Development and Testing of a Renewable Energy-based Thermal Desalination System

by

Zamavangeli Mdletshe

Thesis submitted in fulfilment of the requirements for the degree of
Doctor of Engineering: Mechanical Engineering
in the Faculty of Engineering

Supervisors: Dr V. Msomi

Co-supervisor: Dr O. Nemraoui

Cape Peninsula University of Technology
Bellville, South Africa
February, 2023

DECLARATION

I, Zamavangeli Mdletshe, declare that the contents of this thesis represent my own unaided work, and that the thesis has not previously been submitted for academic examination towards any qualification. Furthermore, it represents my own opinions and not necessarily those of the Cape Peninsula University of Technology.

Sign: 

Date: 13-03-2023

ABSTRACT

In South Africa, membrane desalination has been the desalination method of choice in most cases to assist in attempts to alleviate water scarcity. In this study, an alternative evaporative desalination method was explored called the *adsorption desalination* technique. Evaporative desalination technologies are conventional distillers that are known to consume a significant amount of energy. The adsorption desalination technology emerged to address this issue of high energy consumption of the evaporative desalination technique. Adsorption desalination is an improved version that incorporates the adsorption-desorption refrigeration cycle which is positioned after the boiler for the purpose of capturing and rejecting the adsorbate, the working fluid, of this system. This emerging technology is recognised for its capability to utilise low heat energy to produce potable water.

In this study, the adsorption desalination test rig was developed, constructed and tested using two locally supplied adsorbent materials: silica gel and zeolite. The test rig was at the Mechanical Engineering Department of the Cape Peninsula University of Technology, Bellville Campus, South Africa. After the test rig was constructed, the tests were conducted firstly using electrical energy followed by tests with a hydride of renewable and electrical energy. In performing electrically-driven experiments, a series of eight tests for silica gel were performed, each having varied experimental conditions. Then, the same series of tests were performed for zeolite. Additional to the first series of tests, a series of renewable energy-based tests were performed over 10 days; these tests were performed using the enhanced adsorbent sample comprised of silica gel, zeolite and copper shavings packed on the adsorbent bed.

In this study, the desalination system was a hybrid energised system that was electric and with a solar-driven adsorption desalination technique. As South Africa is a country in the southern hemisphere, its winter stretches from June to the end of August. The first series of experiments were electrically powered. The second series of experiments on the test rig were solar powered, performed in July, a mid-winter month. The experimental output of the second series of experiments demonstrated that mid-winter climate conditions were capable of heating water to above 60^{o}C. This water temperature was then used to trigger desorption of the previously captured water vapour onto the packed adsorbent sample within the test rig which produced more than 30 grams of water vapour when 200 grams of adsorbent material was tested. This was the highest regenerated adsorbate that occurred over two days when the solar irradiation was 415 W/m^2 on day 3 and 410 W/m^2 on day 10.

ACKNOWLEDGEMENTS

Firstly, I would like to thank the Creator of all things for seeing me through this challenging academic journey. Secondly, I thank my supervisor Dr Velaphi Msomi, ngibonga isineke sakho nokungithemba throughout this journey. Uqhubeke ukulwela nokuyiphakamisa indlu yomuntu omnyama. Also, I would like to thank the CPUT's Mechanical Engineering Department workshop staff for their effort in assisting me build the test rig for my study. I thank the department's academic staff for their contribution through advising and motivating me. I thank the larger community of CPUT for their encouragement, from the house parent to the student development office that created a conducive environment for me in the duration of my studies.

Special thanks to my immediate family for their support that came in various ways, I am indeed grateful. Ngiyabonga nina abasezisayini, sengathi engahlala njalo enikhanyisele owasidalayo. Thanks to The TACTSO for their support from the first day I set foot at university till the end, thank you brothers, sisters and leadership. Lastly, I thank my partner in all for the unwavering support.

Thanks to the CPUT VC's Prestigious Award and NRF for their financial support. Opinions expressed in this thesis and the conclusions arrived at are, those of the author, not to be attributed to the funders.

TABLE OF CONTENTS

LIST OF FIGURES

LIST OF TABLES

GLOSSARY

AD- Adsorption Desalination

B. O. P.- bottom of pipe

BV- Ball valve

Con. Red. – concentric reducer

COP- coefficient of performance

CSP- concentrated solar power

Eq.- Equation

ETC- Evacuated tube collector

FT- flow transmitter

GV- gate valve

GOR- gain output ratio

LG- level gauge

MED- Multiple-effect distillation

MENA- Middle East and North Africa

NRV- non-return valve/ check valve

PG- pressure gauge

ppm- part per million

ppt- parts per thousands

PT- pressure transmitter

PVT- photovoltaic thermal

RO- reverse osmosis

RSA- Republic of South Africa

SDWP- specific daily water production

STR- strainer

TDS- Total Dissolved Solids

TT- temperature transmitter

Variac- Variable transformer

CHAPTER 1: INTRODUCTION

1.1 Introduction

Desalination of seawater is a water purification process used to separate salt from saline water and extract the useful potable water using various desalination techniques. This process is fundamentally performed through the two main forms of techniques – membrane and evaporative desalination – but these classifications also exist as hybrid desalination technologies. [1] [2] [3]

In membrane-based desalination, saline water in pressured through a semi-permeable membrane that does not allow unwanted particles to pass through it, only allowing potable water which is further treated for it to be optimal potable water. This technology is more popular than any other desalination methods due to its operational efficiency and scalability. [1] [4]

For an evaporative-based desalination technology to produce potable water from saline water, a temperature difference is applied to the saline water so that there is a phase change or it boils to produce potable water vapour which is later condensed as drinking water. These two methods – the membrane and evaporative-based desalination technologies – are the most used methods for large-scale desalination implementation. [5] [6]

Desalting saline water reduces sodium chloride content to a level that it is suitable for drinking. However, there are other impurities that take longer to be eliminated or reduced, especially if the desalination method used is not based on fluid phase change from liquid to gas. A water treatment process called water softening of hard water is used to improve the integrity of saline water so that this water can be

processed in a membrane desalination machine. This process protects the overall machine from fouling which also prolongs the lifecycle of the membrane of this machine. When softening hard water, chemicals are added to reduce impurities that result from high magnesium and calcium content. This process is primarily used in the pre-treatment phase of the membrane desalination method such as RO desalination technology. This pre-treatment process can be used in an evaporative desalination system by incorporating it; it reduces the temperature required for phase change and, as a result, the problem of scaling is reduced or eliminated in the evaporative desalination technology. [7] [8] [9]

1.2 Background to research problem

The Republic of South Africa (RSA) is a country semi-surrounded by two oceans, the Atlantic and Indian. Regardless of this advantageous geographic location, it is still a potable water scarce country. Ongoing water scarcity warnings have been issued by relevant governmental departments in RSA. This has escalated research conducted by various South African water researchers in recent years. In fact, findings confirm that this water scarcity will be prolonged if little is done to rectify the situation. After the initial water crisis had been identified, suggestions and proposals were brought forward by experts from all sectors with interest in the water industry. This was done with the aim to prevent and alleviate water scarcity in the country. Desalination was one of the methods suggested in response to the water demand. [10-27]

The water crisis in South Africa is not only due to climate change and water demand exceeding water supply but also to poor water management skills and the lack of implementing and maintaining highly efficient water supply infrastructure. Instilling

in water consumers that potable water is a scarce commodity that must not be misused was one method for managing the misuse of water in communities. In support of this, the United Nations Sustainable Development Goal 6 (SDG 6) ensures water access and sanitation for all. This global goal promotes the idea of government investing in water research and development that includes local communities in water resource governance [28]. This heightens the need to invest in water research and building more sustainable water infrastructure to address water scarcity. Involvement of communities would not only minimise the misuse of water but would encourage and include socio-economic activities stemming from active community involvement in water awareness initiatives.

Desalination technology has been proposed in the past to address the water crisis in South Africa. Membrane desalination (reverse osmosis, in particular) is one of the primarily used desalination methods in local municipalities, even though its expensive membrane maintenance costs are acknowledged. [29]

Now, with multiple desalination methods available in the market, this study encourages a thermal desalination technology as an alternative desalination method to RO for RSA. Specifically, a newly developed thermal desalination called adsorption desalination is proposed for RSA [30]. Importantly, in this study, this will be developed, constructed and tested under South African climate conditions.

The adsorption desalination method is a recent thermal desalination technology that remains under intense scrutiny. This technology can be perceived as an improvement of the conventional thermal desalination system. It has two major sub-systems: the evaporator (conventional thermal desalination) and the adsorption-desorption refrigeration cycle. [31]

The adsorbent desalination system has been reviewed meticulously by numerous researchers with the aim of improving and comprehending its thermodynamic boundaries. This system's governing equations are still under development. This is evident in the experimental and numeric studies previously conducted on this system. [32] [33] [34]

Wu et al. [35], studying the thermodynamic cycles that occur in the adsorption desalination systems, found that maximum water production and minimum energy consumption occurs when the evaporator temperature difference is higher than the coolant temperature of the condenser and the adsorbent chambers. In these conditions, their system reached peak performance. EI-Sharkawy et al. [36] also conducted an experiment on this desalination system. They tested, in particular, the adsorbent chambers with a temperature of 30^{o}C inlet cooling water. This system produced a steady 8.2m^{3} of potable water daily. Thu et al. [37], investigating the heat recovery effect between the condenser and evaporator of the adsorption desalination cycle, found that recirculating the outlet coolant from the evaporator to the inlet (coolant) of the condenser reduced the cycle time of the original adsorption desalination system.

1.3 Problem statement

South Africa is clearly facing water shortages. Desalination was declared nationally as one of the viable solutions chosen to address this water crisis. However, membrane is the only desalination method that has been implemented on a large scale. There are various disadvantages associated with membrane which can be reduced through a thermal desalination method. In this study, the emerging adsorption desalination method is proposed for South Africa. This desalination

technology has been deployed successfully in various other places. Therefore, it will be developed, constructed and experimentally tested in South Africa. The aim is to experimentally improve this system by enhancing the adsorbent chamber to achieve the best system output of adsorption desalination using locally available adsorbent materials.

1.4 Research aims and objectives

The primary aim of this study is to develop, construct and test an adsorption desalination system. The following objectives are set for the study:

1. To manufacture and test an adsorption desalination system using locally available adsorbents;
2. To experimentally test the system under South African climate conditions and compare to those of MENA region; and
3. To experimentally enhance the adsorbent chamber of the system.

1.5 Thesis overview

The overview of the thesis for this study is as follows:

Chapter 1 - Background: The background to this study is presented in this chapter which focuses on the overall demand of desalination technology. First, desalination technology is briefly introduced. Secondly, the problem statement is presented. Thirdly, a brief background on the adsorption desalination is discussed. Finally, the aims and objectives of the study are stated.

Chapter 2 - Literature Review: In this chapter, the related literature to the conducted study is reviewed. The review focuses on the emerging adsorption desalination technology that has been previously researched.

Chapter 3 - Development and Construction: This chapter entails the development protocols followed with the construction of the test rig for this study.

Chapter 4 - Experimental Setup and Methodology: In this chapter, the detailed data acquisition systematic procedure is presented based on the final experimental setup of the test rig.

Chapter 5 - Results and Discussion: After capturing the experimental data from the test rig, as in Chapter 4, the results of the system's behaviour at varied testing conditions are presented and discussed.

Chapter 6 - Conclusion & Recommendations: Based on the findings of the experimental study, a conclusion is drawn and recommendations are made for relevant future investigations.

CHAPTER 2: LITERATURE REVIEW

In this chapter, the following sections will be discussed. First, an overview of thermal desalination for South Africa is presented. This overview consists of an analysis of solar irradiation and water salinity for South Africa which is compared with that of the MENA region. Secondly, a review of the three primarily used desalination technologies are presented. Finally, the adsorption desalination technology is reviewed.

2.1 Thermal desalination for South Africa

The use of desalination technology in RSA is gradually growing. This trend is observed through the existence of water research institutions and water-related small, medium and micro enterprises (SMMEs) in the country. If these enterprises get work from the desalination industry, this suggests activities and growth within this emerging market. This is currently the case in RSA even though it is not occurring at as fast a rate as in other countries such as Singapore, Saudi Arabia and Egypt, for example. [38] [39] [40]

There are different kinds of desalination technologies available on the market. Desalination technology can be classified fundamentally as thermal or non-thermal based. This application of desalination technologies depends on various parameters that include existing resources in that area and financial commitment for the proposed desalination plant. Geographic location is one of the most influential parameters when it comes to the selection of the type of desalination method to be used in a particular area, particularly if it is anticipated to be a built on a large scale.

Previous studies have presented a critical review process on how to undertake the selection of a desalination technology. [41] [42] [43]

In South Africa, reverse osmosis (RO) has been the primary desalination method of choice. Over time, however, research studies have shown that it is not only RO desalination technologies that have the potential to supply potable water. The reason why RO has always been the desalination technique of choice in RSA is because of its reasonable energy consumption. But RO desalination had, and still has, the disadvantage of extremely high membrane maintenance costs. Thermal evaporative desalination is an alternative desalination method that has been used for decades but has the disadvantage of a high energy requirement. The challenge of using energy intense desalination technology remains, particularly with the ongoing electricity crisis that is predicted to continue until at least 2025 in RSA. [44] [45]

Now, with the water-energy nexus that has been thoroughly researched globally, this is an opportunity for RSA to review the utilisation of RO desalination technology and consider conventional thermal-based desalination technology without facing constraints for using electricity to desalinate water for consumption purposes. Most importantly, South Africa is abundant with solar energy resources, and this can be manipulated for the benefit of exploring other solar-thermal desalination technologies. Other countries such as those in the MENA region have successfully achieved this, as evidenced by the substantial desalination industry that exists in this region. RSA can address not only water scarcity but also create job opportunities via this growing the desalination industry. [46] [47] [48] [49]

The Witsand Solar Desalination Plant is the first solar thermal desalination plant in Southern Africa to be built in the Hessequa Municipality in the Western Cape. This

plant is producing a reasonable 100 kilolitres of potable water daily. However, this is not a South African desalination technology but an imported French design. Hence, it important for RSA to invest locally to produce independent desalination experts. This will support seasoned desalination experts and generate an eternal industry because water demand is not seasonal; water is an elemental daily requirement. [50] [51] [52] [53]

2.1.1 Influence of solar irradiation on thermal desalination systems

Potable water production through the desalination of seawater has been declared one viable solution for alleviating the global water crisis. For large-scale implementation in solar abundant areas, thermal desalination technologies are more highly recommended than non-thermal. Therefore, solar irradiation is a subject that cannot be overlooked when exploring thermal desalination technology for a country or region with high solar irradiation such as in RSA. In this section, a comparative analysis will be made between RSA and the MENA region. It is evident that RSA gets higher solar irradiation than the MENA region. The MENA region has a solar irradiation range of 3.5 to 5.5 kWh/m^2 while RSA experiences 4.5 to 6.5 kWh/m^2. This clearly indicates that using solar energy advantageously in RSA would be a success if in the MENA region solar thermal energy is successfully used in the desalination industry. [23] [29] [54] [55]

Ahmed et al. [56] presented a review of solar energy technologies that are compatible with desalination technologies. In this study, they highlighted that solar energy is the most suitable energy method for desalination technologies that are energy intense. They also suggested the use of photothermal materials (materials that convert light to heat energy) for the application of increasing the performance

of the membrane distillation and enhancing the energy conversion. Direct solar energy use to drive desalination methods cannot continuously operate desalination plants 24 hours a day. Therefore, solar energy storage in the form of batteries and other thermal methods such as capacitors, sorption, solar fuels, pumped hydroelectric storage (PHS) and compressed air energy storage (CAES) are employed to address this issue. The use of solar energy storage has had a positive impact on the water production of the solar-based desalination plants [57] [58].

Monjezi et al. [59] simulated the incorporation of PVT cells into an RO desalination system suitable for the climate parameters of Egypt, a country with high solar irradiation. In their system, they used seawater as coolant to enhance the efficiency of harvesting solar energy. Energy storage in the form of batteries was used in this study to ensure continuous energy supply. They achieved a reduction of 0.12 kWh/m^3 in the specific energy consumption (SEC) which reduced the required solar panel collection area by 6%.

Stefano et al. [60] innovated a solar thermal distillation system that is geothermally assisted for continuous heating, focusing on the cost effectiveness of this newly developed system that operates 24 hours a day. In their system, they found the SEC to be 5.5 kWh/m^3.

Hoffmann and Dall [61] presented a study on the combination of multi-effect distillation plant and concentrated solar power (CSP) suitable for Arandis, a town in Namibia. Their study justified the practicality of using the hybrid system by focusing on its techno-economics. They determined the system feasible should solar harvesting be used through CSP despite the high initial cost for implementing this dual plant. Even though solar irradiation is a sensitive parameter to a study of this nature, educated assumptions were made due to the unavailability of current data

for the period of their study. The most recent solar irradiation to be recorded for this area was estimated at 2528 kWh/m^2 annually; this guided the estimation.

Valenzuela et al. [62] conducted an experimental investigation on the thermal performance of large parabolic trough solar collectors (PTC). Their study approach was to explore the different angles of the incidence of solar irradiation rays on the solar collectors. It was evident that a low incident angle yields a high direct normal irradiance per square meter. They concluded that the overall performance of the parabolic trough collectors is affected by the incident angle of the solar irradiation rays.

Adsorption desalination has a minimum specific energy consumption of 1.5 kWh/m^3 and reverse osmosis has an energy requirement ranging between 2 to 4 kWh/m^3 of water [63] [64]. South Africa is producing desalinated water using RO, with an estimated maximum of 6.5 kWh/m^2 of solar irradiation. Therefore, the South African solar irradiation on its own renders adsorption desalination a competitive desalination technology for use in South Africa. The low energy consumption of the adsorption desalination, if compared to that of the dominantly used RO, supports the deployment of adsorption desalination for South Africa.

The existing water quality in a location is also an influential factor when selecting a desalination method to address the water shortage. In the next section, water salinity will be reviewed for both RSA and the MENA region.

2.1.2 Influence of water salinity on the performance of desalination systems

A clear comprehension of the existing water salinity of an area or of the saline water feed is critical to the desalination technology that will be used to produce potable

water. A comparison of the MENA region and RSA's seawater water salinity are considered in this section. Studies that investigate water salinity for the purpose of desalination are also presented in this subsection.

The MENA region has higher seawater salinity (36 to 40 ppt) than the seawater salinity off the coast of RSA (35 to 35.8 ppt). The World Health Organization (WHO) reported that the acceptable total issolved solids (TDS) content in potable water should be less than 500 mg/litre (0.5 ppt). It is important to adhere to this standard strictly when desalting seawater for consumption. In the MENA region, the seawater salinity is approximately 40 ppt, suggesting that the desalination systems existing in this region are reducing the seawater's salinity by approximately 80 times in order for it to be drinkable. [17] [65]

Brine is the product of high salt concentration when salt content is separated from saline water to produce potable water. This makes the brine concentration dependent on the salinity of the feed water. Wenten et al. [66], in a mini-review on impact of brine ejected by desalination systems, concluded that a dual plant for water desalination and salt production purposes can reduce energy consumption. Moreover, a system of this nature can assist in saving the environment by recovering the brine as usable salt.

Al-Kaabi et al. [67] examined the sustainability of utilising an seawater reverse osmosis (SWRO) by analysing the water quality (or salinity) and several other factors. In this study, they assessed 19 various locations using a life cycle assessment (LCA) tool to assess the environmental impact of using SWRO, taking into consideration the water salinity available at each of the 19 selected locations. From the analysis, they presented a significant change in environmental impact that

would result from locating a desalination plant in a more suitable area with an optimal seawater salinity.

Pham and Nguyen [68] conducted a theoretical study of a saline water distillation system suitable for Vietnam climatic conditions. In this area, the saline water is recorded to be 35000 parts per million at an average temperature of 30^{o}C. The computation of their model to yield a potable water production of 208kg/h is based on these set conditions.

Fouling is a phenomenon of debris build up at undesired locations of the desalination machine. This clogs the desalination process causing the system to function inefficiently. Fouling in a membrane-based desalination system is due to four factors: operational conditions, membrane properties, foulant characteristics and feed water properties which include scaling. Water salinity level is directly proportional to the scaling that may take place in this system. Therefore, controlling the scaling factor relies on controlling the salinity feed and the operational environment within the distillation process. Tijing et al. [69] presented a review on the occurrence of fouling within a membrane distillation system. In this study, they highlighted scaling as a result of dried-up salt content of the feed water clogging the membrane of this system, recommending that the operational conditions be improved and that the membrane design be optimised so that fouling does not damage the membrane of the membrane distillation system.

From the literature survey in this section, it has been established that water salinity is a critical parameter to investigate prior to the design and implementation of a desalination system to ensure that it is suitable for that specific location. In the next section, a review of the main types of conventional desalination technologies is presented.

2.2 Conventional desalination technologies

Water and energy are basic resources required to drive a country's economy on a daily basis. The balance between these two resources is critical to a country's functionality. The use of non-renewable energy, globally, has revealed its negative impact on the environment. The energy-environment nexus has pushed for a global shift in intense research on clean energy methods for the purpose of sustainable water production while protecting the environment. Renewable energy-based desalination has emerged as a potentially viable solution to address the energy burden attached to the use of desalination technologies. There are various major renewable energy sources, namely solar, geothermal, wind, hydropower and biomass. These time-limited energy sources are naturally available on a cycle basis, meaning that they can only meet energy demands at certain periods but not others. One major development of renewable energy is availing these forms of energy resources whenever there is a demand, and not only at their cycle convenience. [70] [71] [72]

Compain [73] presented a study on solar energy methods compatible with desalination plants. This study confirms that reverse osmosis (RO) stands unchallenged and focus should be on developing the RO method as it benefits from the advantage of operating during the night. Their study further suggests that multi-effect distillation (MED) and multi-stage flash (MSF) are not recommended to be solar powered because these desalination methods are acknowledged as energy intense and regarded as technologies still needing to be proven. Therefore, it is important to explore solar thermal energy storage to enable solar energy-based desalination technologies to operate 24 hours a day. In doing so, focus should not

be shifted from utilising renewable energy to save the environment and the production of potable water in a more sustainable manner. [72]

In the subsequent sections, three desalination technologies are reviewed. Reverse osmosis (RO), multi-effect distillation (MED) and multi-stage flash (MSF) are highly utilised desalination technologies; consequently, intensive research and development has been dedicated to these three systems [74] [75] [76]. Later, the adsorption desalination technology will also be reviewed.

2.2.1 Progress in developing reverse osmosis desalination systems

Reverse osmosis (RO) desalination, a membrane-based desalination technology, is the most used technology to produce potable water. It is currently regarded as the most energy efficient method when compared to thermal evaporation desalination technologies. Even though this is dependent on the feed salinity level, RO has by far proven to be an energy efficient desalination technology [77]. However, RO has high membrane maintenance costs and corrosion defects which can be eliminated by including pre-treatment processes [78]. Numerous pre- and post-treatment processes included in this technology protect the integrity of the membrane and produce high quality potable water. These additional processes can be considered a disadvantage because they increase the cost of implementing and operating this desalination technology. Therefore, RO desalination is suitable in instances of desalinating low saline water that has low solid contents. This will reduce or eliminate the pre-treatment process stage.

Kaya et al. [79], conducting a study on utilising the combination of photovoltaic and reverse osmosis based on Abu Dhabi conditions, recommended that this hybrid

desalination system be used in this city instead of the more frequently used MSF and MED thermal desalination systems. This study initially established that desalination of seawater will increase in the near future. In their analysis, they recommend capitalising on the falling price of solar PV units, affordable energy consumption or RO, as a major cost decrease of RO components. Their study suggests how to switch from the use of unclean energy to clean solar energy to drive desalination plants in this region. Moreover, they suggest that evaporative desalination is not environmentally sustainable due to its high energy requirement, concluding with a recommendation to switch to reverse osmosis.

Chu et al. [80] developed and analysed the performance of an SWRO plant implemented on large scale. A comprehensive analysis technique was used to determine optimal design parameters for an SWRO plant. Water quality is one aspect that was evaluated. Also, in reviewing the cost of the process of drawing seawater from the ocean into the plant, they found that using a dissolved air bio-ball floatation (DABF) system would reduce the overall plant operation costs incurred at the inlet system setup. The DABF system is designed to prevent organic material from entering the plant. After the feed seawater water has gravitated through the DABF before the inlet of the plant, the seawater is pre-treated using the optimal dual media filtration (DMF) process. Other parameters such as the split partial, simulation, output water quality check and specific energy consumption were presented in their study as well.

Elmaadawy et al.'s [81] study aimed to address the use of non-renewable energy in large-scale RO plants. This is attained by proposing the use of renewable energy so that the environment is protected from possible harmful outcomes of using unclean energy to produce potable water through RO. In this study, various off-grid hybrid energy supply methods such as solar, wind turbine and battery energy

sources are incorporated to the existing diesel-powered RO desalination system. They found that this hybrid energy system can yield profit after a period of two and half years. The optimal physical size parameters of the hybrid energy system were presented. The hybrid energy system ensured the lowest possible carbon emissions when the environmental analysis was conducted. This study serves as a guide for policy makers and professions with related work when considering the integration of hybrid energy systems for RO plants implemented on a large scale.

Alsarayreh et al. [82] conducted a numerical study wherein they investigated the performance and energy consumption of a medium scale brackish water reverse osmosis (BWRO) model. An energy recovery device (ERD) was collaborate with the BWRO model to evaluate the energy consumption of the model. It was determined that the energy consumption of the improved model deceased when ERD was incorporated onto the original model. As a result, the configuration of the newly developed model was determined to be feasible. Other parameters such as the feed flow rate, pressure and temperature were also assessed, and it was determined that these respective parameters likewise impact the water recovery of the model.

Kettani et al. [83] modelled the RO plant that would operate 24 hours per day based on Chtouka Ait Baha (Morocco) parameters. This large-scale model was tested using a series of four different power sources: scenario 1: the grid; scenario 2: PV together with the grid; scenario 3: lead acid batteries together with PV and grid; and scenario 4: lead acid batteries together with the grid and CSP units. After modelling each scenario, series of tests evaluated the cost of running the RO desalination plant when the respective energy methods were used. They proposed that for Morocco's conditions, scenario 2 should be implemented first; and then later on, CSP units could be implemented to power a large-scale RO plant to produce potable water at an energy cost-effective price in the near future.

2.2.2 Progress in developing multi-effect desalination systems

Multiple-effect distillation (MED), a thermal evaporative desalination technology in use for several decades, was initially used in the chemical industry to extract sugar from sugar cane syrup. This process was later applied in the seawater desalination industry. MED technology distils water progressively over multiple stages; hence, a 'multiple effect' to produce potable water. Unlike RO, MED does not require intense pre-treatment processes. Also, high saline water feed is not sensitive to this technology as in the RO process. MED can distil feed water with an approximate temperature of 70^{o}C, but preferably at a lower temperature to prevent scaling and fouling within the system. The gained output ratio (GOR) is the ratio of the water produced to the steam generated in the first effect or stage. Research shows that having more stages (effects) to range between three to six impacts the GOR which then increases the systems performance ratio (PR). However, there is still room for improvement in determining the parameters affecting the water production of this technology. [84] [85] [86] [87]

Carballo et al. [88], in a study that established the optimal operational conditions for the MED pilot system, used a previous theoretical model. They improved the system by focusing on the two main indexes: specific exergy consumption and energy efficiency. Other indexes such as the PR, specific water consumption and specific thermal energy consumption were used to analyse the system. They observed that in maximised criteria, the mass flow rate through the stages was proportional to the potable water produced by the system. It was concluded that each index yields different favourable conditions when they were optimised. The specific exergy

consumption index yields low quality energy demand and the specific energy consumption yields low temperature heat in the system.

Wang et al. [89] simulated an MED model that was experimentally validated. This study presented the daily potable water production of the newly developed distillation plant with four to six effect stages. The developments of this model focused on using low grade thermal energy to attain a better performing MED model. It was observed that the developed model outperformed the conventional MED model by 25 to 60%.

Alhaj et al. [90] addressed the need to explore other energy methods to drive the MED system. In their study, they intended to achieve optimal operating conditions of an MED system when solar energy is used to drive this desalination system. Solar linear *Fresnel* collectors were used to drive the system, as the energy system used in a desalination system is critical in any study. It was observed that the solar collector unit accounted for 60% of the implementation costs of the entire system. The remaining 40% was shared between the cost of the actual MED plant and the energy storage.

Brine discharge into the environment by evaporative desalination methods has been an ongoing problem. Guo et al. [91] conducted a theoretical study on a solar powered zero liquid discharge (ZLD) spray evaporator MED system, with three effect stages. In this study, they experimented with light spray droplets onto the tube bundle with the aim of addressing scaling within the stages. This resulted in zero brine discharge when the seawater was being desalinated. The system was unfortunately feasible with a simulated 500^{o}C temperature supply.

2.2.3 Progress in developing multi-stage flash desalination systems

Multi-stage flash (MSF) together with RO are the leading desalination methods used frequently in the desalination of seawater industry. Unlike MED and other thermal desalination technologies, MSF desalination is a preferable technology due to its daily water production and cost-effectiveness. MSF desalination also progressively desalinates the working fluid; it has effective stages ranging between 18 to 25. The global shift of elimination electrically driven desalination technologies is trending; however, this technology is still not yet purely driven by solar thermal energy. It still requires a degree of electrical energy to operate. Studies have observed that MSF has proven reliable, particularly in energy abundant countries. The GOR and PR are two of the economic parameters used to gauge the MSF desalination performance. [92] [93] [94]

Scaling is common in phase change-based desalination methods. Hawaidi and Mujtaba [95] mathematically investigated the parameters that contribute to scaling within an MSF desalination system. Initially, they distinguished that fouling factor is a measure representing the degree of scaling occurring in desalting systems. They then proceeded to present the results of their study, suggesting scaling as an undesirable phenomenon that occurs over time, causing the system to require more energy to operate. According to Hawaidi and Mujtaba, this is due to the build-up of scales on the tubes which hinders effective heat transfer and as a result, compromises the rate at which the system will produce water.

AL-Rawajfeh et al. [96] modelled and developed a (once-through) OT-MSF and (brine-recycle) BR-MSF distiller configuration to analyse the scale formation within the distiller. They found that scale formation is proportional to the temperature existing within the distiller when anti-scalant is not used to protect the surfaces

exposed to saline or brackish water. It was established that the use of anti-scalant reduced the fouling factor and protected the internal surface of the distiller. Similar behaviour was observed in both simulated configurations and the simulation was also validated experimentally.

Kalendar and Griffiths [97], experimentally examining the performance of an MSF desalination test rig, investigated the effect on heat transfer when using a plain and an enhanced tube (of varying diameters) in the evaporator and condenser units. They found that the enhanced tubes yield a better overall heat transfer when two different coolant flow rates were tested. The heat transfer coefficient yield by the enhanced tube was found to be 2,13 for the plain tubes.

Darawsheh et al. [98] conducted an experimental investigation on the solar driven MSF desalination system that incorporates multistage vacuum chamber. They assessed the performance of the MSF desalination using governing equations of specific feed flow rate, specific available energy consumption, specific thermal energy input and efficiency of water distillation. In their study, they observed that by controlling the system's pressure condition by lowering the pressure progressively from 0 kPa to -20 kPa, the system yielded a distillation rate of 0.671 L/h to1.038 L/h, respectively.

2.3 Progress in developing adsorption desalination systems

In the latter sections, the three most commonly used desalination methods are discussed. There are different classifications of water desalination techniques, of which the emerging desalination technology called the adsorption desalination technology falls under the evaporative desalination method. The adsorption

desalination is a newly developed thermal desalination method that entails a combination of two main sub-systems: the conventional thermal evaporation desalination and the adsorption-desorption refrigeration cycle. [99]

This desalination technology is an original patent of Ng et al. [100]. In a conventional thermal evaporation desalination method, potable water is produced by boiling saline water and then shortly thereafter condensing it straight from the evaporator. In the adsorption-desorption based desalination system, the potable water vapour (adsorbate) produced in the evaporator is captured by the adsorbent (i.e., silica gel) to increase the rate of the condensation process so that the specific daily water production of this kind of desalination system is increased. The adsorption-desorption cycle is a thermo-physical cycle that has two basic agents: the adsorbent and the adsorbate. An adsorbent is a physical porous material that attracts the adsorbate. Frequently used adsorbents are silica gel, zeolite and activated alumina, which is available in different grades. The hydrophilic physical property of adsorbents makes it possible for the water vapour to be adsorbed from the evaporator (faster if compared with the conventional desalination method). This water vapour is later rejected or desorbed into the condenser due to hydrophobic phenomenon. [101] [102] [103] [104]

Ali et al. [105] presented a newly developed adsorption desalination model that consists of an ejector-assisted configuration. The adsorbent material that was used in this thermodynamic model was silica gel. The theoretical investigation of the developed desalination system showed significant improvement when compared with that of the original system. The specific daily water production (SDWP) of their system was estimated to produce 46m^3 per tonne per day, significantly high if compared to conventional adsorption desalination systems that have an SDWP ranging between eight to 15m^3 per tonne per day.

Raj and Baiju [106] presented a theoretic model for the adsorption desalination cycle. In their study, they observed that controlling the operational parameters such as the coolant temperature influences the water production of the system. Based on analysis, they concluded that a high performing adsorption desalination system is a result of low temperature (10 to 20^0C) water cooling for the adsorbents and condenser and high hot water temperature (70 to 85^{o}C) for the adsorbents.

Bai et al. [107] modelled an adsorption cooling desalination system that was experimentally validated. The three main foci of their study were to assess the influence of the seawater salinity on the modelled system; to experimentally investigate the newly developed adsorbent on the desalination system; and to develop the mathematical model to accurately predetermine the behaviour of the adsorbent beds of the desalination system. Other parameters such as the effect of adsorption and desorption and the effect of various coolants circulating in the system were observed. In these observations, the system's performance was analysed when the parameters were controlled, with their system experimentally producing an amount of 18m^3 per day of SDWP.

Li et al. [108] presented a study wherein they numerically analysed the heat and mass transfer of three different adsorbent packing scenarios. Scenario 1 to 3 each consisted of two types of adsorbents packed around a fin tube. The heat transfer was further explored at different fin pitch lengths. After developing their model, they found that the optimal configuration yields an SDWP of 7.5m^3 per day.

2.3.1 Parameters influencing horizontal falling film evaporator performance

Evaporators are devices used in various sectors such as desalination, dairy processing, petrochemical, and numerous other industries for various distillation processes. Evaporators come in two main types: the flooded and the falling film evaporator. The flooded evaporator has a heat exchanger fully submerged under the fluid that is subjected to the heat. In a falling film evaporator, the dynamic fluid is distributed from the top of the evaporator onto the heat exchanger (or the tube bundle). The falling film evaporator is more energy efficient than the flooded evaporator because the flooded evaporator has to overcome a temperature difference of a stagnant pool of fluid which consumes a substantial amount of energy.

The falling film evaporator is further classified into two kinds: the horizontal and the vertical falling film evaporator [109] [110] [111]. In a horizontal falling film evaporator, the tube bundle is horizontally arranged and in the vertical evaporator, the tube bundle is vertically arranged. Both evaporators have the top distributor dispensing the fluid to be heated by the respective tube bundles [112] [113] [114]. Emphasis will be on the horizontal falling film for this present study. A horizontal falling film evaporator has several parameters that are controlled in order for it to yield an optimal heat transfer from the tube bundle to the dynamic fluid. This heat transfer determines the throughput of the evaporator. However, the coefficient of heat transfer is also dependent on the physical parameters – structural, geometric and fluid flow pattern properties [115]. Literature has captured the three traditional patterns that can occur when a falling film cascades from the distributor down the horizontally arranged tubes. These conventional fluid patterns are in the form of droplets, columns and sheet patterns flowing down the inter-tube bundle.

Structural parameters refer to the external surface finish of the tube bundle. Previous researchers have explored this using the plain copper tubes as a tube

bundle. However, it has been established that enhancing the external surface of the tube bundle improves the falling fluid flow pattern. This also increases the surface area of the heat exchanger (tube bundle) which improves its efficiency [116]. Studies demonstrate that of the three patterns, the sheet pattern is the most desirable because it does not leave any undesirable dry patches on the external surface of the tube bundle when there is temperature difference. [117] [118]

Chen et. al [119] experimentally investigated an enhanced tube bundle, establishing that on a plain tube bundle, the fluid tends to not form a sheet pattern. As they advanced with observations, they found that as the tube bundle was further enhanced, the flow pattern improved. Very few studies are dedicated to the physical aspects of the falling film evaporator. Instead, the majority of studies focus more on the heat transfer coefficient of the evaporator.

Jin et al. [120], experimenting on the falling film evaporator, investigated the impact of film flow rate and heat flux on the overall heat transfer performance of the evaporator. In studying a four-tube evaporator with refrigerant R134a, they observed that the heat transfer coefficient of the top tube of the bundle is higher than that of the tubes further below the tube bundle. Similarly, they determined that the inter-tube bundle pitch is directly proportional to the heat transfer coefficient.

Shen et al. [121] prepared experimental test rigs of three different geometrically positioned horizontal tube bundles. In set 1, a triangular tube arrangement formation was set; set 2 was a rotated square arrangement; and set 3 was a square pitch tube bundle arrangement. The impact of the four parameters – spray density, saturation temperature, overall temperature difference and inlet steam velocity – on the heat transfer coefficient was observed on each test rig. It was found that the spray density and saturation temperature are directly proportional to the heat transfer coefficient,

while the heat transfer coefficient is inversely proportional to the overall temperature difference of each evaporator test rig. The inlet steam velocity was found to have no influence on the heat transfer coefficient.

Researchers prepare the tube bundle in various ways to achieve an optimal flow pattern. For example, plain tubes and other possible surface preparations can be employed to externally enhance the tube bundle [122]. Mdletshe et al. [116], enhancing the tube bundle longitudinally in their study, also witnessed an improvement in the flow pattern as it cascaded down the tube bundle. Geometric parameter refers to the arrangement or positioning of copper tubes within the tube bundle, which can be square or staggered. The physical geometric study of tube arrangement is critical for sufficient surface wettability and steady fluid flow as it cascades down the bundle.

The horizontal tube bundle arrangement contributes to the performance of the evaporator by positioning the tubes in such a way that this reduces or eliminates dry patches on the tube bundle. Various studies have been conducted on the positioning of the tube bundle for the falling film evaporator [120] [122]. The geometric parameters include the size, number and positioning of the horizontal tubes and the top fluid distributor. This, as a result, determines the optimal physical size of the evaporator. Structural parameters include the surface finish and material selected for the tubes of the horizontal tube bundle of the evaporator. The fluid related properties – such as the Reynolds number, Prandtl number and Nusselt's number of the fluid – are sensitive parameters that affect the performance of the evaporator. The mere fact that this type of evaporator operates at low temperature difference is why it has been employed frequently in the adsorption desorption-based desalination technology. This also eliminates the disadvantage that other thermal evaporation desalination systems have of scaling. [123] [124]

2.3.2 Use of adsorption desorption cycle in thermal desalination systems

The adsorption cycle is a thermophysical reversible cycle triggered by cold water circulation through a packed adsorbent bed to absorb (attract) an adsorbate (vapour) onto a physical porous surface area of an adsorbent (silica gel). The reverse of this cycle is called the desorption cycle which is triggered by hot water circulation to desorb (reject) the adsorbate (vapour) off the surface area of the adsorbent (silica gel). This thermodynamic cycle has been previously investigated both experimentally and theoretically. [125] [126] [127]

An adsorbent granular captures the adsorbate onto its porous surface. The capability of an absorbent to adsorb is called its adsorption affinity, which varies for different adsorbents. However, to trigger the adsorption or desorption affinity, a temperature difference is required which is commonly via a cold or hot water circulation.

Kim et al. [128] studied the initial time lag (ITL) together with the effect of using multiple adsorbent beds and the effect of the input-stream temperatures on the performance of the adsorption desalination. In questioning the practicality of the existing governing equations for controlling the adsorbent desalination, they found that ITL is practically sound compared to the use of conventional heat and mass transfer rates. This was based on the good performance that was observed from the overall system when using ITL.

Ali et al. [129] conducted a study on a solar driven adsorption desalination system suitable for climatic conditions in Egypt. Silica gel of 13.5 kgs adsorbent was used in their system that yielded a specific daily water production of 10.5 litres per day and a COP of 0.5. Assuit, the city in Egypt where this adsorbent system was based,

has a solar irradiation ranging from 0.5 to 0.8 kW/m^2 on average throughout the year.

Olkis et al. [130] also conducted a similar study, using 0.2 kgs of silica gel adsorbent in this smallest test rig to-date of an adsorption desalination system. The test rig novelty is for the understanding and advancement of the temperature swing of this system. Ultimately this test rig is to enable tests of various adsorbent materials in small quantities instead of using large adsorbent quantities.

Du et al. [131] explored solar heating for the adsorption desalination. Their study focused primarily on optimising the solar collection for the purpose of supplying hot water to the system at cost effective units. This was achieved by methodically selecting an optimal and cost-effective solar collection area unit. In this study, when solar heating was used, it was found that 0.03 to 0.04 CNY/MJ was the overall cost. A precise guide on how to design a solar-driven adsorption desalination emerged from this study.

Thu et al. [132] conducted a numeric study of a four-bed adsorbent desalination system which was experimentally validated. In their study, they observed the cycle period of the system when the internal heat energy was reused between the evaporator and condenser. This suggests that the outlet coolant of the evaporator (which is cooler water) is used at the inlet of the condenser to extract the heat in the condenser. A cycle period of 360 seconds was observed when 70°C hot water was used in this system.

Finally, the adsorption desorption cycle in a desalination system plays the significant role of increasing the rate at which the water vapour is extracted from the evaporator to the condenser. As a result, this optimises the daily water production of an evaporation desalination system when it has incorporated the adsorption desorption

cycle. In the next section, the existing adsorption desorption desalination systems will be presented.

2.3.3 Historic adsorption desalination systems

In this section, a summary of several documented adsorption desalination systems or plants are presented. This thermal desalination technology by design considers the critical issue of having lower energy consumption [133]. However, it has a shortfall of a historic poor coefficient of performance (COP). Hence, the gain output ratio (GOR) is a commonly used ratio to quantify the performance of this system. A review of the adsorption desalination systems available in various countries is tabulated below, with the daily water produced by those systems presented.

TABLE 1: REPRESENTING THE REVIEWED EXISTING ADSORPTION DESALINATION SYSTEMS

Investigator	Country	Daily Water Production
[30]	Singapore	3.6 m^3/day
[36]	Singapore	8.2 m^3/day
[37]	Singapore	4.3 m^3/day
[125]	Egypt	25kg/day
[134]	China	100kg/h
[135]	Egypt	40 m^3/day
[136]	China	4.69 m^3/day
[137]	Singapore	10 m^3/day
[138]	UK	10 m^3/day

[139]	UK	10 m^3/day
[140]	UK	8.4 m^3/day
[141]	Iran	9.58 m^3/day
[142]	UK	10.9 kg/day
[143]	Saudi Arabia	6.3 m^3/day

The adsorption desalination system is a promising emerging desalination technology that has been studied quite intensely in a relatively short span of time. Fortunately, while it still has substantial room for improvement, it can be beneficial in addressing the global water shortage. Hence, it is investigated in this study in an effort to solve the serious, perpetual water shortages in South Africa.

To date, the adsorption desalination system has undoubtedly established that it can function as a viable solution to address water scarcity globally. Alnajdi et al. [31] suggested in their study that improving the characteristics of the adsorbent may lead to better comprehension of this system which would result in reducing the adsorption desorption cycle time, implying a higher SDWP. Therefore, developing and testing the adsorbent chambers of this system is still open for further investigation.

2.4 Summary

The reviewed literature has clearly distinguished that adsorption desalination technology is a potential technique for addressing potable water scarcity in South Africa. In the literature reviewed, studies revealed how researchers have capitalised on undesirably hot climate conditions for the good purpose of producing potable water. Regions such as the MENA and other countries such as Singapore, China and the UK have demonstrated the use of renewable solar energy to drive thermal

desalination systems. In these regions, adsorption desalination technology in particular was determined to be a successfully employed desalination method despite the high seawater salinity in these areas.

This present study intends to experimentally develop a model that will be built and tested under South African climatic conditions. After testing this experimental model, its performance, based on the daily water production, will be compared to the performance of existing adsorption desalination systems available in various regions around the world.

CHAPTER 3: DEVELOPMENT AND CONSTRUCTION

As pre-experimental work, a conference proceedings article was produced in the construction phase to size and analyse the distributor pipe preparation and tube bundle; those results were published as follows:

Z. Mdletshe, V. Msomi, O. Nemraoui. (2021). The effect of modifying the external surface of copper tubes used in a falling film fluid of a horizontal tube bundle. *Materials Today: Proceedings*, 45(45), 5689-5694.

This chapter presents the development and construction of a test rig of the adsorption desalination system. For this study, the test-rig consists of two main components: the evaporator and adsorbent beds. In this study, solar thermal energy was explored in addition to electrical energy as an energy source to heat water for the adsorbent bed, to trigger desorption. Therefore, a third component, the solar collector, was an additional sub-system featured. Firstly, the development of the falling film evaporator is presented. Secondly, the development of the adsorbent bed is presented. And finally, the solar harvesting unit used to heat the water circulating through the 50L geyser for desorption in the adsorbent bed is presented.

The hot water in this entire study was required in two places – in the evaporator and in the adsorbent bed – to desalt saline water to produce potable water vapour and for desorption, respectively. It should be noted that the hot water circulating through the evaporator was at all times electrically heated, leaving only the adsorbent bed to be heated using solar heated water; but initially electrical energy was used for experimental tests of desorption. This system was erected using materials supplied

by local South African vendors. Recycled materials were used where possible to lower the construction cost.

3.1 Adsorption desalination test rig

The studied desalination system pipe and instrumentation diagram presented in Figure 3.1 illustrates the general flow of the system with an indication of a few instrumentations to give the gist of the working fluid flow and location of the major components on the schematic. Even though the constructed desalination test rig was for the purpose of desalinating seawater, the shell of the evaporator was constructed out of carbon steel and mild steel so material cost was reduced. Ideally, a food grade stainless steel should have been used.

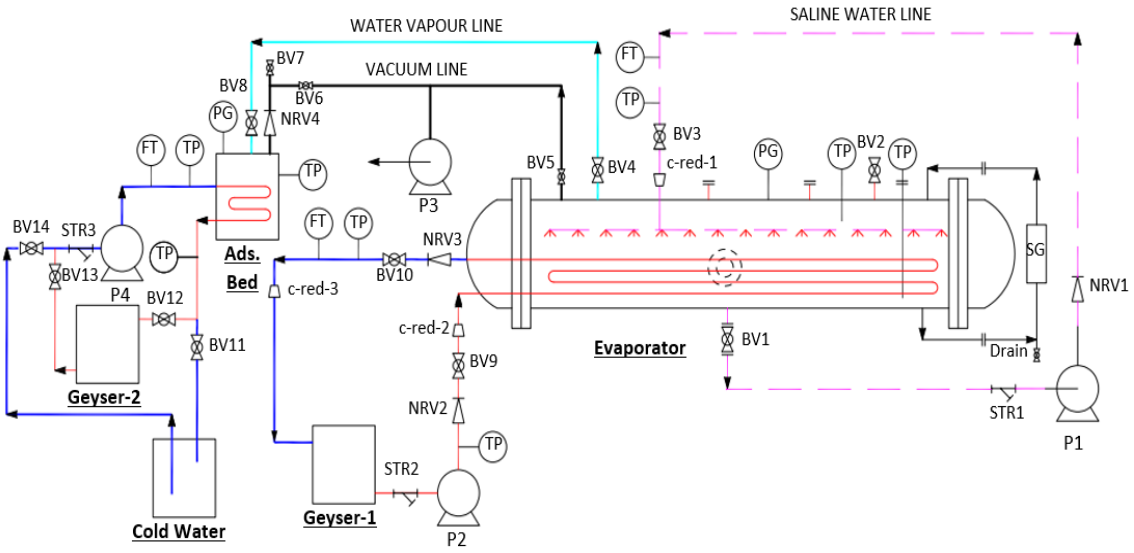

FIGURE 3.1: P&ID OF ADSORPTION DESALINATION SYSTEM

The P&ID (Figure 3.1) flows as per instructions presented below. The diagram shows the fluid flow and not the testing procedure details, but rather the system's fluid flow after the adsorbent sample was loaded in the 'Ads. Bed' (see Figure 3.1).

Step 1 – Start at the 'BV2' saline feed is manually injected into the evaporator. After the saline water is injected into the evaporator, a vacuum is created using a vacuum pump (P3) to the set desired pressure condition. 'BV5' is then closed.

Step 2 – The hot water from the electrical geyser is circulated through the evaporator coil using pump 'P2'.

Step 3 – When the evaporator's coil temperature stabilises, the magnetic centrifugal pump 'P1' is switched on, causing the saline water in the evaporator to recirculate from the 'BV1' of the evaporator to the sprinkler nozzles or top distributor pipes of the evaporator, which then cascades down over the coil or tube bundle of the evaporator. The saline water is boiled as it falls as a thin falling fluid film over the tube bundle. This saline water is circulated until on the 'SG' site level glass, the water level is significantly low, signalling a low water level inside the evaporator.

Step 4 – Cold water circulation through pump 'P4' is switched on for cold water to circulate through the adsorbent bed.

Step 5 – When sufficient water vapour is produced from boiling the falling film fluid at controlled pressure in the evaporator, 'BV4' and 'BV8' are opened, letting the desalinated water vapour into the adsorbent bed to trigger adsorption, using a pressure difference that is sustained by the vacuum pump.

Step 6 – When the adsorbate in the adsorbent bed is captured sufficiently for that set pressure condition, 'BV14' and 'BV11' are closed and 'BV13' and 'BV12' are

opened for hot water circulation to begin desorption of adsorbate off the packed adsorbent sample.

Step 7 – When sufficient heat transfer, relative to the geyser's water temperature, has transferred to the adsorbent bed, 'BV6' is opened, ensuring that 'BV5' remains closed. The water vapour is rejected with the aid of pressure difference and thermal build up in the adsorbent bed; this is a result of heated water pumped through 'P4' from 'Geyser 2'. This water vapour is released through 'P3'. The mass changes due to the accumulation of potable water vapour adsorbed by the adsorbent are logged on a digital scale that was constructed and subsequently presented in this chapter.

Step 8 – The end.

3.2 Falling film evaporator fabrication

The use of a falling film fluid on a horizontal tube bundle evaporator for the application of an adsorption desalination has previously been practiced by several researchers, as reviewed in Chapter 2. Alternatively, a vertical tube bundle can be used depending on the industry or the working fluid of the system; for example, in dairy product distillers this method is frequently utilised. Instead of a falling film evaporator, a flooded evaporator is yet another method that can be employed for fluid distillation processes. In this present study, a horizontal falling film fluid evaporator was used.

Ideally food grade conduits, such as stainless steel 316 and 304, were to be used to contain consumable products such as the potable water that will be produced in this study. However, to render the test rig financially feasible, it was recommended that the shell of the evaporator in this study be constructed using less expensive

materials that can be processed with the existing manufacturing processes available in the CPUT Mechanical Engineering Department. To lower the construction cost, recycled carbon steel 16-, 4- and 2-inch pipes were purchased from Brackenfell Steel to manufacture the shell of the evaporator unit on site. The constructed evaporator shell is presented in Figure 3.2.

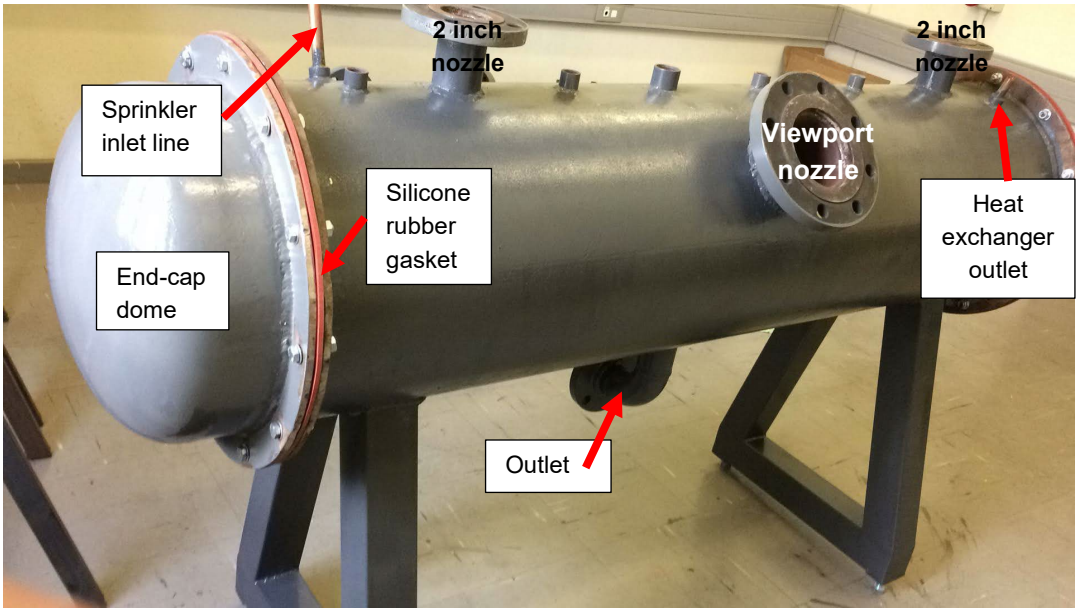

FIGURE 3.2: EVAPORATOR SHELL

Listed below are the items used in preparing and assembling the evaporator:

- Evaporator shell fabricated on site (16-inch pipe and 16-inch end cap)
- Evaporator heat exchanger fabricated on site
- Silicone rubber gaskets: 3mm thick
- Level site glass: ϕ10mm
- View port fabricated on site
- Y-type strainer: 15mm

- Non-return valve: 15mm & 22mm
- Ball valves: 15mm, 25mm
- Thermocouples, PT100
- Flow transmitter YF-S201: 15mm
- Complex pressure gauge: 15mm
- Concentric reducers: 22mm to 15mm
- Plug: 15mm

3.2.1 Development of tube bundle

The evaporator consists of two components: the heat exchanger, referred to as a horizontal tube bundle installed inside the shell of the falling film evaporator; and the shell. Due to limited processes and handling equipment available on site, plain Ø15mm copper tubes were used as the tube bundle, even though previous researchers have successfully experimented with enhanced tube bundles, as presented in the literature review. The development of the evaporator heat exchanger is presented in this sub-section.

The initial working space of the falling film evaporator was Ø409mm, restricted by the shell internal diameter of the 16-inch carbon steel pipe with a length of 1,7m, but the heat exchanger's effective length was 1,4m. The heat exchanger baffle, which was the frame structure that supported the copper pipes – the tube bundle that served the purpose of heat transfer (Figure 3.3) – is constructed of a carbon steel 10mm thick plate. Holes were drilled on site using a milling machine. Ten columns of Ø15mm holes were drilled at a centre-to-centre pitch of 30mm. The tube bundle holes were prepared in alignment with the top distributor pipe holes but with two sets or rows. Two of the baffle plates were prepared in this regard.

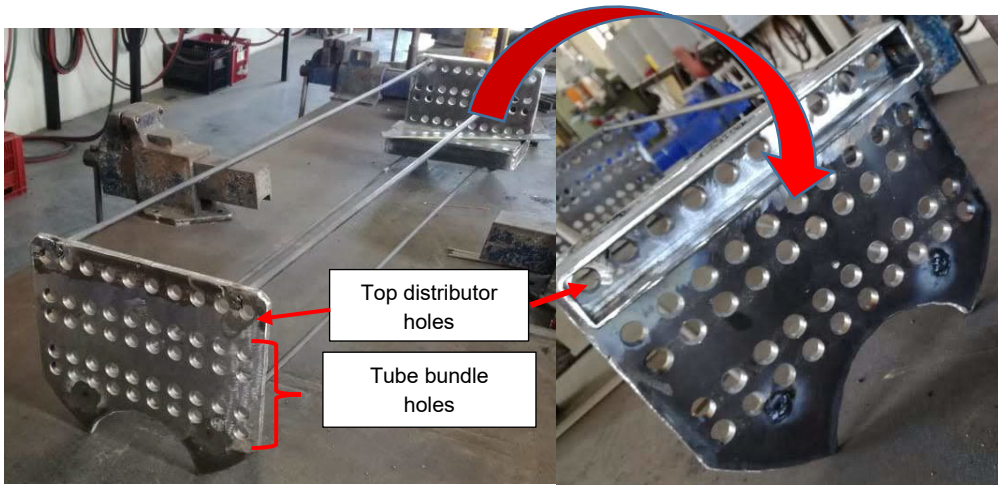

FIGURE 3.3: BAFFLE PLATE

The top fluid distributor pipe construction is critical in attaining good falling film fluid that would yield sufficient vapour or distillation throughput. There have been a number of studies dedicated to the design of the fluid distributor for the falling film evaporator [120], [121]. Mathematical modelling and experimental studies have been conducted by researchers to achieve an optimal fluid distributor [118], [119]. In this present study, the fluid distributor was experimentally investigated and developed. With observations it was noted that the distributor pipe of Ø15mm with Ø2.5mm (CNC drilled holes) at a centre-to-centre pitch of 8mm was optimal, taking into consideration the limits of the machines available on site (see Figure 3.4). The pre-test experiments were conducted to select the optimal configuration to manufacture the tube bundle. Pre-experimental study results leading to the selection of optimal pitch size were documented and published. [116]

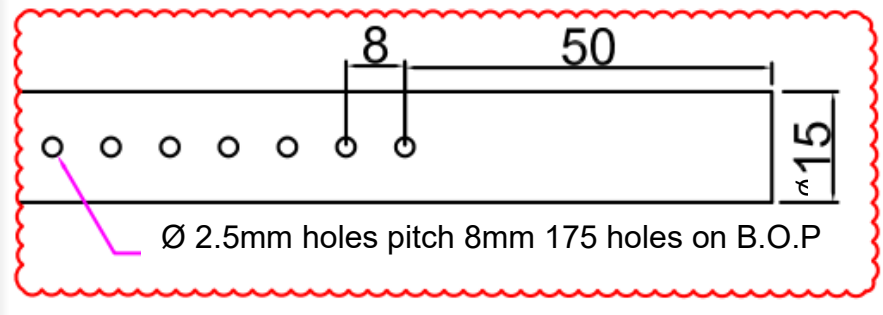

FIGURE 3.4: DISTRIBUTION PIPE PREPARATION

In the reviewed literature, the importance of having an optimal fluid film flow over the tube bundle was established. In this study, as a pre-experiment, different distributor pipe samples with different pitch holes were prepared to experimentally assess an optimal distributor that yields good fluid coverage over the tube bundle. From the aforementioned pre-experiment, as part of this study, the optimal geometric parameters were determined for the location of the top distributor and the pitch size of the holes [116]. A pitch of 8mm and Ø2.5mm holes were the optimal dimensions of the top distributor pipe located 45mm above the top pipe of the tube bundle centre-to-centre dimension (see Figure 3.4). The complete pictorial assembly of the tube bundle is presented in Figure 3.5. The illustration of the fluid cascading from the top distributor pipe down the tube bundle is shown in Figure 3.5 when test water was injected into the top distributor pipes. This was to assess if the fluid flow sufficiently covers the circumference of the horizontal pipes of the tube bundle.

FIGURE 3.5: EVAPORATOR HEAT EXCHANGER

After testing the flow coverage supplied by the top distributor, it was observed that the inlet has room for improvement, so further developments were made. Initially, the inlet was on the one side supplying a length of 1,4m x 10 of top pipes. Insufficient fluid coverage on the further end was observed. The top distributor's inlet was modified to optimise the fluid distribution amongst the top distributor pipes. Even though the alteration would not impact the total flowrate into the top distributor, the alteration improved the distribution of the fluid coverage over the tube bundle's length by having multi-injection points injecting into the top bundle at various locations.

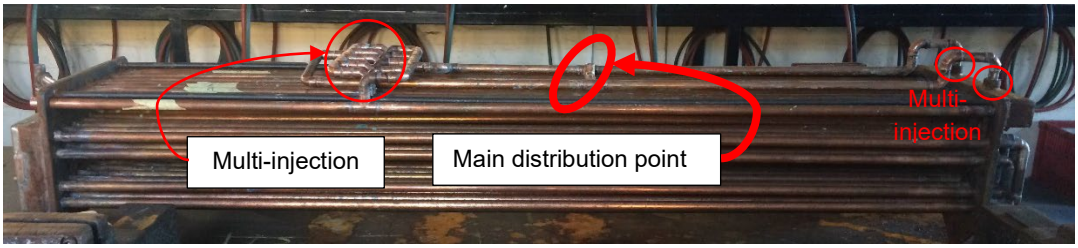

FIGURE 3.6: MODIFIED HEAT EXCHANGER

Therefore, instead of having a single inlet point (Figure 3.5) to the top distributor pipes, multi-injection points were created for even fluid distribution coverage over the tube bundle (Figure 3.6).

The evaporator's heat exchanger (tube bundle) was later tested for leakages by charging an air supply line at the inlet and connecting a temporal positive pressure gauge at the outlet. The leak test was done only once before installing the tube bundle into the shell of the evaporator. The ball valve 'BV' was opened and the air was injected into the tube bundle until the pressure gauge reached 6kPa; then the ball valve was closed and air leakages were assessed by listening to determine if air was being released from the tube bundle. Also, the pressure gauge was observed after closing the ball valve to determine if there was a pressure drop due to air leakages. The air leakage setup for the tube bundle is shown in Figure 3. 7.

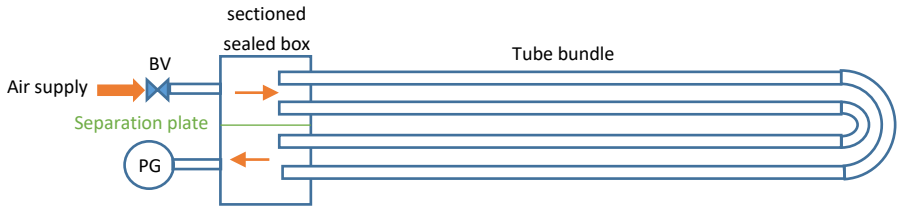

FIGURE 3.7: TUBE BUNDLE LEAKAGE TEST

3.3 Adsorbent bed fabrication

One adsorbent chamber was constructed out of a degassing chamber. The degassing chamber constructed from metal body was modified for the purpose of housing the adsorbent bed and the adsorbent coil, which served as the heat exchanger within this chamber to bring about temperature difference. The initial

state of the degassing chamber consisted of two components: a 12-litre chamber and a 30mm thick clear acrylic as a top sealer of the chamber. On the acrylic topping, two holes were drilled using a bench driller for the inlet and outlet line of the adsorbent coil. Additional 12mm holes were drilled for the purpose of connecting an insert for the vacuum line, the evaporator connection line to transport the water vapour (adsorbate), and small 6mm holes for the cables of the temperature probe of the adsorbent container and cable holes for the loadcell and its clamping fix point. The chamber was sealed airtight after inserting the components by a steel metal putty material sealer.

3.3.1 Development of adsorbent heat exchanger

The adsorbent heating and cooling coil was constructed using an Ø15mm and Ø22mm copper pipe. Along this coil, a copper strip of 0.75mm thick was clamped to transfer the temperature change from the body of the heat exchanger pie to the adsorbent bed. The copper strip was fixed onto the coil and hanging freely into the packed adsorbent material in the copper container that was seated onto the plate form of the loadcell fixed at the bottom of the adsorbent chamber. The final details of the adsorbent bed are shown in section 4.3.2 in Figures 4.8 and 4.9.

3.4 Solar water heating unit for desorption activation

An evacuated tube collector (ETC) unit was used to heat the water that was used to trigger desorption in the adsorbent bed. The hot water from the ETC unit was stored in the 50-litre geyser tank. Figure 3.8 shows the directional flow of the inlet and outlet

of the ETC unit's manifold, where the actual heat exchange from the harvested solar energy ultimately occurs. The complete solar unit installation of the ETC unit, illustrated in Figures 3.8 and 3.9, was installed at the roof of the CPUT Mechanical Engineering Department, with the geyser and circulation pump situated indoors at the laboratory. A Ø15mm pex-aluminium-pex composite pipe, and respective fitting, served as connection lines between the geyser, the pump and ETC manifold unit. A frame supporting the ETC manifold was constructed using galvanised steel structures that were prepared on site. The frame elevated the manifold to a height of 1,36m perpendicular to the ground. While the glass tubes fix to the manifold, the hypotenuse side had a length of 2m.

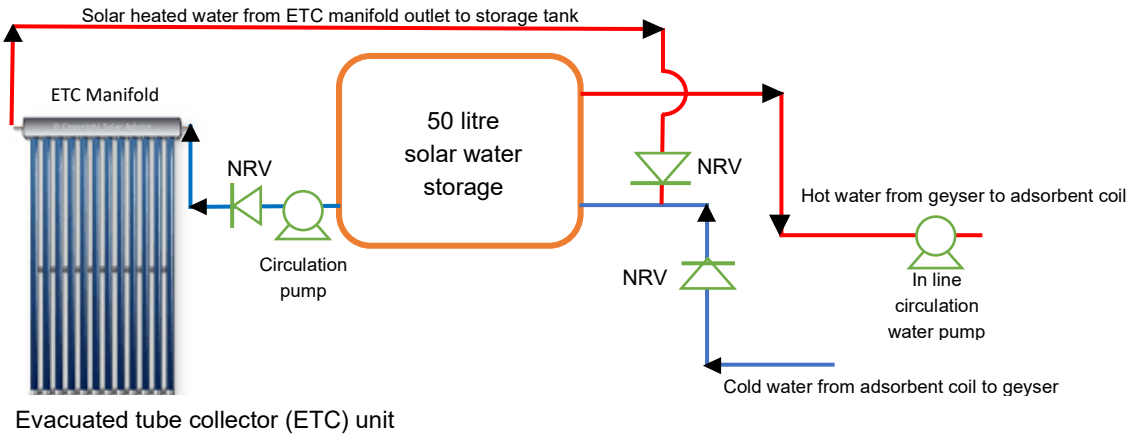

FIGURE 3.8: ETC UNIT

FIGURE 3.9: INSTALLED ETC UNIT

The pipe network illustrated (Figure 3.8) demonstrates the pipe and instrumentation that were used on the pipe line to give a general overview of the fluid flow of the solar sub-system. The pipe and equipment size used in this section of the test rig were kept constant at 15mm diameter pipe throughout.

3.5 Summary

Processes and equipment used to construct the model are presented in Appendix B. The working fluid – potable water vapour in this study – was transported via a 16mm nylon pipe line amongst the evaporator, adsorbent chamber and vacuum pump of the test rig. However, it was anticipated that working fluid would be prone to pre-condensation before reaching its destination. To prevent this from occurring, insulation of all components including the inter-connection pipe lines was introduced to the system, using the thermal foam and insulation blanks to cover the pipes, evaporator and adsorbent chamber. This was done following the construction and

assembly of the system. Continuous examination for leakages in the system (in both construction and data acquisition phases) was undertaken. After assembling the system, all data acquisition devices were connected to the computer for data capturing. In the next chapter, the data acquisition setups are presented in detail.

CHAPTER 4: EXPERIMENTAL SETUP AND METHODOLOGY

In this chapter, the experimental and data acquisition setup of the test rig is presented. The experimental procedure that was followed to test the studied adsorption desalination test rig is also presented. The testing procedure was re-iterated at varied experimental parameters and when modifications were made on the system. After presenting the experimental setup and procedure in this chapter, the discussion of experimental results will be presented in Chapter 5.

4.1 Data acquisition setup

The data acquisition setup of the test rig is presented in the following manner. Firstly, the falling film evaporator data capturing points are presented. Secondly, the electrically heated hot water geyser for the evaporator's heat exchanger setup is presented. Thirdly, the adsorbent bed data acquisition setup is presented. Finally, the experimental setup of the solar harvesting unit for the purpose of heating water to trigger the desorption cycle in the adsorption bed is presented in this sub-section.

4.1.1 Falling film evaporator experimental setup

A falling film evaporator has a dual process with the purpose of boiling saline water to produce potable water vapour. The dual fluid flow process encompasses two closed loop circulations simultaneously taking place within the evaporator. The primary hot water circulation circulates through the heat exchanger 'tube bundle' and the secondary circulation is the flow of saline water (initially cold) sprinkled onto

the external side of the heat exchanger within the evaporator using a magnetic centrifugal pump, since the evaporator's experimental environment is under controlled vacuum pressure conditions.

Since the evaporator was for experimental purposes, exploring varied controlled parameters such as the pressure and temperature for both primary and secondary circulation loops were tested. The evaporator of the studied test rig was set to be tested at different pressures, at varying vacuum pressures. A vacuum pump and a manual ball valve served to draw a vacuum in the evaporator. The varied test conditions were pronounced as 'Set 1' to 'Set 3', later discussed in sub-section 4.3. A pressure gauge (-100 to 100kPa) was used to monitor the pressure inside the evaporator. For the primary cycle, a PT100 thermocouple was connected at the inlet and outlet , TT1 and TT2 respectively, as per Figure 4.1. Three temperature sensors were positioned at different levels within the evaporator, as follows: TT5: sensor placed 20mm from the ID of the BOP of the evaporator; TT6: sensor was placed 150mm from ID of the TOP of the evaporator; and TT7: sensor was placed 20mm from ID of the TOP of the evaporator. The thermocouples were connected to the Pico Technology PT104 data logger that was connected to the computer for the temperature data to be captured. To monitor the water level inside the evaporator, a water level site glass was used. This component also had a drain cock at its lowest end as one of the evaporator drainage points apart from 'BV3' (see Figure 4.1). A schematics of the components on the evaporator is shown in Figure 4.1.

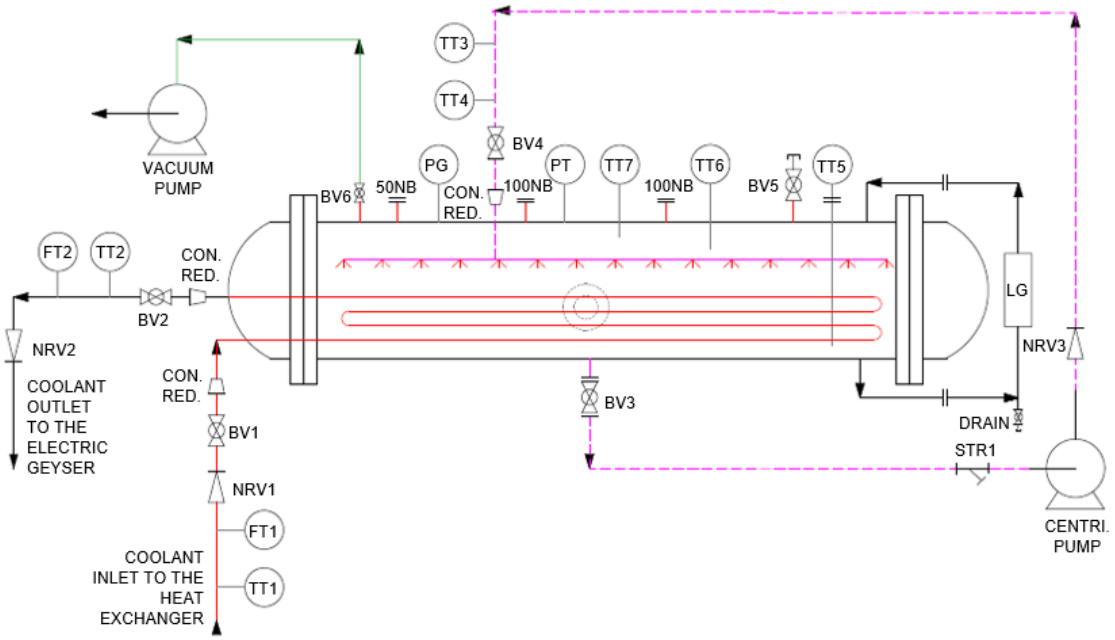

FIGURE 4.1: EVAPORATOR EXPERIMENTAL SETUP

The evaporator was initially tested separately from the entire system. This preliminary experiment was performed to ensure that there are no leakages in the tube bundle. This was successfully done by installing a flow transmitter at the inlet and outlet of the heat exchanger coil. When the primary cycle was switched on, the mass flow rate at the inlet had to remain constant; leakages along the tube bundle implied that there were leakages Also, the mass flow transmitter was installed to monitor the flow-rate through the tube bundle when boiling of saline water was performed in the evaporator. All data were acquired electronically using a data logging system, and the pressure was manually logged for every pressure condition set. A view port glass was used to observe inside the evaporator to determine if any distillate was being produced.

4.1.2 Geyser for evaporator heat exchanger experimental setup

The electrically powered 50 litre geyser supplied hot water to the heat exchanger of the evaporator. The installed geyser has the capacity of adjusting and setting the desired temperature. This allows the evaporator to be tested at various temperature ranges from 35°C to 72°C. Water outlet from the geyser (Figure 4.2) feeds the primary loop cycle of the evaporator. The variable transformer was another point of voltage regulation or control, whose effect was manifested in the change in temperature of the primary water loop of the evaporator. Also, the built-in temperature regulator of the electric geyser adjusted the water temperature for the tube bundle of the evaporator.

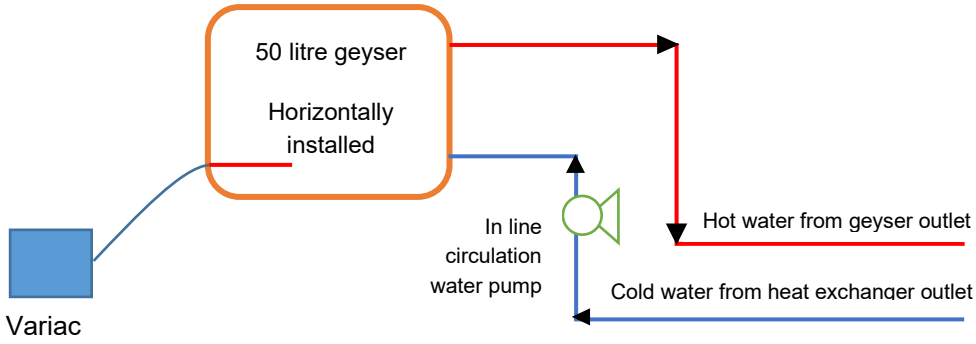

FIGURE 4.2: HOT WATER GEYSER FOR EVAPORATOR'S HEAT EXCHANGER

4.1.3 Adsorbent bed experimental setup

In the adsorbent chamber, the cooling coil has two inlet points – one to cater for the hot water circulation and the second to cater for cold water circulation to trigger desorption and adsorption. To monitor the temperature of the coolant water circulating in the adsorbent coil, two temperature sensors at the inlet and outlet

points were installed. To monitor the flow-rate, a flow-rate transmitter was installed at the inlet of the coil. On the adsorbent chamber, an analogue pressure gauge was installed (-100 to 100 kPa). A temperature probe was inserted and sealed through the body of the top acrylic lid of the chamber to track the temperature change in the packed adsorbent copper container inside the chamber (Figure 4.3). A vacuum ranged pressure gauge monitored the pressure difference within the chamber. All the monitoring devices were connected to the data logger for data acquisition. The adsorbent chamber had a vapour line from the evaporator for adsorption to take place. On the adsorbent chamber provision was made for a vacuum outlet which was used interchangeably for releasing the effective working fluid (the potable water vapour).

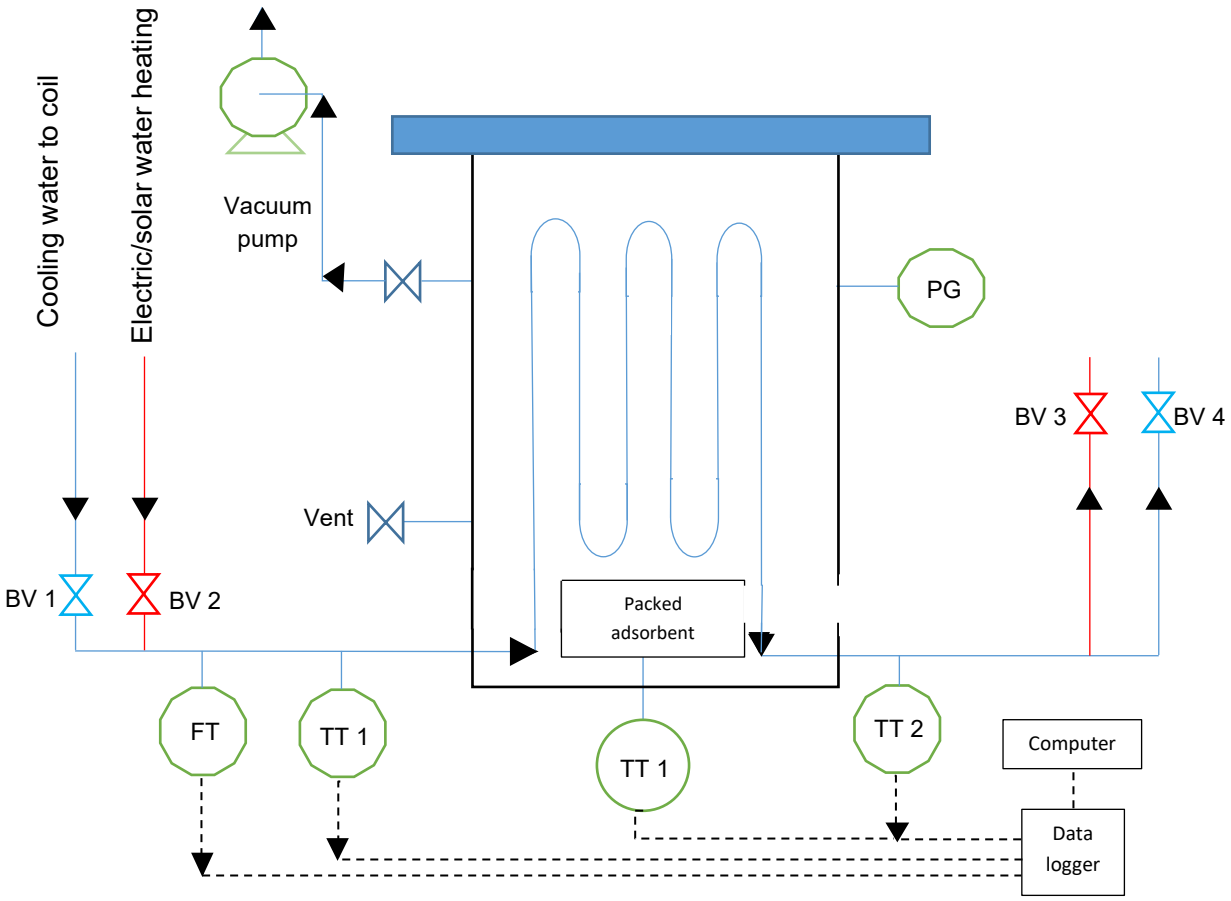

FIGURE 4.3: ADSORBENT CHAMBER TEST SETUP

4.1.4 Solar water heating unit for desorption cycle setup

The electric water geyser was initially used and later on switched to renewable energy powered geyser. During the use of solar energy to drive the desorption cycle the system still consisted a portion of electrical driven components. A solar water heating unit was used for the adsorbent bed coil to activate the exothermic-based desorption cycle. The solar water heating unit was catered for in an evacuated tube collector (ETC) unit, on Figure 4.4. The unit was initially installed with 10 tubes and gradually increased to its maximum. The maximum capacity of the tubes that the header manifold could withstand was 20 tubes. Solar irradiation was the key factor that contributed to the output temperature of the solar water heating unit. Below is the illustration of the initial installation of the ETC. The tubes were added progressively throughout the performance of experiments to observe the impact of a single tube.

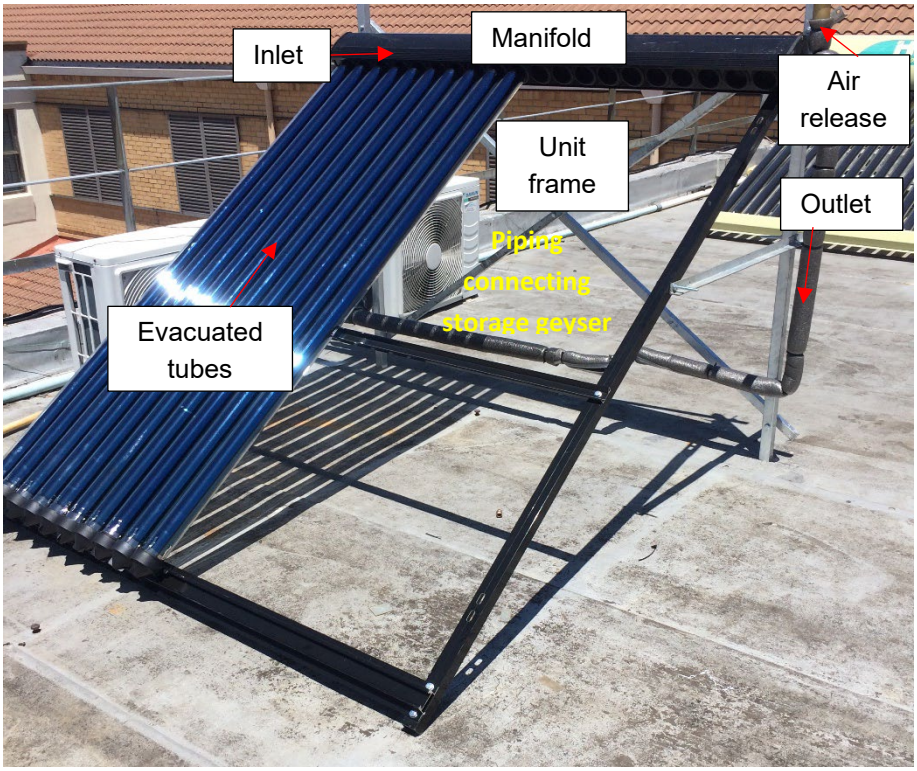

FIGURE 4.4: SOLAR WATER HEATING UNIT INSTALLATION

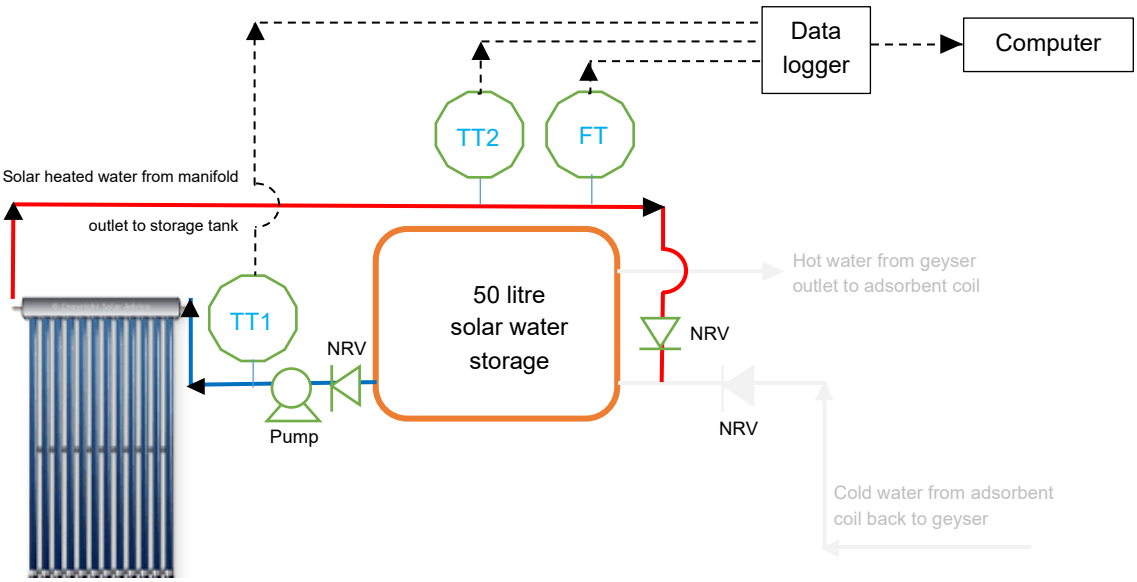

Evacuated tube collector (ETC) unit installed at the roof top

FIGURE 4.5: SOLAR WATER HEATING TEMPERATURE DATA ACQUISITION SETUP

The temperature at the outlet and the inlet of the manifold of the ETC unit was logged using the PT100 temperature probes. Data were captured throughout the day to keep track of the temperature difference in the geyser that resulted from the solar intensity harvested through the evacuated tubes installed on the roof of the CPUT Mechanical Engineering Department. The flow-rate of the water circulating through the manifold and storage geyser remained constant and was monitored using the flow transmitter indicated (FT in Figure 4.5).

Parallel to capturing the data of the solar heated water temperature, the weather station nearby on the same roof captured the solar intensity, humidity and wind speed. The solar intensity was the useful data for this study, which will later be discussed in the results section. The solar heated geyser water (by solar intensity) was for the triggering of the desorption cycle, as presented in Chapter 5.

4.2 Modification of system

Due to high thermal losses encountered within the test rig that caused premature condensation, vapour lines were modified. Initially, the vapour conduits were 100NB carbon steel pipe. These were changed to 16mm diameter nylon pipes; hence, the 100NB blanked off (on Figure 4.1) outlets on the body of the constructed evaporator. The pipe lines transporting water vapour from the evaporator to the adsorbent chamber were eventually changed due to pre-condensation occurring in the metal conduits. All experiments were performed on the newly modified system with different vapour conduits. Significant vapour movement was observed after this modification. To monitor the vapour captured in the adsorbent bed, a digital scale was initially placed beneath the whole adsorbent bed unit, but this did not give significant results. The scale was then placed inside the adsorbent bed (see Figure

4.6) and the sample size of the adsorbent material was reduced, yielding significant results.

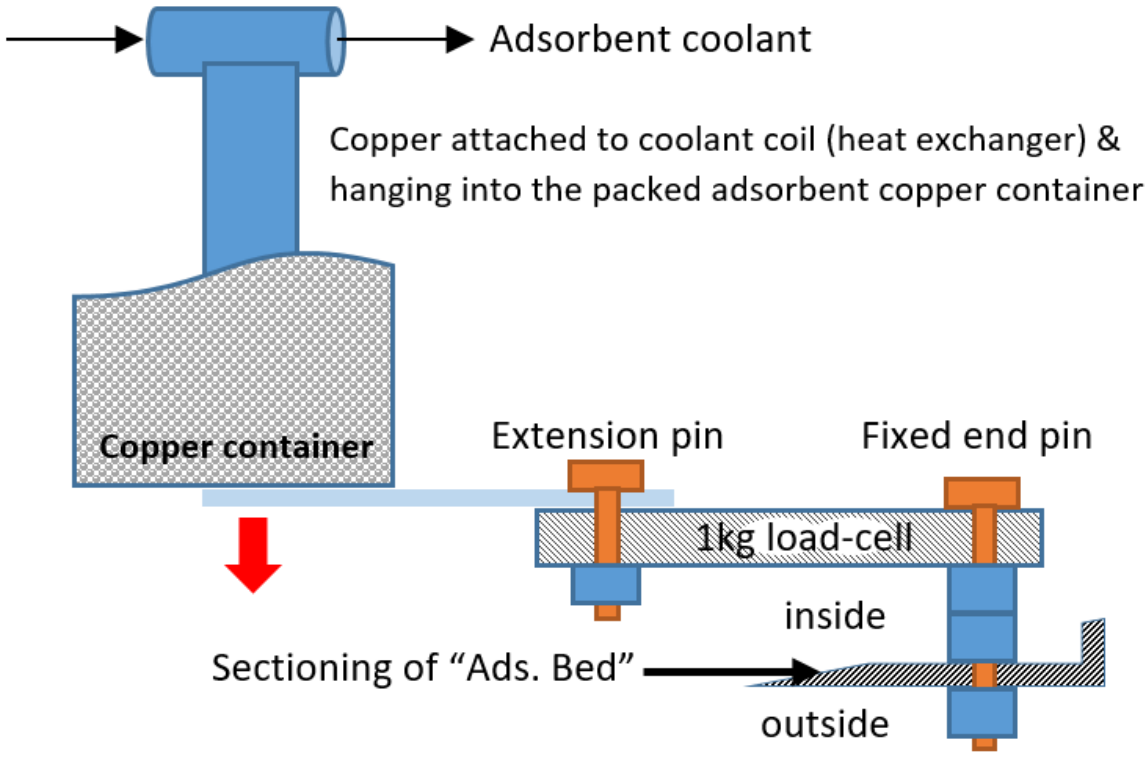

FIGURE 4.6: INSIDE ADSORBENT BED

4.3 Experimental procedure

After construction and data acquisition equipment was set up, the experiments were conducted based on the procedure presented in this section. It should be noted that the renewable energy-based tests were designed to be performed during the day because the evacuated tube's performance was dependent on solar intensity to heat the water stored in the 50-litre geyser. The vapour lines were nylon conduits throughout the system for the purpose of transporting water vapour and to avoid

pre-condensation. Therefore, the experimental procedure presented was on the basis of the final design and modified setup.

Before any operation, the solar water heating kick starts at sunrise so that the solar heated water can be used later for the desorption cycle. During the day, the water temperature increased due to the accumulation of heat from the day's gradual increase of solar intensity.

The testing procedure for a purely electrically driven setup was organised in the following manner. The hot water providing temperature change in the evaporator was from the 50-litre electric geyser that had varying temperatures ranging from 35^{o}C to 72^{o}C. After setting the desired geyser temperature, the pump circulating the hot water from the geyser to the heat exchange was switched on until the temperature in this primary cycle had a temperature difference of less than 5^{o}C between the inlet and outlet. The saline feed water was injected into the evaporator. The desired vacuum pressure (below atmospheric pressure) was set using a vacuum pump. All evaporator valves were sealed. The secondary cycle was switched on, where the saline water circulation pump went through for saline water to cascade from the top distributor pipes downwards over the tube bundle that has the geyser's hot water circulation inside. This dual process ran until sufficient water vapour was produced in the evaporator and observed through the 100NB viewport glass of the evaporator. The vacuum pump maintained the pressure in the evaporator at the desired pressure value.

There was one adsorbent bed of silica-gel and zeolite. Each adsorbent was tested at a time, and a mixture was also tested to assess its performance. Then the produced water vapour was moved from the evaporator into the adsorbent bed. The pressure in the adsorbent was lowered below atmospheric pressure that existed in

the evaporator. Therefore, the transportation of the water vapour from the evaporator to the adsorbent bed was via the pressure swing. The pressure ratio between the evaporator and the adsorbent gradually stabilised as the water vapour moved from ‘higher pressure’ (the evaporator) to ‘lower pressure’ (the adsorbent). While the water vapour was flooding the adsorbent bed, the vacuum pump was constantly running to sustain a controlled testing condition. While the adsorbent material was accumulating water vapour on its porous surface with cold room temperature ($<30^{o}C$), water circulation was flowing through the coil embedded in the adsorbent material to assist in triggering of the adsorption cycle.

For desorption to take place using the solar heated water as a result of the peak solar irradiation of each day, the highest daily water temperature was used to trigger desorption of the tested adsorbent sample. On days where the peak water temperature had a temperature difference of $\pm4^{o}C$ as compared to other days, no further adsorption and desorption tests were performed. For those days, only observations of solar water heating were presented. Moreover, the adsorption and desorption output of those days were deemed as similar to those of the previous days with similar peak water temperatures within $\pm3^{o}C$. The recovered adsorbate was rejected out of the adsorbent chamber into the atmosphere. The two adsorbents were tested at varied conditions individually, as a combination at varied conditions and as an enhanced combination using copper shavings. The experiments were to assess how much water vapour was produced at the desorption phase when solar irradiation varied each day for 10 days to heat the water that was used in the desorption phase.

In the subsequent sub-sections, more detailed experimental test performance protocols are presented. It should be noted that some tests were reiterated but with minor adjustment in the experimental setups and adsorbent material test samples

to access the enhanced performance of the test rig. The results of the experimental tests are discussed in Chapter 5.

4.3.1 Pre-Test: Testing of the evaporator to produce water vapour

Initially, the tests on the falling film evaporator were conducted to demonstrate the production of water vapour using the setup (on Figure 4.7).The subsequent procedure followed from the feed fluid to the production phase of water vapour. First, saline water was injected through ‘BV2’ and the valve was closed. ‘Geyser-1’ was switched on and the desired temperature was set on ‘Geyser-1’ on the built-in thermostat. ‘BV9’ and ‘BV10’ were opened, pump ‘P2’ was switched on and the primary cycle was live. This brought about the temperature difference in the tube bundle inside of the evaporator. ‘BV1’ and ‘BV3’ were opened, pump ‘P1’ was switched on and the secondary cycle was live. The outlet of secondary cycle was inside the evaporator that had ‘nozzles’ or small holes that sprinkled the saline water over the heated primary cycle tube bundle. As the saline water was cascading over the now heated tube bundle, heat from the tube bundle dissipated towards the cascading tube bundle all inside the shell of the evaporator. While the primary and secondary cycles were circulating simultaneously, ‘BV5’ was opened and the vacuum pump ‘P3’ was switched on to lower the pressure below atmospheric pressure, varying to suit the desired experimental plan as tests were progressively performed. Distillate was produced and condensate was observed on the view port glass located at the centre of the evaporator’s body.

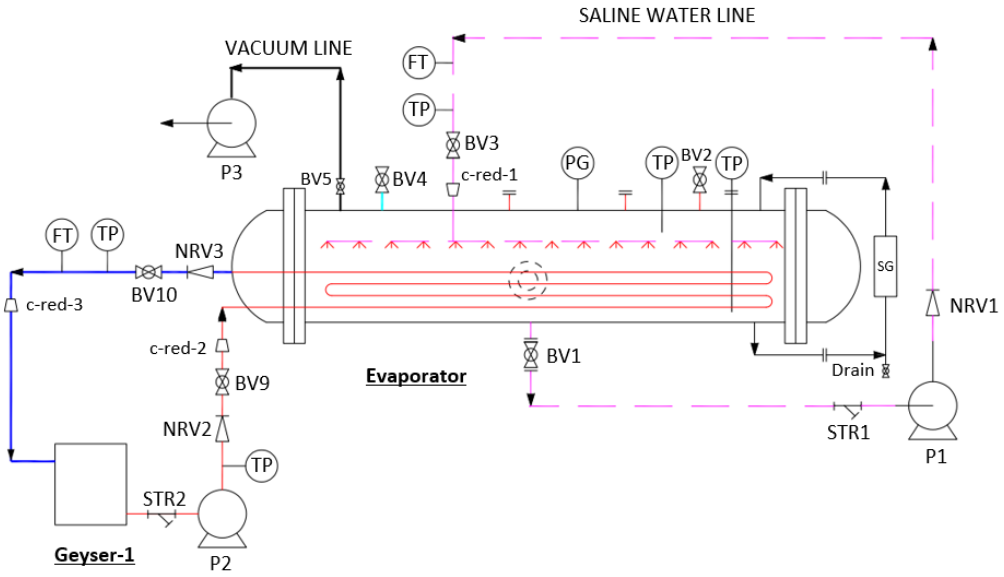

FIGURE 4.7: FALLING FILM EVAPORATOR

After the process of producing water vapour (distillate) was established, capturing this water vapour using the adsorbent material was undertaken. This was done by conducting a series of experimental tests as presented in the subsequent sections.

4.3.2 Electrical Tests: Testing of the adsorbent bed using electrical energy for desorption

Additional to the falling film evaporator pre-test, the adsorbent bed was connected, as per Figure 4.8. This experimental setup was the final setup that was later on enhanced for performance. All tested adsorbent materials samples were alternated within this setup, repeatedly, performing the same procedure at varying parameters of the vacuum pressure, temperature change in the primary cycle and the coolant water circuit flowing through the adsorbent bed (Figure 4.9). Other test conditions were explored in the experiments to assess the performance of the system. Initially,

the ‘Geyser-2’ was electrified using electrical energy. Electrical energy was used to power the geyser for Test 2 to Test 6. Only at Test 7 was renewable energy used as a source of solar energy to heat the water for the desorption cycle to be triggered for ‘Geyser-2’. ‘Geyser-1’ was constantly electrically powered throughout the experiments. Figure 4.6 shows the detailed schematics of the setup inside the adsorbent bed.

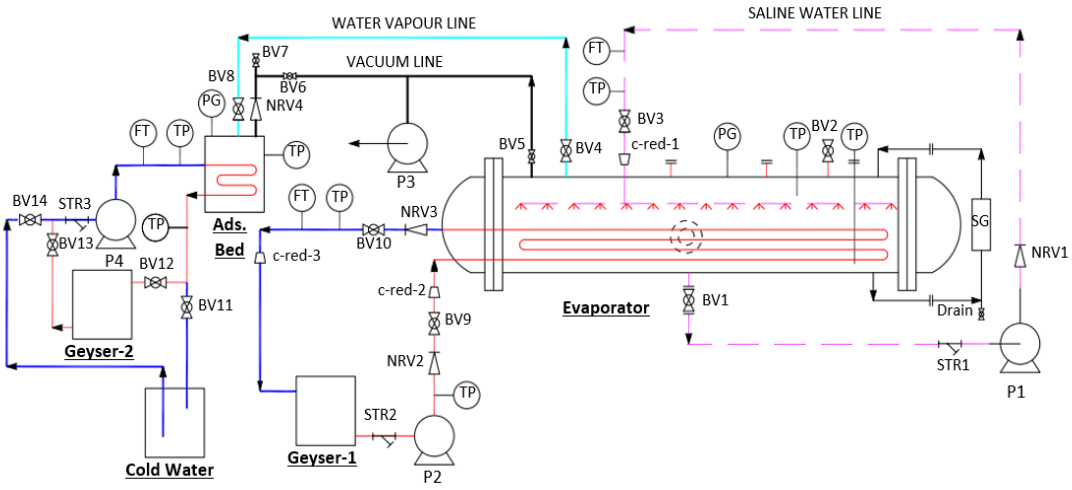

FIGURE 4.8: ELECTRICALLY DRIVEN TEST RIG

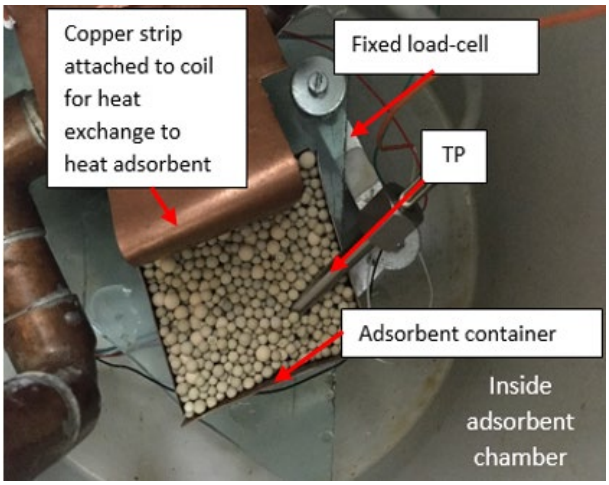

FIGURE 4.9: INSIDE THE ADSORBENT BED TOP VIEW

At the adsorbent bed, a copper strip was attached to the coolant coil. The copper strip transferred the thermal heat to the packed adsorbent container position on top of the load cell that measured the mass difference of the adsorbent inside the container as the water vapour was adsorbed and desorbed. The ‘TP’ in Figure 4.9 measured the temperature difference within the adsorbent container. The load cell was connected to the HX711 amplifier and then to the Arduino Uno which was connected to the computer that digitally logged the mass changes of the load cell every second (Figure 4.6 and Figure 4.9).

4.3.3 Test 1, 3 & 5: Testing of silica gel

Silica gel adsorbent of 200 grams of was packed into the copper container (see Figure 4.9). After packing the adsorbent, the water vapour was flooded into the adsorbent bed via pressure difference. Detailed parameters are tabulated and presented in Chapter 5 as discussion of experimental results.

4.3.4 Test 2, 4 & 6: Testing of zeolite

Likewise, for zeolite adsorbent material, a sample of 200 grams was experimented on. The same procedure was repeated to that of silica gel. It should be noted that even though the sample was at this point zeolite, this adsorbent material was repeatedly tested for various parameters to comparatively assess its performance with the silica gel when the pressure and temperature varied.

4.3.5 Test 7: Testing of the combination of silica gel and zeolite

In the Test 7 series of experiments, 100 grams of silica gel and 100 grams of zeolite were mixed and shaken thoroughly to ensure even mixture. The combination was then placed on the plate-form of the scale to experiment on this hybrid adsorbent sample.

4.3.6 Test 8: Testing of enhanced adsorbent bed using copper shavings

The best performing test outputs observed from previous test conditions are replicated. The difference at this point was the addition of 50 grams of copper shavings mixed with hybrid adsorbent samples. The effect of enhancing the adsorbent samples is observed in both the adsorption and desorption phases. The effect at the desorption phase was the most critical as it is the most effective and useful production process of the test rig.

4.3.7 Test 9: Solar water heated for desorption using evacuated tubes

Instead of using electrical energy to power the 50-litre geyser to trigger desorption in the adsorbent bed, a solar water heating mode was switched on, by switching off the electrical geyser 1 and using the ETC Unit to heat water (see Figure 4.7).

The best performing samples and testing conditions are repeated with the desorption coolant using solar heated water. These were the final testing conditions for this study. This test was performed over 10 days during the day to make use of solar energy to heat the water for triggering desorption. It should be noted that solar

water heating was solely for the adsorbent bed use only. Other sections of the study utilised electrical energy.

4.4 Summary of experimental performances

Below is a summative overview of the experimental procedure adhered to in performing the experiments, to experimentally test the constructed test rig. Test 1 to Test 8 were purely electrically driven. The series tests, of Test 9 were solar energy-based. The solar heated water of Test 9 were for the purpose to trigger desorption of the investigated adsorbent within the adsorption desalination test rig. An error analysis on the special scale built and used is found On the Appendix C

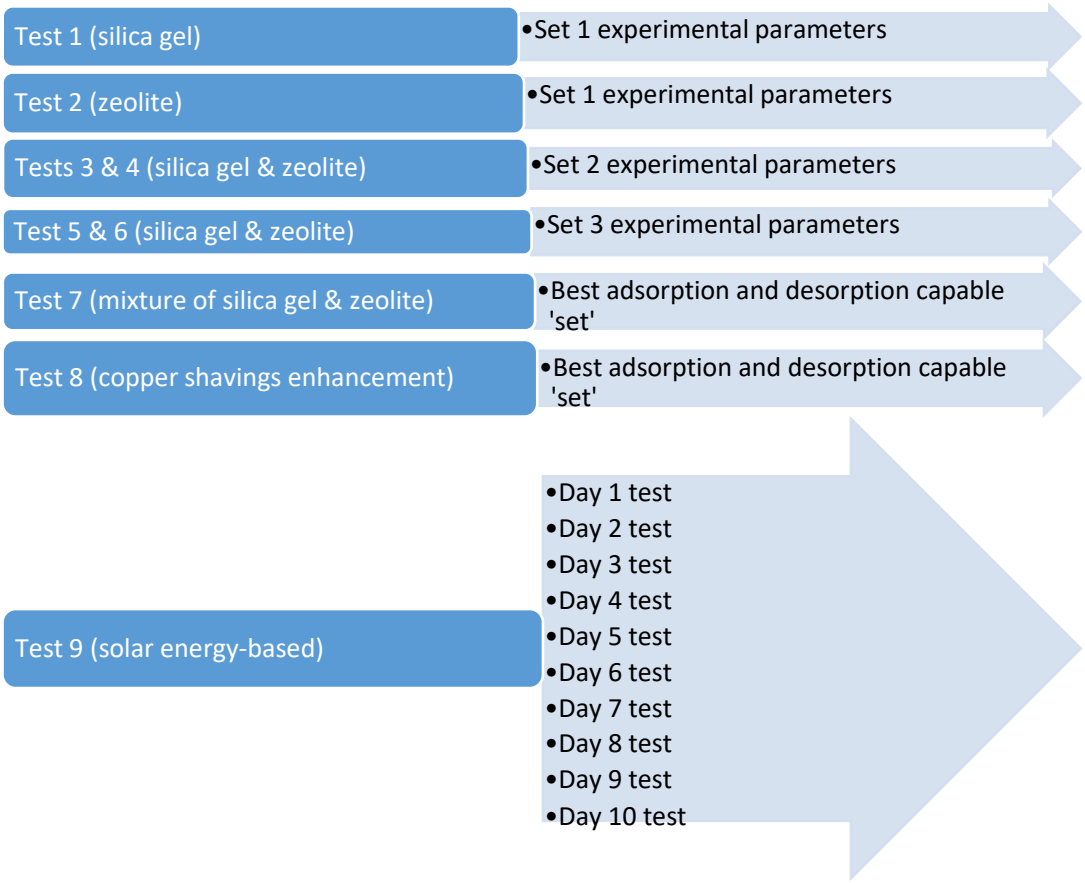

CHAPTER 5: RESULTS AND DISCUSSION

Some parts of this chapter have been published in journal articles:

Z. Mdletshe, V. Msomi, O. Nemraoui. (2022). Experimental investigation of the adsorbents using pressure and thermal swing for adsorption and desorption. *Results in Engineering*, 15 (100513).

Z. Mdletshe, V. Msomi, O. Nemraoui. (2023). Solar water heating based on Bellville weather conditions in winter. *Renewables: Wind, Water and Solar,* 10 (2).

The experimental investigation results are discussed in this chapter. It should be noted that water vapour and its hydrophilic and hydrophobic affinity to the subject adsorbent materials were the critical and valuable constituents of this study. Therefore, the performance of the entire system was based on experimentally assessing the capability of adsorption and desorption of locally supplied silica gel and zeolite at various environmental conditions.

5.1 Experimental results from the studied test rig

In this research study, 18 experimental test were conducted in total to assess the developed and constructed test rig. Initial tests were performed and progressively the test conditions were improved so that the desorption phase, which is the last stage at the adsorbent bed, yielded the best results through better test conditions and the enhancement of the adsorbent bed per objectives presented in Chapter 1.

A pre-experimental test was conducted to assess the evaporator's ability to produce water vapour, which was the distillate of the test rig. Results from the first test of the evaporator initially failed to produce any water vapour when the evaporator was operating at atmospheric pressure. Therefore, reducing the pressure by 0.1kPa below atmospheric pressure produced insignificant distillate, which was observed visibly on the viewport glass of the evaporator when desalination was conducted at this controlled pressure. The temperature of the inlet to the tube bundle was maintained at 40^{o}C for this test. The pressure was then lowered further to -10kPa and significant distillate was observed as the pressure was progressively lowered.

5.1.1 Test 1 Results: Experimental results of silica gel

The experimental test conditions of Test 1 adsorption, on Figure 5.1 (a); and Test 1 desorption, on Figure 5.1 (b) were performed under the tabulated parameters (Table 2). For Test 1, it was observed that under these conditions the adsorption phase of the silica gel sample took less than 1000 seconds to reach saturation for the set pressure sustained by the vacuum pump. After the silica gel adsorbent could no longer adsorb the water vapour, a hot water circulation in the adsorbent bed was switched on for desorption to take place – Figure 5.1. However, desorption did not immediately take place: there was a time lag for the heat to transfer from the coolant to the copper strip and finally to the packed adsorbent, which triggered the desorption or rejection of the previously captured water vapour. Significant desorption or rejection of water vapour off the adsorbent was witnessed after the hot water at 95^{O}C (geyser temperature) was circulating through the adsorbent coil. This was evident on Test 1 temperature profile (Figure 5.2).

TABLE 2: SET 1 – PARAMETERS FOR TEST 1 & 2

Parameter	Value
$P_{evaporator}$	-10 kPa
$P_{adsorbent}$	-60 kPa
$T_{average\ evaporator}$	52°C
$T_{set\ geyser\ desorption}$	95°C
$T_{in\ adsorbent}$	30°C

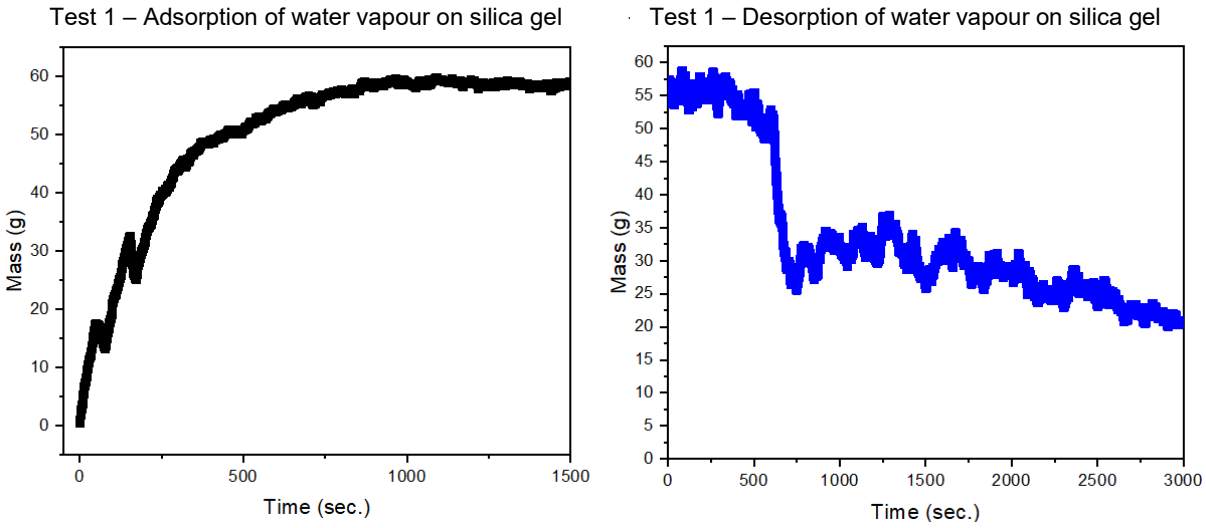

(A) (B)

FIGURE 5.1: (A) ADSORPTION; (B) DESORPTION FOR SILICA GEL TEST

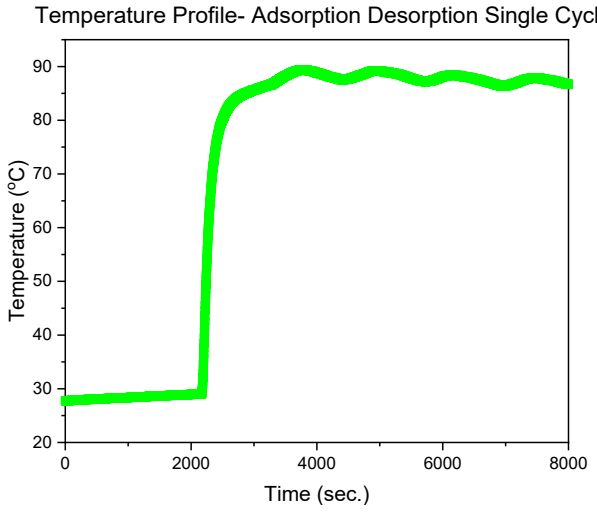

FIGURE 5.2: TEMPERATURE PROFILE OF SILICA GEL TEST

5.1.2 Test 2 Results: Experimental results of zeolite

It should be noted that the testing parameters for Test 2 for adsorption on Figure 5.3 (a), were the same as for Test 2 for desorption on Figure 5.3 (b) on Table 2. Zeolite was the adsorbent observed in the test presented in this sub-section. The amount of adsorbate adsorbed onto zeolite was slightly lower than that of silica gel when both experimental test conditions were the same. However, desorption performance of zeolite in this test condition was higher than that of silica gel. It was observed that of 58g of water vapour that was captured, only 48g was desorbed when the hot water circulation was circulating through the adsorbent coil. Unlike silica gel, this demonstrated that in these testing conditions it was capable of desorbing an amount of 39g of water vapour when all test conditions were the same for both adsorbent materials (Figure 5.3). A similar temperature behaviour for a single cycle, like that in Figure 5.4, was witnessed throughout the performances of the experiments: the temperature increased when the adsorbent hot water from the geyser was opened. However, there were thermal losses along the line and within the adsorbent chamber, which was later improved as discussed in section 5.2.

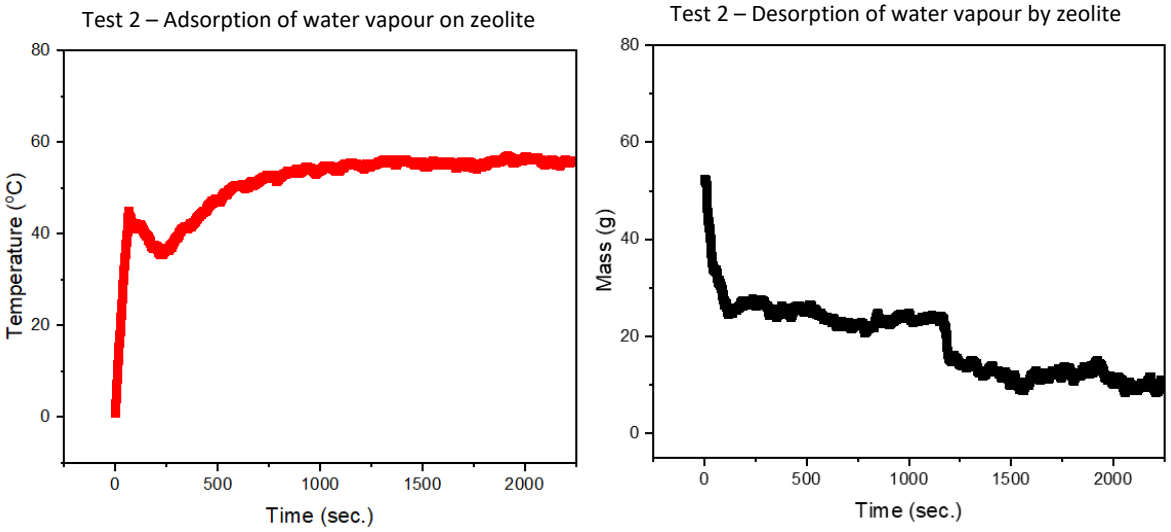

(A) (B)

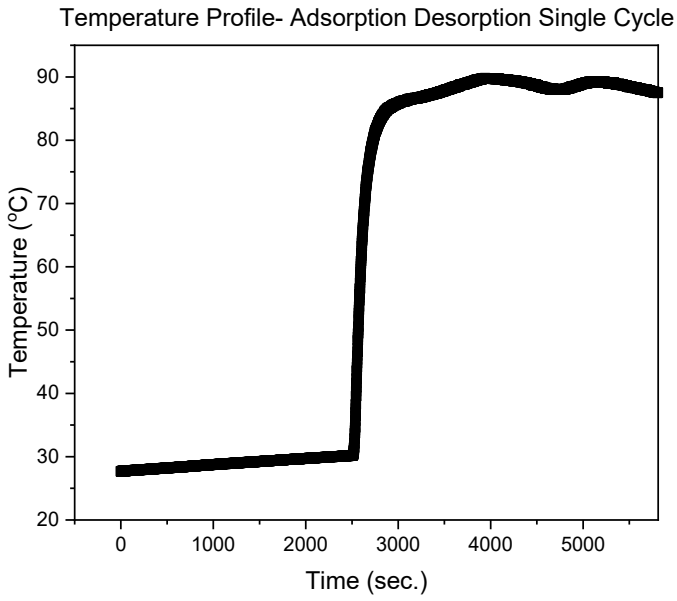

(C)

FIGURE 5.3 : (A) ADSORPTION; (B) DESORPTION & (C) TEMPERATURE PROFILE ZEOLITE FOR (TEST 2)

5.1.3 Test 3 & 4 Results: Experimental results of silica gel & zeolite

Test 3 (testing of silica gel) and Test 4 (testing of zeolite) demonstrated nearly similar behaviour to the first two tests but in this case, lower water vapour uptake was observed in both adsorbent materials. However, the saturation point at the set parameters was reached much quicker – under 500 seconds for Set 2 – as tabulated in Table 3. It was observed that for desorption zeolite rejected its adsorbate faster than silica gel. Silica gel took double the period of zeolite to desorb its adsorbate (see Figure 5.5). Zeolite, upon reaching 5g residual adsorbate during desorption, could no longer reject the adsorbate any further at 600 seconds for when the hot water circulation was opened to trigger desorption.

TABLE 3: SET 2 – PARAMETERS FOR TEST 3 & 4

Parameter	Value
$P_{evaporator}$	-10kPa
$P_{adsorbent}$	-40kPa
$T_{average\ evaporator}$	52°C
$T_{set\ geyser\ desorption}$	95°C
$T_{in\ adsorbent}$	30°C

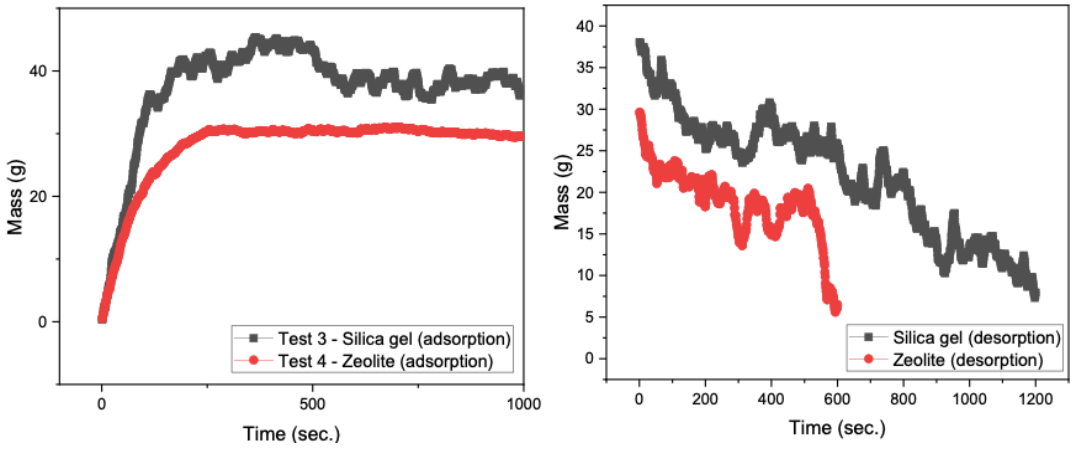

(A) (B)

FIGURE 5.4: (A) ADSORPTION & (B) DESORPTION OF (TESTS 3 & 4)

5.1.4 Test 5 & 6 Results: Experimental results of silica gel & zeolite

Set 3 (see Table 4) demonstrated the highest uptake of adsorbate and rejection of adsorbate for silica gel test sample (see Figure 5.5). It was observed that the adsorbate mass accumulated onto the packed silica gel was 65g. When Set 3 parameters were now tested using a zeolite adsorbent sample, it was observed that the adsorbent uptake was 30g. Similar to the previous tests, silica gel out-performed zeolite. From the three sets of parameters, Set 3 produced the best experimental results for silica gel for both adsorption and desorption phase. For adsorption to take place, the coolant water temperature circulating through the evaporator's tube bundle was 35^{o}C for Set 3 and for Sets 1 and 2, it was 52^{o}C. This could be the reason why silica gel could easily adsorb the adsorbate that was produced at the evaporator using Set 3 testing conditions. From the observations of the three set parameters, it is evident that the lower the boiling temperature at the evaporator used to produce the adsorbate, the easier it was to adsorb that adsorbate. If the evaporator coolant's temperature was high, the adsorbate was not easily adsorbed by the adsorbent.

TABLE 4: SET 3 – PARAMETERS FOR TEST 5 & 6

Parameter	Value
$P_{evaporator}$	-10kPa
$P_{adsorbent}$	-55kPa
$T_{average\ evaporator}$	35^{o}C
$T_{set\ geyser\ desorption}$	95^{o}C
$T_{in\ adsorbent}$	30^{o}C

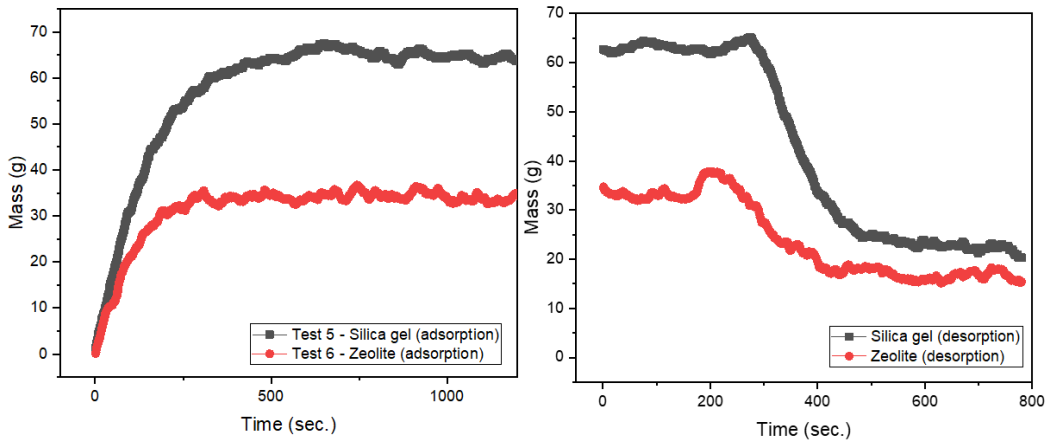

(A) (B)

FIGURE 5.5: (A) ADSORPTION & (B) DESORPTION OF TESTS 5 & 6

Therefore, Set 3 parameters was the best performing set of Sets 1, 2 and 3. The parameters used in Tests 5 and 6 were that of Set 3. This set was used in all tests going further until the final batch of experiments, including experiments of the enhanced adsorbent bed tests and the solar energy-based tests. It should be noted that the significant experimental data output of this study was at the desorption phase, the rejected distillate. The highest rejected adsorbate was 40g which was observed in Set 3; consequently, Set 3 was the determined choice for proceeding with more experimental tests.

5.1.5 Test 7 Results: Experimental results of combined adsorbent

Based on the output yield by the three pairs of experiments, the set that produced high adsorption and desorption was used to test the combined adsorbents and the enhanced adsorbent bed.

A radar graphical summary of adsorption and desorption performance of silica gel and zeolite is presented in Figure 5.6 and Figure 5.7, respectively. Figure 5.6

confirms that silica gel showed good adsorption performance in all sets. Silica gel was capable of adsorbing a minimum of 40g of adsorbate, which was 20% of its original dry mass of silica gel. The highest mass that silica gel adsorbed was 65g. However, the useful adsorbate was the one accounted for during the desorption process which was determined by the difference between adsorption mass and desorption mass. In the case of Set 3 (Figure 5.6), this was the highest adsorbate desorbed, computed as 43g of adsorbate regenerated.

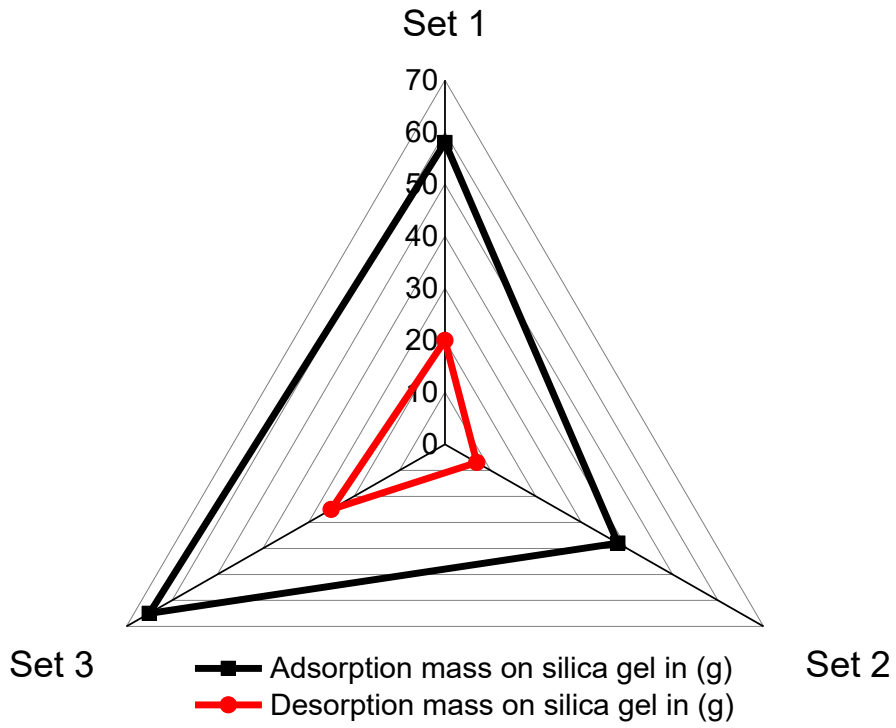

FIGURE 5.6: RADAR GRAPH OF SILICA GEL ADSORPTION & DESORPTION CAPACITY AT DIFFERENT SETS

A graphical summary of zeolite's test performance is presented in Figure 5.7. In this test, it was observed that only Set 1 yielded significant adsorption capacity of 58g adsorbate. Set 2 and Set 3 underperformed: even though they showed some

desorbed adsorbate, it was insignificant when compared to that of silica gel in these two sets. Zeolite demonstrated inconsistent experimental results. Therefore, mixing zeolite with silica gel was tested to assess its performance when combined with another adsorbent material, with test result presented later (see Figure 5.8).

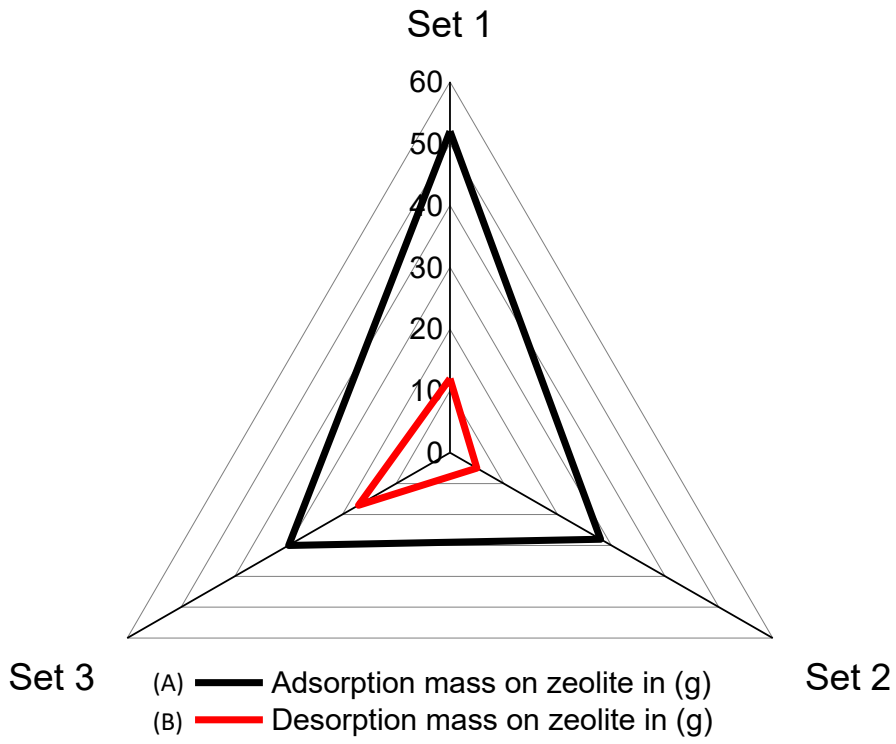

FIGURE 5.7: RADAR GRAPH OF (A) ZEOLITE ADSORPTION & (B) DESORPTION CAPACITY AT DIFFERENT SETS

When 100g of dry zeolite was mixed with 100g of silica gel, using Set 3 parameters to test, it was observed that the adsorption capacity was lower than that of purely silica gel (Test 5) but higher than that of zeolite (Test 6) when tested at similar experimental conditions. For the combined adsorbent test, a maximum of 45g of adsorbate was adsorbed and 26g of adsorbate was desorbed.

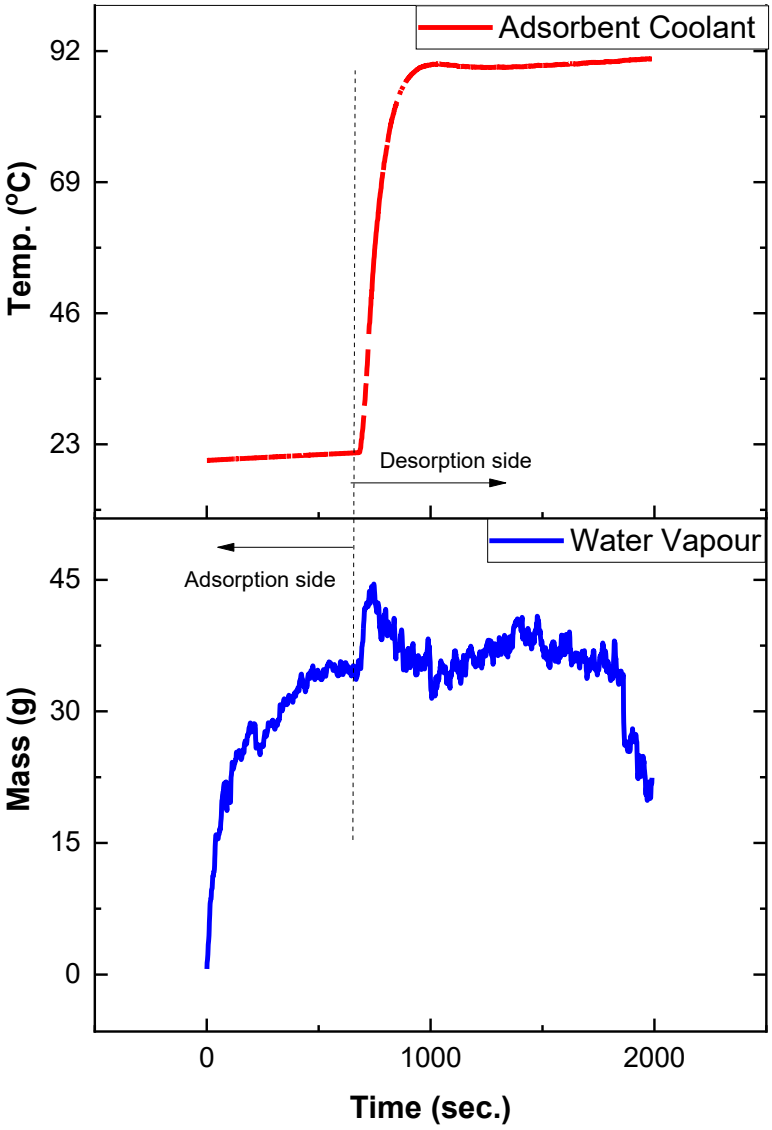

FIGURE 5.8: COMBINED ADSORBENTS -TEST 7 RESULTS

Further tests were performed on the enhanced mixed adsorbents. The enhancements were an addition of copper shavings mixed well with the two adsorbents. Set 3 was also used for this test.

5.1.6 Test 8 Results: Experimental results of enhanced adsorbent bed

After adding the copper shavings to enhance thermal distribution within the adsorbent bed, observations (see Figure 5.9) demonstrated a significant effect that contributed to both adsorption and desorption. A uniform desorption rate was observed: within the time frame of 2000 seconds, 32g of residual adsorbate was left after 55g of adsorbate had been adsorbed. Therefore, if the hot water circulation was retained longer, this would increase the desorbed adsorbate making the test rig produce more distillate.

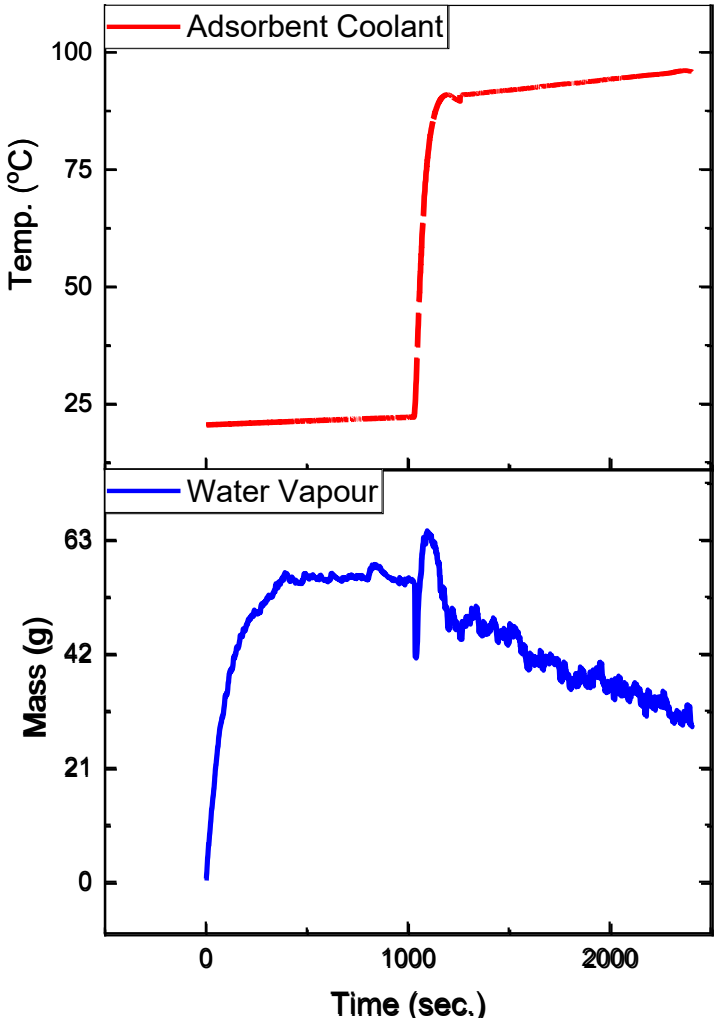

FIGURE 5.9: COPPER SHAVINGS ENHANCED ADSORBENT BED - TEST 8 RESULTS

5.2 Experimental results of a series of solar-based tests

Instead of using electrical energy as the energy source to heat the adsorbent coolant water, solar heated water was used to trigger the desorption cycle. The energy distribution of the test rig (Figure 5.10) represents all electrified appliances within the test rig. There were two 50L geysers of which each accounted for just above 21% of the overall system's power consumption when the entire system was powered solely by electricity. When one geyser was switched to solar power, this portion of electrical energy was deemed saved and the remaining balance of energy was retained as electrical energy to drive the system. Therefore, when the system was using solar energy to heat the water of the second geyser, the system was operating as a hybrid energy system of electrical and solar energy. The total amount of power rating of the electrical components used in the system amounts to 100% power used by the system. The equation used to workout the energy distribution of the system was as follows:

$$P_{50L\ Electric\ Geyser\ 1} + P_{Evaporator\ Pump} + P_{Magnetic\ Pump} + P_{Vacuum\ Pump} + P_{Adsorbent\ Pump} + P_{50L\ Electric\ Geyser\ 2} + P_{evacuated\ Tubes\ pump} = P_{Sum\ within\ the\ electric\ driven\ system} = 9.45\ kW$$

See Figure 5.10 for actual power rating of components. All energy distribution were worked out in this sequence, with the numerator of its respective power rating divided by the total power rating of the :

$$=(P_{50L\ Electric\ Geyser} \div P_{Sum\ within\ the\ electric\ driven\ system}) \times 100$$

$$=(P_{Evaporator\ Pump} \div P_{Sum\ within\ the\ electric\ driven\ system}) \times 100$$

$$=(P_{Magnetic\ Pump} \div P_{Sum\ within\ the\ electric\ driven\ system}) \times 100$$

$$=(P_{Vacuum\ Pump} \div P_{Sum\ within\ the\ electric\ driven\ system}) \times 100$$

$=(P_{Adsorbent\ Pump} \div P_{Sum\ within\ the\ electric\ driven\ system}) \times 100$

$=(P_{evacuated\ Tubes\ pump} \div P_{Sum\ within\ the\ electric\ driven\ system}) \times 100$

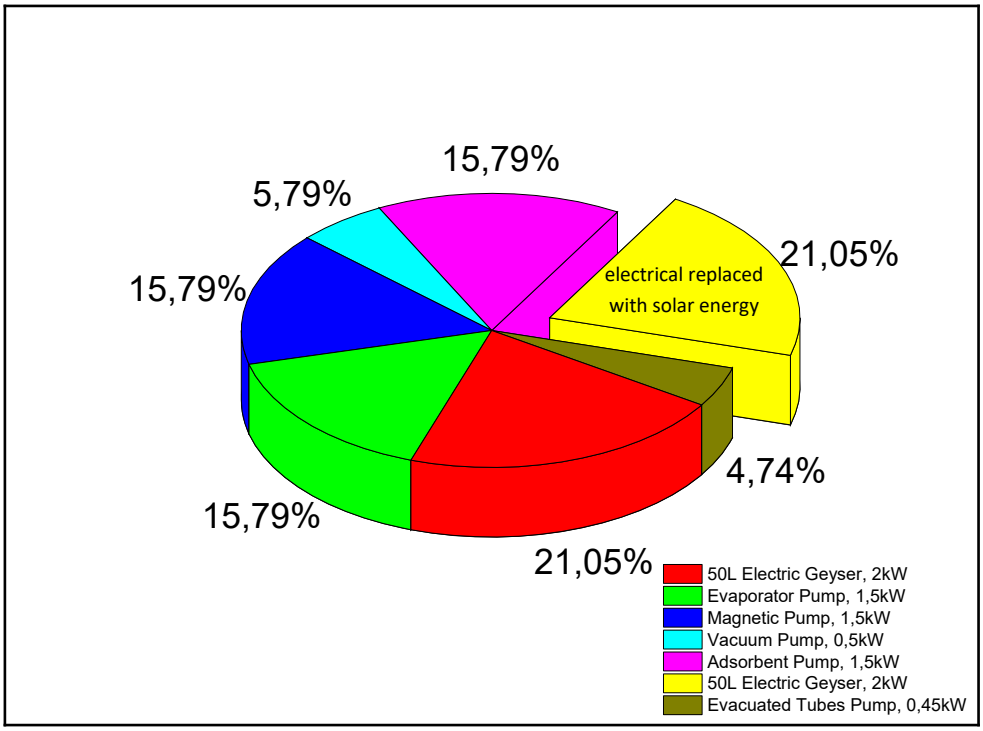

FIGURE 5.10: ENERGY DISTRIBUTION OF THE TEST RIG

The experimental test results from this point onward were utilising solar heated water for desorption. Data collected for the solar irradiation, outdoor temperature and actual temperature difference within the solar geyser were captured for 10 days in total, in addition to the eight experiments that were purely an electrically driven experimental setup. This was to observe the potential that solar water heating can contribute to cutting down on electrical energy use. The outcome of the ETC unit, which was the solar heated water of the tests, was dependent on the outdoor temperature and most of all, the solar irradiation. The peak water temperature yield by this solar water heating unit was later experimented onto the test rig to test how much yielding distillate it could regenerate with the solar heated water in the

desorption phase, from the previously captured water vapour of the adsorbent. The aim of this portion of the experiments was to test the desorption capability of the local adsorbent materials using South Africa's solar energy for the application of the desalination system under study.

5.2.1 Solar-based test results day 1

After the adsorption of the water vapour was complete from the evaporator into the adsorbent bed, desorption was triggered using thermal swing to reject the water vapour off the adsorbent sample. The use of the 20-tubed ETU was employed to heat the water that triggered the desorption phase. Day 1 was clear sky with 370 W/m^2 of solar irradiation, an outdoor temperature peak of 25,8^oC that yielded the 50L water stored in the solar geyser to reach a maximum temperature of 58^oC (see Figure 5.11). The distillate produced was 7,84 grams.

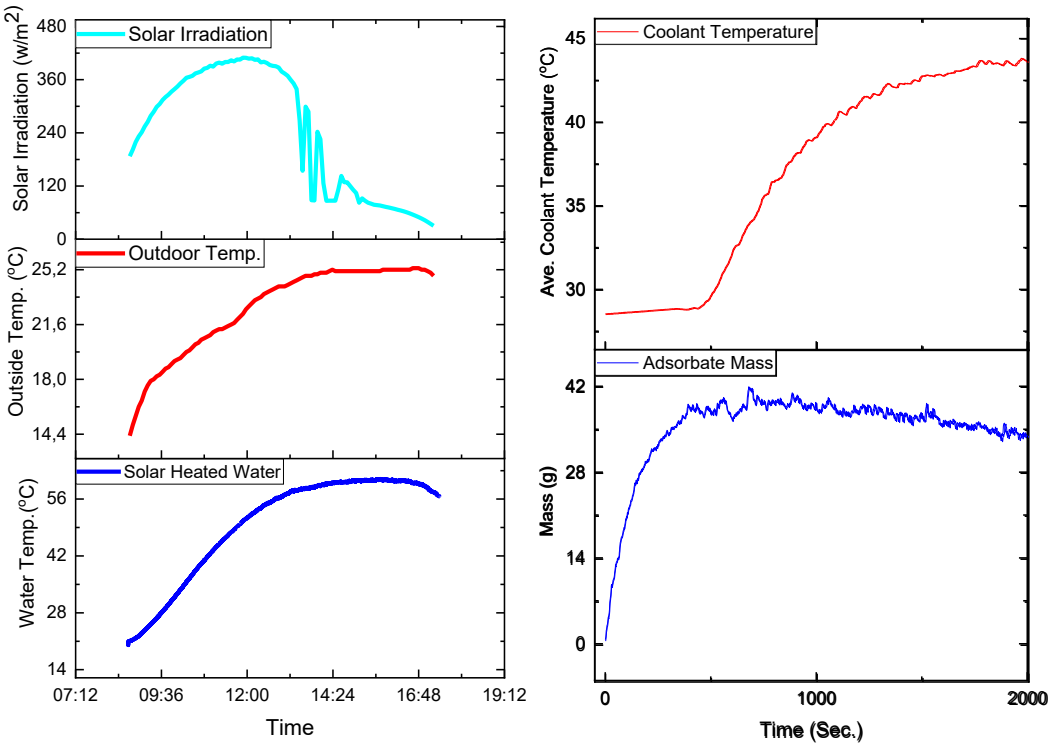

(A) (B)

FIGURE 5.11: (A) DAY 1 SOLAR WATER HEATING; (B) ADSORPTION & DESORPTION

A significant increase in the day's temperature between 09:30 and 13:00 was observed, with the maximum water temperature of this day occurring at 15:30. After this point, the solar irradiation decreased drastically which directly affected the water temperature. Data acquired on the 03-07-2022.

After gathering the solar energy-based data that yielded the water temperature of the solar geyser, the solar heated water was tested to assess how much distillate or water vapour could be produced when the desorption coolant was 58°C. This water coolant temperature did not produce significate distillate.

5.2.2 Solar-based test results day 2

The observations made on day 2 (on Figure 5.12) of solar-based experiments demonstrated the highest water temperature of all 10 days at 66,7°C. The solar irradiation of this day was 456 W/m^2, with as outdoor temperature of 22°C. The experimental results showed that the water vapour rejected during the desorption phase yielded by the stored water in the geyser was observed as 27,29 grams per 200 grams of adsorbent material. Data acquired on the 04-07-2022.

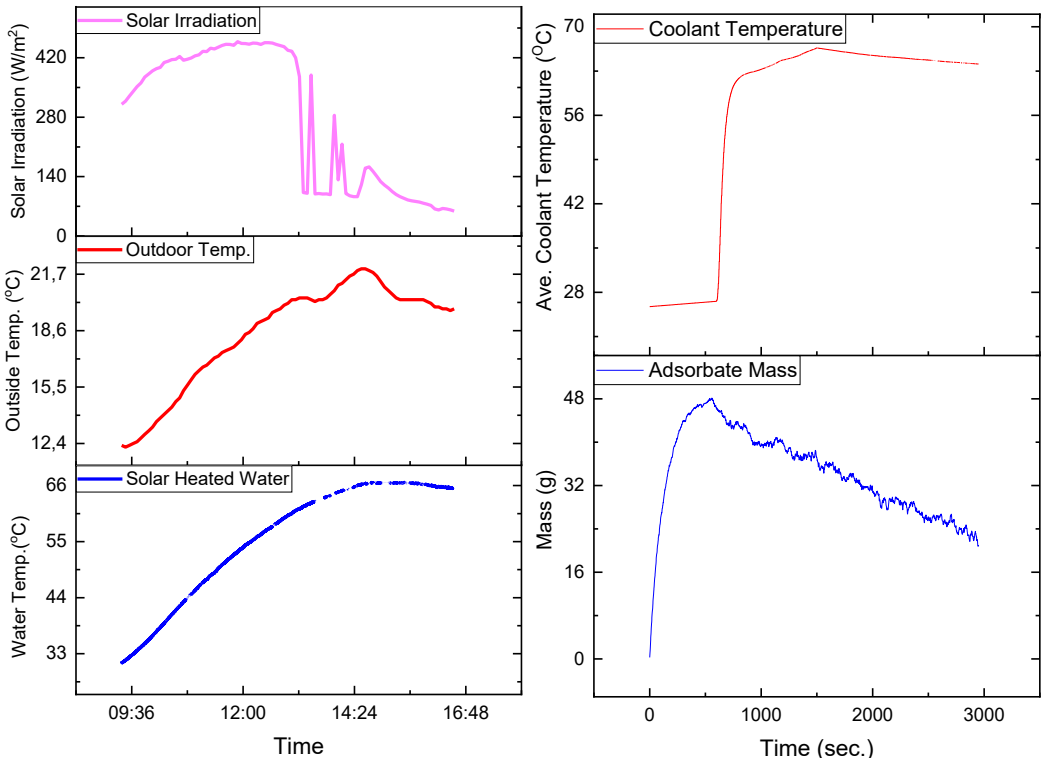

FIGURE 5.12: (A) DAY 2 SOLAR WATER HEATING; (B) ADSORPTION & DESORPTION

5.2.3 Solar-based test results day 3

Experimental day 3 of solar water heated experiments was a sunny day with a peak of 415 W/m^2 solar irradiation, an outdoor temperature of 17,8^{o}C that yielded a maximum water temperature of 62,3^{o}C. On this day, the water vapour distillate produced using the hot water from the solar geyser to desorb the captured adsorbate was 31,26 grams per 200 grams of adsorbent sample (on Figure 5.13). Data acquired on the 05-07-2022.

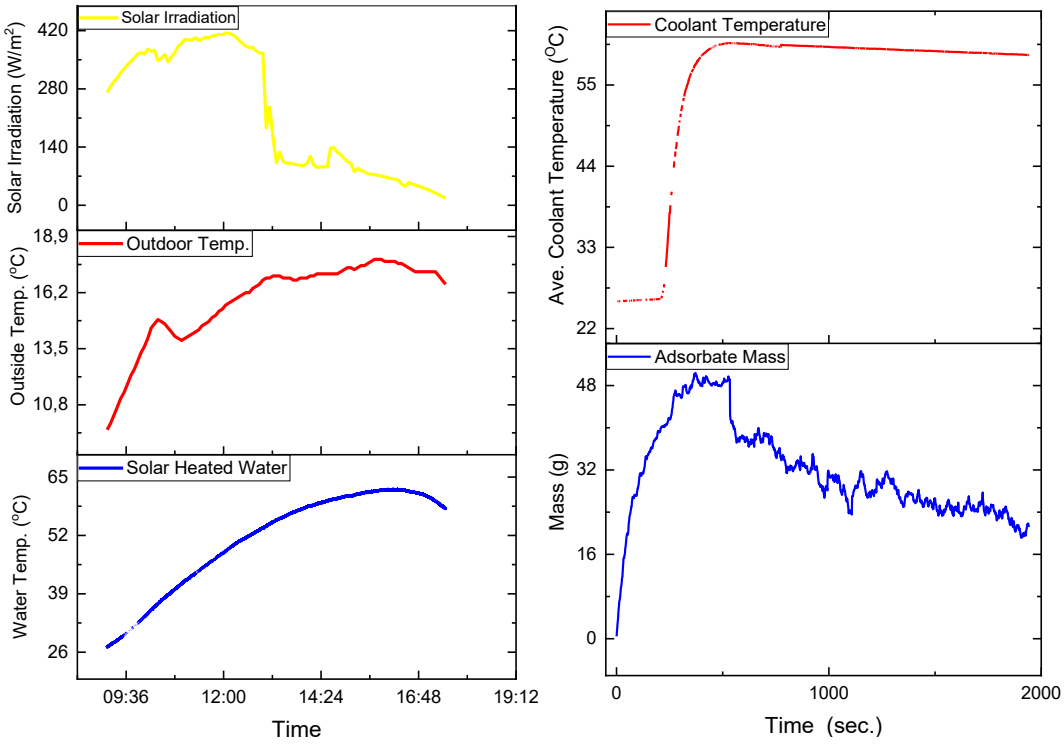

(A) (B)

FIGURE 5.13: (A) DAY 3 SOLAR WATER HEATING; (B) ADSORPTION & DESORPTION

5.2.4 Solar-based test results day 4

On day 4 of solar energy-based experiments, it was observed that the peak solar irradiation was 434 W/m^2, the peak outside temperature was 16,6^{o}C and the maximum water temperature yield was 54,6^{o}C. The maximum water temperature used for desorption to regenerate water vapour was observed as 15,64g as per Figure 5.14. Data acquired on the 06-07-2022.

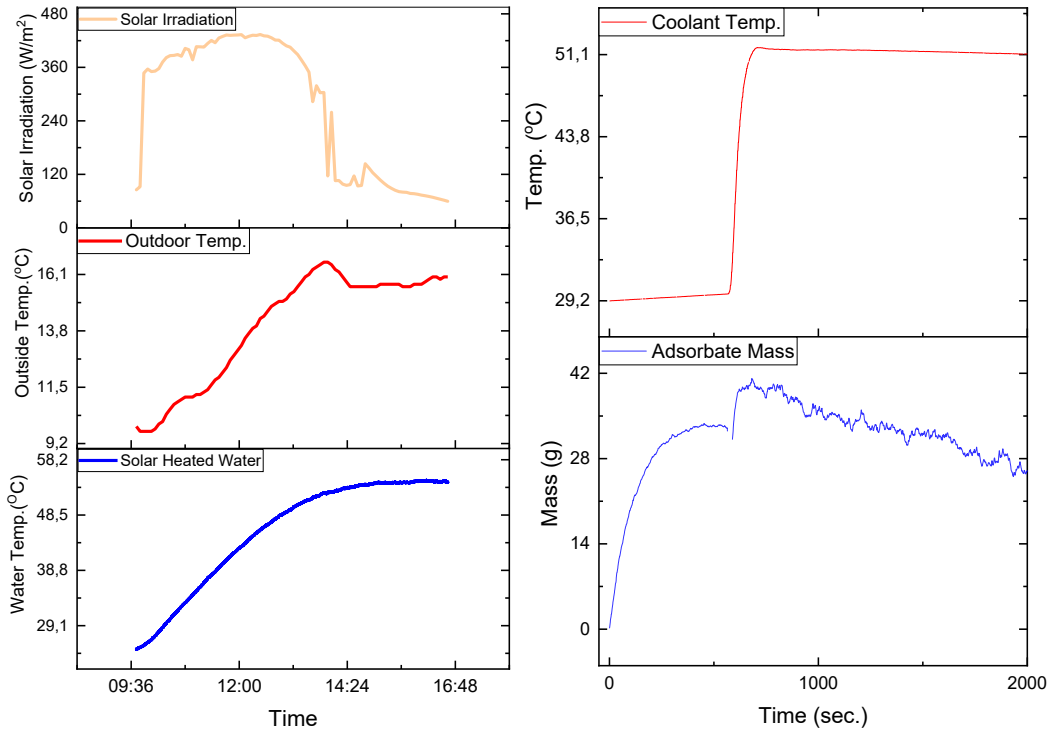

FIGURE 5.14: (A) DAY 4 SOLAR WATER HEATING; (B) ADSORPTION & DESORPTION

5.2.5 Solar-based test results day 5

On day 5 of running the experiments, it was observed that the weather was overcast, prohibiting solar rays from propagating through the clouds unhindered. Evident on the solar irradiation graph were numerous peaks and valleys that depicted inconsistent solar ray harvesting. This reoccurred throughout day 5. The maximum solar irradiation observed on day 5 was 243W/m^2, the peak outdoor temperature was 17,4^{o}C and the maximum solar geyser water temperature was 41^{o}C. The distillate regenerated from the adsorbent bed at desorption temperature 41^{o}C was insignificant, an amount of 7,03 grams (on Figure 5.15). Data acquired on the 07-07-2022.

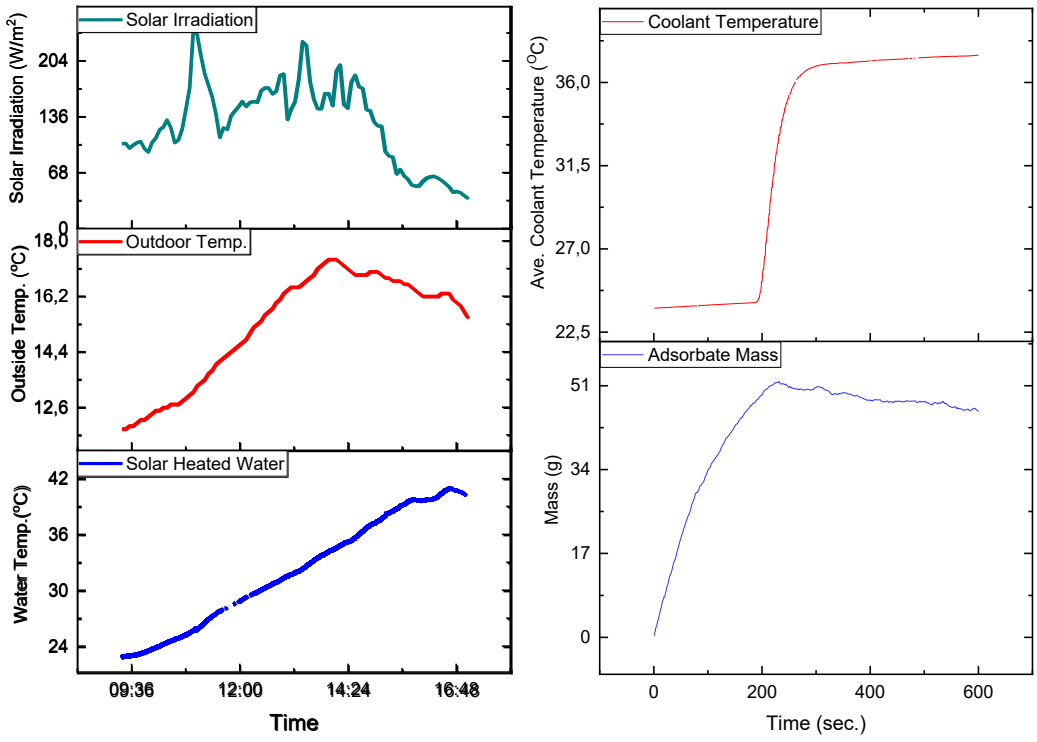

(A) (B)

FIGURE 5.15: (A) DAY 5 SOLAR WATER HEATING; (B) ADSORPTION & DESORPTION

5.2.6 Solar-based test results day 6

On day 6 of solar-based experiments, the maximum solar irradiation experienced was 457 W/m^2, the maximum outdoor temperature was 19.1^{o}C and the peak water temperature in the 50L storage geyser was 64^{o}C.The desorbed distillate of day 6's hot water is based on the outcomes observed on day 2 because the water temperature difference was 2^{o}C; as this temperature difference was minor, it was anticipated that it would yield the same amount of distillate as observed in day 2 (on Figure 5.16). Data acquired on the 08-07-2022.

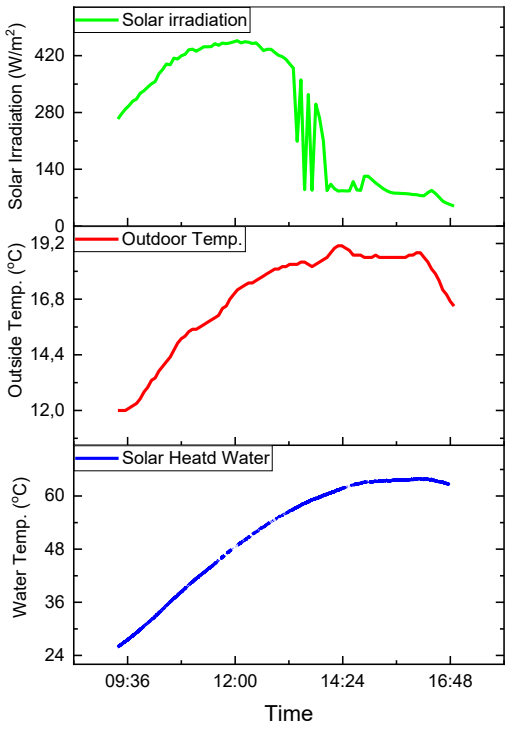

FIGURE 5.16: DAY 6 SOLAR WATER HEATING

5.2.7 Solar-based test results day 7

Day 7 of solar-based experiments was cloudy, demonstrating the lowest peak solar irradiation of all days, at 177 W/m^2. The peak outdoor temperature was 16,7ºC. The water temperature produced for this day was the lowest of all days at 30,4ºC. It was concluded that this water temperature would not trigger any desorption based on the comparative observation of the output of day 5 that yielded insignificant distillate results when the stored water reached a maximum of 41ºC. On day 7, as the water temperature was 10ºC lower than on day 5, it was anticipated that this water temperature would not yield any significate distillate (on Figure 5.17). Data acquired on the 09-07-2022.

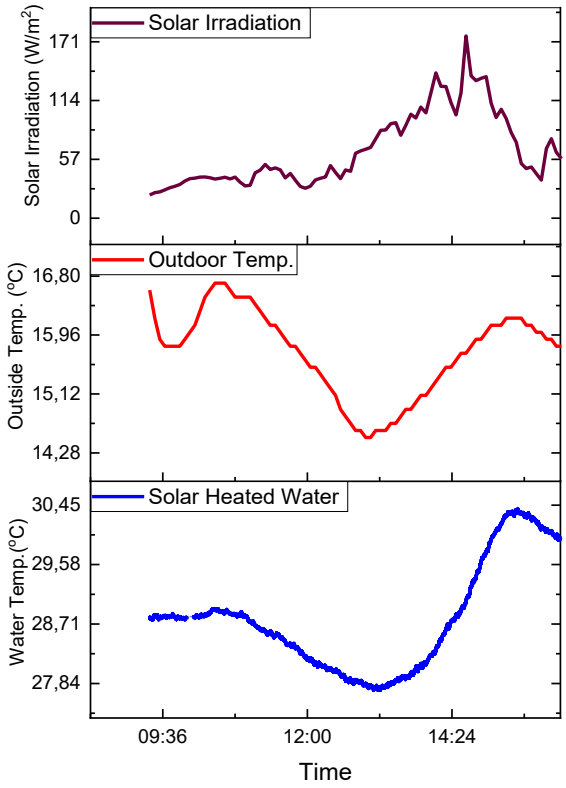

FIGURE 5.17: DAY 7 SOLAR WATER HEATING

5.2.8 Solar-based test results day 8

Day 8 was both a sunny and cloudy day with a peak solar irradiation of 494 W/m^2, the second highest solar irradiation of the 10 days. The outdoor temperature was 17°C. Day 8 environmental conditions produced a peak water temperature of 52,6°C. The desorption output of day 8 was deemed similar to that observed in day 4 because of the minimal water temperature difference that was observed between day 8 and day 4 peak water temperature output (on Figure 5.18). Data acquired on the 22-07-2022.

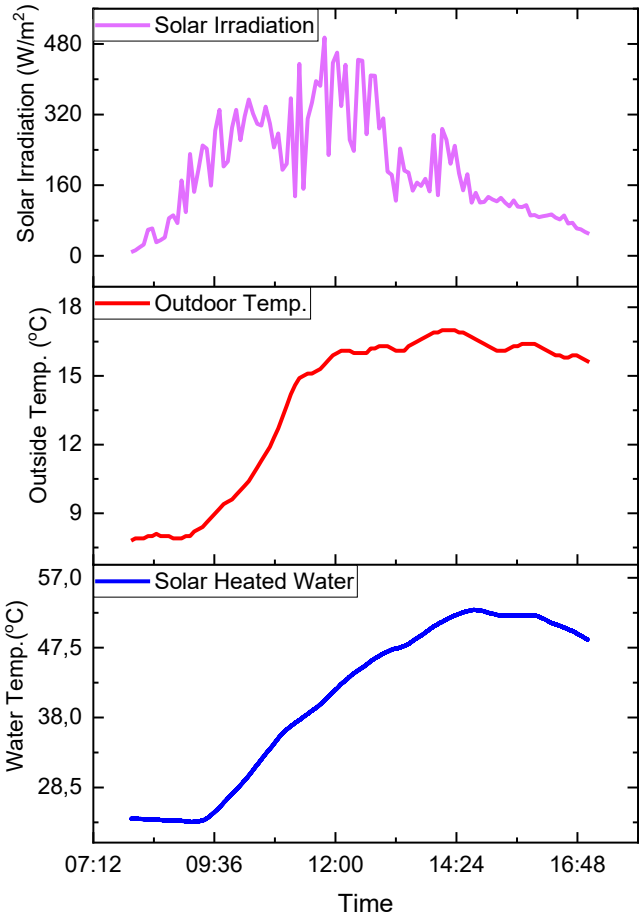

FIGURE 5.18: DAY 8 SOLAR WATER HEATING

5.2.9 Solar-based test results day 9

Day 9 of solar-based experiments was a both sunny and cloudy day as reflected in Figure 5.19. The constant fluctuation of solar irradiation indicates the cloud cover interfering between the harvesting of solar rays. On this day, the peak solar irradiation was 501 W/m^2, the highest of all the days. The peak outdoor temperature was 15.5^{o}C, which was the lowest outdoor temperature of all days of solar-based experiments. The maximum water temperature produced for this day was 53.4^{o}C. The distillate produced was with reference to that of day 4 because of the small peak water temperature difference observed on those two days. Data acquired on the 23-07-2022.

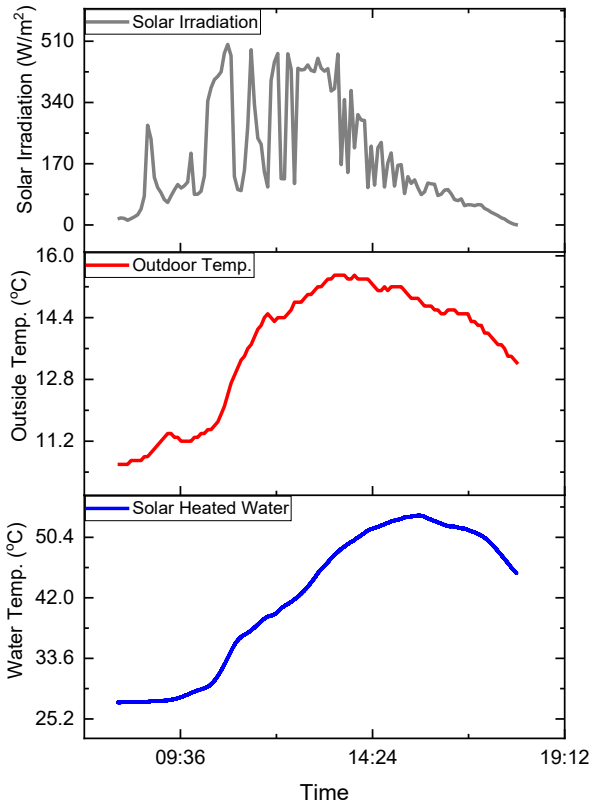

FIGURE 5.19: DAY 9 SOLAR WATER HEATING

5.2.10 Solar-based test results day 10

The experimental data collected from day 10 of the solar-based test showed that the sky had a clear cloud cover allowing the sun rays to experience no hindrance and thereby benefit from smooth solar irradiation, on Figure 5.20. The maximum solar irradiation on this day was 409.8 W/m^2, the outdoor maximum temperature was 24.7^{o}C and the maximum water temperature that this day's condition could reach was 62,3^{o}C. Therefore, using this water temperature, the test rig was tested for how much distillate could be produced at desorption phase when 62,3^{o}C of water coolant in the adsorbent bed was used. It was observed that day 3 and day 10 had the same maximum hot water output; therefore, the distillate produced was deemed as the same form as the basis of day 3's adsorbate distillate output which was 31,26 grams per 200 grams of adsorbent sample. Data acquired on the 25-07-2022.

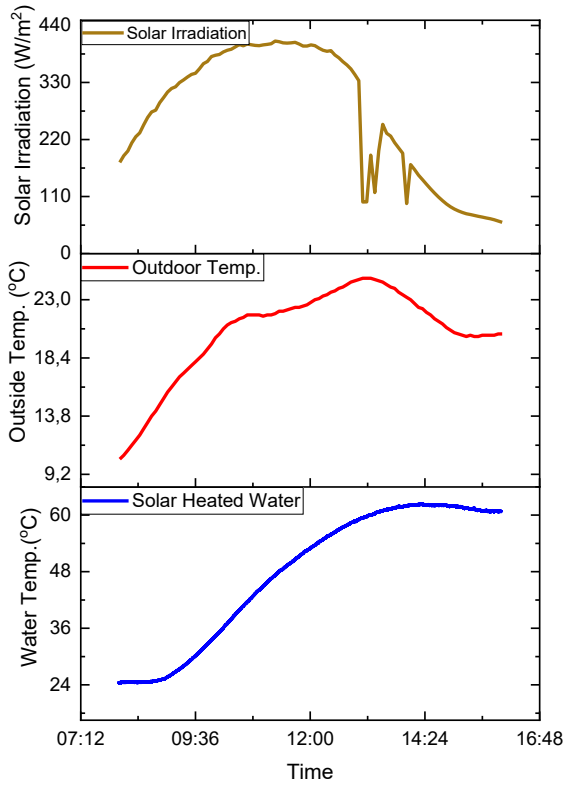

FIGURE 5.20: DAY 10 SOLAR WATER HEATING

5.3 Summary of experimental outcome of solar energy-based desalination

In this section, a summary of the data collected for 10 days in July 2022 is presented graphically on Figure 5.21. Concurrently, the rejected water vapour during desorption is also presented for the water temperature that was yielded by the daily solar irradiation.

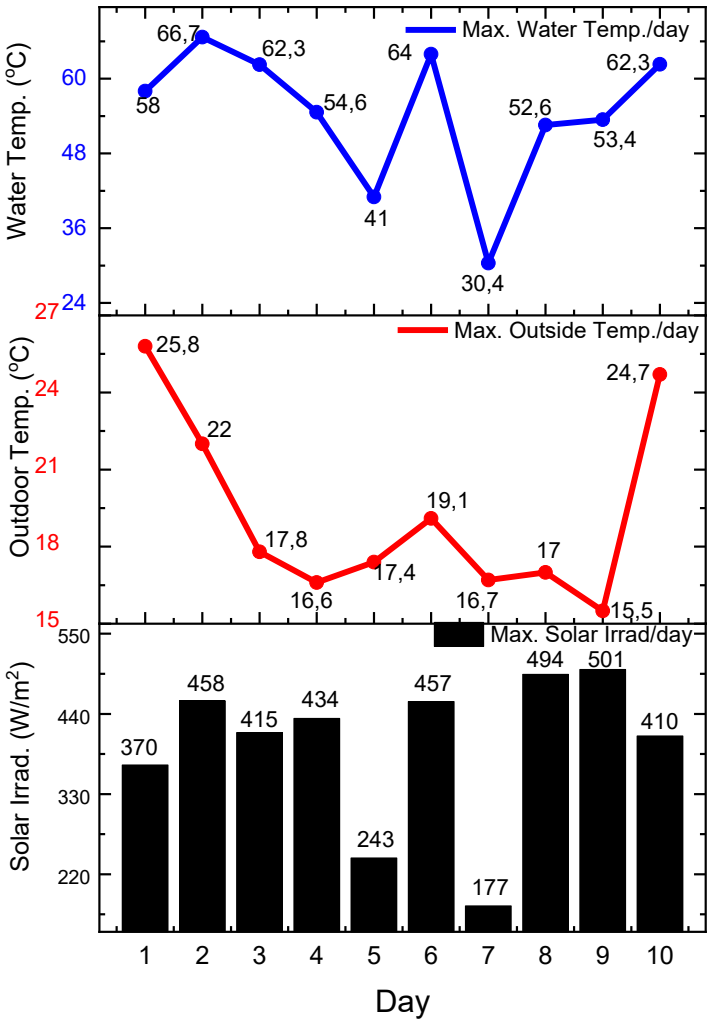

FIGURE 5.21: SOLAR-BASED DAILY OUTPUT

It was observed that day 9 experienced the highest solar irradiation, although it did not have the highest peak water temperature stored in the geyser. Day 8 had the second highest solar irradiation, followed by day 2. However, it was observed that neither solar irradiation nor outdoor temperature can be relied on independently determine the output of the water temperature at the geyser storage; rather, these parameters can be analysed as a combination to conclude the overall impact of the weather conditions on the water temperature output. Other parameters such as wind speed and outdoor humidity were side-lined for this study; data analysis was limited to solar irradiation, outdoor temperature and cloud cover observed each day.

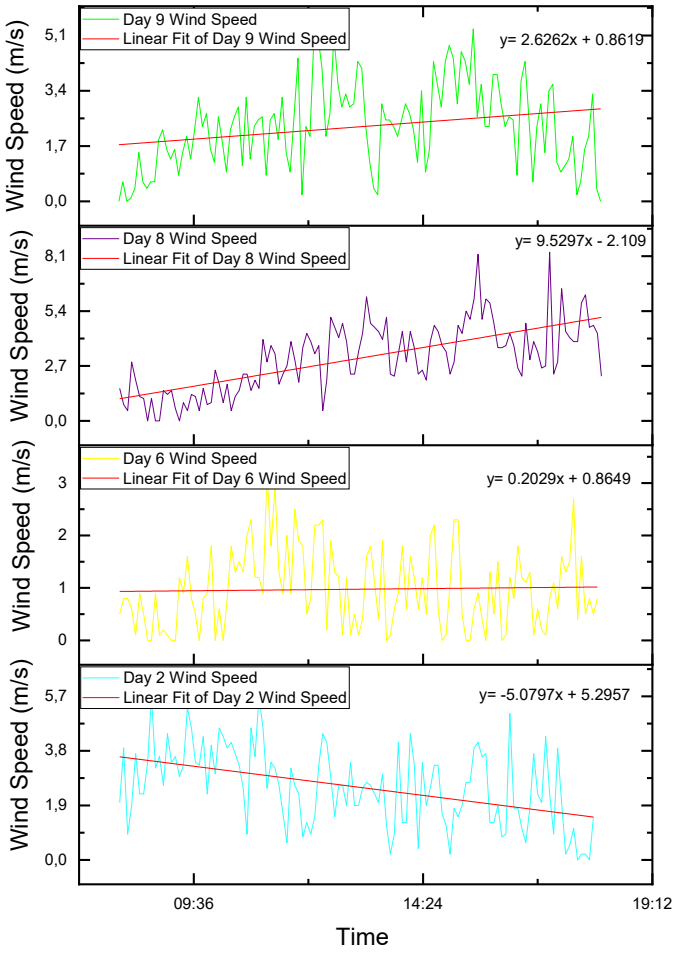

FIGURE 5.22: WIND SPEED FOR DAY 2, DAY 6, DAY 8 & DAY 9

However, due to day 9 having the highest solar irradiation but not yielding the anticipated hot water temperature, the impact of the wind speed was scrutinised. It was observed that the top four days of solar irradiation (day 9, day 8, day 6 and day 2) were influenced by the wind speed. It was observed that on day 2, where the wind speed gradually decreased throughout the day, the temperature of the solar heated water was hotter than that of the days when the wind speed gradually increased throughout the day to more than 4m/s. This was likewise observed in day 2, day 9 and also day 8. Day 9 and day 8 both had higher solar irradiation than day 2. The wind speed of day 2 gradually decreased from 3.8m/s which was overall slower than the previously mentioned two days. The graphical presentation of the linear fit curve of the wind speed demonstrates the respective wind speeds (see Figure 5.22). The wind speed of these days, if analysed comparatively with the solar irradiation, leads to the conclusion that wind speed impacts the solar harvesting that directly impacts the output temperature of the solar heated water.

CHAPTER 6: CONCLUSION & RECOMMENDATIONS

Renewable energy-based desalination is a critical necessity for RSA, especially with the ongoing load-shedding and alarming water shortage. This study focused on an emerging desalination system called the adsorption desalination method. The conceptualisation of this system stemmed from the conventional thermal distiller or evaporative desalination method but having the addition of the adsorption-desorption refrigeration cycles. Locally available adsorbent materials were explored in this study to test the constructed desalination system using local environmental conditions of South Africa. Initially, the system was electrically powered, following which the experiments incorporated solar energy as a source of energy to heat water that was utilised to trigger the desorption cycle of the adsorption-desorption refrigeration cycle.

6.1 Conclusion

In the experimental performances, the following observations culminated in the following conclusions. It was observed that at the adsorption phase, saturation of adsorbent is not only dependent on its capability of adsorbing but rather co-dependent on conducive experimental conditions under which the adsorption was performed. This was observed when the same amount of adsorbent sample (200 grams) when tests were run at varying environmental conditions yielded different adsorptive capabilities. It was not only hydrophilic and hydrophobic properties that were contributing factors, but also but the environment under which the adsorbent materials were tested notably influenced the performance of the adsorbent samples. Therefore, manipulating the test conditions to achieve optimal output was critical for

good system output. The adsorption phase pressure conditions were critical to transporting the water vapour into the adsorbent bed, a pressure swing method facilitating the adsorption phase of the experiments. In the desorption phase, thermal swing was utilised to evacuate the previously captured water vapour off the surface of the subject adsorbent. Even in the case of thermal swing as the catalyst to achieved effective desorption, it was still critical that vacuum pressure conditions were maintained throughout the performance of the experiments.

6.2 Test rig outcomes

In this study, the throughput yield was based on how much potable water vapour was accumulatively desorbed by the two adsorbent materials (silica gel and zeolite) over time. The conventional adsorption desalination system encompasses the condenser unit which is not inclusive of this study. In this study, the throughput of the test rig was the desorbed water vapour off the adsorbent porous surface during desorption; this rejected distillate was regarded as the output of the test rig in this study.

When the tests were conducted, there were four core experiments: the testing of the silica gel and zeolite individually; the combination of the two adsorbents; the combination of the two adsorbents together with copper shavings, all three of which were electrically driven. The fourth series of tests were the best performer of the three groups tested using solar energy for the desorption cycle. In this sub-section, the concluding remarks on all four core tests will be presented in addition to the discussion in Chapter 5. It is important to note that this research study focussed primarily on the adsorbent bed even though all sub-stations independently influenced the operations of the test rig.

Individual adsorbent test output: Independent tests of silica gel and zeolite results demonstrated that silica gel was the better performing adsorbent material of the two for the application of the adsorption desalination system. Silica gel outperformed zeolite in two of the three test parameters. Unlike silica gel, zeolite demonstrated inconsistent experimental outputs below the outputs of silica gel.

Combination of adsorbents test output: Even though zeolite demonstrated inconsistent behaviour when the experiments were performed with zeolite alone, when zeolite was mixed with silica gel, it was observed that zeolite retards the adsorption desorption capabilities of silica gel. Comparing Test 5 and Test 7 made evident that with the adsorbent samples exposed to the same testing conditions, Test 5 still emerged as a better performer than Test 7 for both adsorption and desorption capabilities.

Enhanced combination of adsorbents test output: Intriguing experimental behaviour was observed when the adsorbent bed was enhanced, an adsorbent bed comprising silica gel, zeolite and copper shavings mixed and shaken well before installing this onto the special scale place inside the adsorbent chamber. A more uniform desorption phase behaviour was observed after adding copper shavings to enhance the thermal distribution in the adsorbent bed. This had an impact on the rate at which desorption was occurring, as observed in the experiment inclusive of copper shavoing. The longer the hot water was allowed to circulate, the more water vapour was recovered at a uniform rate. The water vapour recovered was equivalent or deemed as the water produced by the test rig.

Renewable energy-based test output: Even though evacuated tubes do not operate between dusk and dawn, this solar water heating technology unit demonstrated reliability and sustainability as a solar energy harvesting technology for the

application of solar water heating. This solar water heating unit was capable of heating water from 19°C to above 66,7°C in mid-winter in South Africa, with solar irradiation ranging from 176.6 W/m^2 (on day 7) up to 501 W/m^2 (on day 9), with the capability of triggering desorption that regenerated a maximum of 31,26g of water vapour on day 3 where 415 W/m^2 and 17,8°C experimental data was observed. Therefore, featuring solar water heating (evacuated tube) technology in this study is indeed a technically sound option. In comparison to when the test rig was operated 100% with electrical power, replacing the electric 50L geyser with a solar powered geyser was clearly beneficial. Even though the renewable energy-based tests were hybrid, converting one geyser into a solar geyser contributed to the reduction of electrical energy utilised in the test rig.

6.3 Recommendations

The temperature at the adsorbent bed during adsorption phase was maintained at 30°C and below throughout the performance of all tests to support the packed adsorbent material in capturing the water vapour. Also, controlled pressure differences were used as a tool to transport water vapour and to ensure adsorption effectively occurred. However, it is recommended for future work that temperatures, lower than 30°C be explored as one potential catalyst to trigger or support adsorption to occur. It was witnessed that in the adsorption phase, if insufficient cooling or hot temperatures over 40°C were experienced in the adsorbent bed during adsorption phase, this resulted in the adsorbent underperforming by failing to reach maximum potential if compared with the adsorbent exposed to testing conditions that had sufficient cooling during the adsorption phase.

For desorption to effectively take place, hot water circulating through the adsorbent coil from the geyser (initially electric then later solar) was observed as yielding significant desorption results at 60^0C to 80^{o}C; this agrees with the findings of previous studies [144]. Therefore, it is also recommended that a smaller adsorbent sample size (smaller that 200g as tested in this study) be used to further investigate the behaviour of adsorbents. A smaller size implies a reduced energy requirement to investigate the adsorbent material on small scale.

The system was quite sensitive to minor pressure and temperature changes. Therefore, insulation quality and test conditions of the system are critical to the performance outcome of this system. It is recommended that future work investigate effective ways for this system to operate under vacuum conditions.

An additional recommendation for future work concerns automating this test rig to better monitor performance to help extract more data and to help in observing and monitoring the system's behaviour in careful detail.

Finally, finding suitable and affordable equipment to log the data under vacuum pressure test conditions was a challenge. Related instrumentation studies suitable for this test rig are recommended for future work.

BIBLIOGRAPHY

[1] H. Rabiee, K. R. Khalilpour, J. M. Betts, N. Tapper, Chapter 13 - Energy-Water Nexus: Renewable-Integrated Hybridized Desalination Systems, Editor(s): Kaveh Rajab Khalilpour, Polygeneration with Polystorage for Chemical and Energy Hubs, Academic Press, 2019, pp. 409-458.

[2] T. Younos, K. E. Tulou, "Overview of Desalination Techniques," *Journal of contemporary water research & education*, vol. 132, pp. 3-10, 2005.

[3] A. Alkaisi, R. Mossad, A. Sharifian-Barforoush, "A Review of the Water Desalination Systems Integrated with Renewable Energy," *Energy Procedia*. vol. 110, pp. 268-274. 2017.

[4] N. A. Ahmad, P. S. Goh, L. T. Yogarathinam, A. K. Zulhairun, A. F. Ismail, "Current advances in membrane technologies for produced water desalination," *Desalination*, issue 493, Article 114643, 2020.

[5] S. Atkinson, Singapore's first large-scale dual-mode desalination plant is now on stream," *Membrane Technology*, vol. 2020, issue 11, pp. 6, 2020.

[6] M. T. Mito, X. Ma, H. Albuflasa, P. A. Davies, "Reverse osmosis (RO) membrane desalination driven by wind and solar photovoltaic (PV) energy: State of the art and challenges for large-scale implementation," *Renewable and Sustainable Energy Reviews*, vol. 112, pp. 669-685, 2019.

[7] R. Hu, T. Huang, G. Wen, Z. Tang, Z. Liu, K. Li, "Pilot study on the softening rules and regulation of water at various hardness levels within a chemical crystallization circulating pellet fluidized bed system," *Journal of Water Process Engineering*, vol. 41, Article 102000, 2021.

[8] Z. Yao, L. E. Peng, H. Guo, W. Qing, Y. Mei, C. Y. Tang, "Seawater pre-treatment with an NF-like forward osmotic membrane: Membrane preparation,

characterization and performance comparison with RO-like membranes," *Desalination*, vol. 470, Article 114115, 2019.

[9] S. Alsadaie, I. M. Mujtaba, "Crystallization of calcium carbonate and magnesium hydroxide in the heat exchangers of once-through Multistage Flash (MSF-OT) desalination process," *Computers & Chemical Engineering*, vol. 122, pp. 293-305, 2019.

[10] Geography Statistics of South Africa. World Atlas, Online. 2020.

[11] T. Goga, E. Friedrich, C. A. Buckley, "A LCA (Life Cycle Assessment) comparison of wastewater reclamation and desalination for the eThekwini municipality – a theoretical study," WISA, 2016.

[12] G. A. Thopil, A. Pouris, "A 20 year forecast of water usage in electricity generation for South Africa amidst water scarce conditions," *Renewable and Sustainable Energy Reviews*, vol. 62, pp. 1106-1121, 2016.

[13] Amatola water, "Desalination an alternative solution to SA's water supply challenges," nd.

[14] H. Ngobese, "Desalination plant relieves KZN drought," Vuk'uzenzele. 2017.

[15] The Chemical Engineer, "First solar-powered desalination plant for South Africa," 2018.

[16] Z. Donnenfeld, C. Crookes, S. Hedden, "A delicate balance water scarcity in South Africa," Southern Africa Report, 2018.

[17] World Health Organization, "Guide for drinking water quality," nd.

[18] D. M. van Tonder, C. J. S. Fourie, J. M. Maree, “Development of a Solar Desalination Plant,” *South African Journal of Geology,* vol. 119 issue 1, pp. 39-46, 2016.

[19] B. B. Haldenwang, “The state of water in South Africa- are we heading for a water crisis? Vol 7 No 01,” 2020.

[20] “A CSIR perspective on water in South Africa,” CSIR Report No. CSIR/NRE/PW/IR/2011/0012/A, 2010.

[21] Department of Energy, “Forecasts for electricity demand in South Africa (2017-2015) using the CSIR sectoral regression model for the integrated resource plan of South Africa,” Prepared by CSIR, 2017.

[22] DWAF South Africa, “Quality of domestic water supplies. Vol 4: Treatment Guide,” WRC Report No TT 181/02, 2002.

[23] L. J. Laubscher, “Techno economic viability of desalination processes in South Africa,” Masters Thesis, North-West University, 2011.

[24] Forest & Sullivan, “Municipal and industrial sectors drive South African desalination plants markets,” *Membrane Technology*, vol. 2007, issue 7, pp. 8-9, 2007.

[25] C. L. Blersch , J. A. du Plessis, “Planning for desalination in the context of the Western Cape water supply system,” *Journal of the South African Institution of Civil Engineering,* vol. 59, issue 1, pp. 11-21, 2017.

[26] G. Rencken, “Largest sea-water desalination plant in South Africa is supplied in record time,” Membrane Technology, vol. 2011, issue 3, pp. 9, 2011.

[27] D. Kitley, “A costing analysis of reverse osmosis desalination plants powered by renewable energy and their potential for South Africa,” Masters Thesis, University of Cape Town, 2015.

[28] United Nations, “Sustainable development goals. Goal 6: Clean water and sanitation,” 2020.

[29] K. N. Turner, K. Naidoo, J. G. Theron, J. Broodryk, “Investigation into the cost and operation of South African desalination and water reuse plants. Vol 2: Current status of desalination and water reuse in Southern Africa,” WRC Report No TT 637/15, 2015.

[30] K. C. Ng, K. Thu, B. B. Saha, A. Chakraborty, “Study on a waste heat-driven adsorption cooling cum desalination cycle,” *International Journal of Refrigeration*, vol. 35, issue 3, pp. 685-693, 2012.

[31] O. Alnajdi, Y. Wu, J. K. Calautit, “Toward a Sustainable Decentralized Water Supply: Review of Adsorption Desorption Desalination (ADD) and Current Technologies: Saudi Arabia (SA) as a Case Study,” *MDPI-Water,* vol. 12, Article 1111, 2020.

[32] D. Zejli, R. Benchrifa, A. Bennouna, O. K. Bouhelal, “A solar adsorption desalination device: first simulation results,” *Desalination*, vol.168, pp. 127-135, 2004.

[33] K. C. Ng, H. T. Chua, C. Y. Chung, C. H. Loke, T. Kashiwagi, A. Akisawa, et al*.,* “Experimental investigation of the silica gel-water adsorption isotherm characteristics,” Applied Thermal Engineering, vol. 21, pp. 1631-1642, 2001.

[34] H. T. Chua, K. C. Ng, W. Wang, C. Yap, X. L. Wang, “Transient modelling of a two-bed silica gel-water adsorption chiller,” *International Journal of Heat Mass Transfer*, vol. 47, pp. 659-669, 2004.

[35] J. W. Wu, E. J. Hu, M. J. Biggs, “Thermodynamic cycles of adsorption desalination system,” *Applied Energy,* vol. 90, issue 1, pp. 316-322, 2012.

[36] I. I. El-Sharkawyb, K. Thu, K. C. Ng, B. B. Saha, A. Chakraborty, S. Koyama, “Performance Improvement of Adsorption Desalination Plant: Experimental Investigation,” *International Reviews of Mechanical Engineering*, vol. 1, pp. 25-31, 2007.

[37] K. Thu, B. B. Saha, A. Chakraborty, W. G. Chun, K. C. Ng, “Study on an advanced adsorption desalination cycle with evaporator–condenser heat recovery circuit,” *International Journal of Heat and Mass Transfer,* vol. 54, issue 1–3, pp. 43-51, 2011.

[38] “Municipal and industrial sectors drive South African desalination plant markets,” *Membrane Technology*, vol. 2007, issue. 7, pp. 8-9, 2007.

[39] J. Eke, A. Yusuf, A. Giwa, A. Sodiq, “The global status of desalination: An assessment of current desalination technologies, plants and capacity,” *Desalination*, vol. 495, Article 114633, 2020.

[40] “LG Chem supplies membranes for Egypt's largest desalination plant,” *Membrane Technology*, vol. 2017, issue 8, pp. 3, 2017.

[41] J. Andrianne, F. Alardin, “Thermal and membrane process economics: Optimized selection for seawater desalination,” *Desalination,* vol. 153, issue 1–3, pp. 305-311, 2003.

[42] A. A. B. Rújula, N. K. Dia, “Application of a multi-criteria analysis for the selection of the most suitable energy source and water desalination system in Mauritania,” *Energy Policy*, vol. 38 issue 1, pp. 99-115, 2010.

[43] Z. Wang, Y. Wang, G. Xu, J. Ren, “Sustainable desalination process selection: Decision support framework under hybrid information,” *Desalination,* vol. 465, pp. 44-57, 2019.

[44] J. J. Schoeman, A. Steyn, “Nitrate removal with reverse osmosis in a rural area in South Africa,” *Desalination.* vol. 155, issue 1, pp. 15-26, 2003.

[45] A. Mansouri, M. Hasnaoui, A. Amahmid, S. Hasnaoui, “Feasibility analysis of reverse osmosis desalination driven by a solar pond in Mediterranean and semi-arid climates,” *Energy Conversion and Management,* vol. 221, Article 113190, 2020.

[46] P. A. Hohne, K. Kusakana, B. P. Numbi, “Optimal energy management and economic analysis of a grid-connected hybrid solar water heating system: A case of Bloemfontein, South Africa,” *Sustainable Energy Technologies and Assessments*, vol. 31, pp. 273-291, 2019.

[47] I. Ozturk, “Sustainability in the food-energy-water nexus: Evidence from BRICS (Brazil, the Russian Federation, India, China, and South Africa) countries,” *Energy,* vol. 93, pp. 999-1010, 2015.

[48] T. R. Ayodele, J. L. Munda, “Potential and economic viability of green hydrogen production by water electrolysis using wind energy resources in South Africa,” *International Journal of Hydrogen Energy*, vol. 44, issue 33, pp. 17669-17687, 2019.

[49] L. Nhamo, T. Mabhaudhi, B. S. Mpandeli, C. Dickens, C. Nhemachena, A. Senzanje, D. Naidoo, S. Liphadzi, A. T. Modi, “An integrative analytical model for the water-energy-food nexus: South Africa case study,” *Environmental Science & Policy*, vol.109, pp. 15-24, 2020.

[50] Y. Zhou, “Evaluating the costs of desalination and water transport,” *Water Resources Research,* vol. 41, pp. 1-10, 2005.

[51] S. Hoseinzadeh, R. Yargholi, H. Kariman, P. S. Heyns, “Exergoeconomic analysis and optimization of reverse osmosis desalination integrated with geothermal energy,” *Environmental Progress & Sustainable Energy*, vol. 39, issue 5, Article e13405, 2020.

[52] The Chemical Engineer. (2018). *First solar-powered desalination plant for South Africa*.

[53] Creamer Media’s Engineering News. (2019). *Africa’s first solar-powered desalination plant passes 10 000 kl mark*.

[54] H. Kariman, S. Hoseinzadeh, P. S. Heyns, “Energetic and exergetic analysis of evaporation desalination system integrated with mechanical vapor recompression circulation,” *Case Studies in Thermal Engineering,* vol. 16, Article 100548, 2019.

[55] Global solar atlas. (2021). Solargis. Online.

[56] F. E. Ahmed, R. Hashaikeh, N. Hilal, “Solar powered desalination – Technology, energy and future outlook,” *Desalination*, vol. 453, pp. 54-76, 2019.

[57] V. G. Gude, N. Nirmalakhandan, S. Shuguang Deng, “Integrated PV-thermal system for desalination and power production,” *Desalination and Water Treatment*, vol. 36, issue 1-3, pp. 129-140, 2011.

[58] Y. Hou, R. Vidu, P. Stroeve, “Solar energy storage methods,” *Industrial & Engineering Chemistry Research*, vol. 50, issue15, pp. 8954–8964, 2011.

[59] A. A. Monjezi, Y. Chen, R. Vepa, A. E. B. Kashyout, G. Hassan, H. E. Fath, A. E. Kassem, M. H. Shaheed, “Development of an off-grid solar energy powered

reverse osmosis desalination system for continuous production of freshwater with integrated photovoltaic thermal (PVT) cooling," *Desalination,* vol. 495, Article 114679, 2020.

[60] F. Stefano, G. Valentina, B. Roberto, L. Vito, G. Riccardo, "Setting up of a cost-effective continuous desalination plant based on coupling solar and geothermal energy," *Desalination,* vol. 500, Article 114854, 2021.

[61] J. E. Hoffmann, E. P. Dall, "Integrating desalination with concentrating solar thermal power: A Namibian case study," *Renewable Energy*, vol. 115, pp. 423-432, 2018.

[62] L. Valenzuela, R. López-Martín, E. Zarza, "Optical and thermal performance of large-size parabolic-trough solar collectors from outdoor experiments: A test method and a case study," *Energy*, vol. 70, pp. 456-464, 2014.

[63] N. Ghaffour, S. Lattemann, T. Missimer, K. C. Ng, S. Sinha, G. Amy, "Renewable energy-driven innovative energy-efficient desalination technologies," *Applied Energy*, vol. 136, pp.1155-1165, 2014.

[64] H. Nassrullah, S. F. Anis, R. Hashaikeh, N. Hilal, "Energy for desalination: A state-of-the-art review," *Desalination*, vol. 491, Article 114569, 2020.

[65] Aquarius Sea surface salinity from space. 2021. NASA. Online.

[66] I. G. Wenten, D. Ariono, M. Purwasasmita, M. Khoirudin, "Integrated Processes for Desalination and Salt Production: A Mini-Review," in *AIP Conference Proceedings*, vol. 1818, Article 020065, 2017.

[67] A. Al-Kaabi, H. Al-Sulaiti, T. Al-Ansari, H. R. Mackey, Assessment of water quality variations on pre-treatment and environmental impacts of SWRO desalination," *Desalination*, vol. 500, Article 114831, 2021.

[68] N. H. Pham, V. T. Nguyen, "Proposed Research on Saline-Water Distillation for Living by Utilizing Waste Heat from Industrial Steam Boilers," in *5th*

International Conference on Green Technology and Sustainable Development (GTSD) pp. 505-510, 2020.

[69] L. D. Tijing, Y. C. Woo, J. Choi, S. Lee, S. Kim, H. K. Shon, “Fouling and its control in membrane distillation—A review,” *Journal of Membrane Science,* vol. 475, pp. 215-244, 2015.

[70] A. M. Hamiche, A. B. Stambouli, S. Flazi, “A review of the water-energy nexus,” *Renewable and Sustainable Energy Reviews,* vol. 65, pp. 319-331, 2016.

[71] J. Xu, Y. Li, H. Wang, J. Wu, X. Wang, F. Li, “Exploring the feasibility of energy self-sufficient wastewater treatment plants: a case study in eastern China,” *Energy Procedia,* vol. 142, pp. 3055-3061, 2017.

[72] M. W. Shahzad, M. Burhan, D. Ybyraiymkul, K. C. Ng, “Desalination with Renewable Energy: A 24 Hours Operation Solution,” in *Water and Waste Treatment*, IntechOpen, 2019.

[73] P. Compain, “Solar Energy for Water desalination,” in *1st International Symposium on Innovation and Technology in Phosphate Industry, Procedia Engineering*, vol. 46, pp. 220-227, 2012.

[74] K. C. Ng, M. W. Shahzad, “Sustainable desalination using ocean thermocline energy,” *Renewable and Sustainable Energy Reviews*, vol. 82, pp. 240-246, 2018.

[75] H. Mokhtari, M. Sepahvand, A. Fasihfar, “Thermoeconomic and exergy analysis in using hybrid systems (GT+MED+RO) for desalination of brackish water in Persian Gulf,” *Desalination*, vol. 399, pp. 1-15, 2016.

[76] S. Loutatidou, H. A. Arafat, “Techno-economic analysis of MED and RO desalination powered by low-enthalpy geothermal energy,” *Desalination,* vol. 365, pp. 277-292, 2015.

[77] J. Kim, K. Park, D. R. Yang, S. Hong, “A comprehensive review of energy consumption of seawater reverse osmosis desalination plants,” *Applied Energy*, vol. 254, Article 113652, 2019.

[78] T. A. Otitoju, R. A. Saari, A. L. Ahmad, “Progress in the modification of reverse osmosis (RO) membranes for enhanced performance,” *Journal of Industrial and Engineering Chemistry*, vol. 67, pp. 52-71, 2018.

[79] A. Kaya, M. E. Tok, M. Koc, “A Levelized Cost Analysis for Solar-Energy-Powered Sea Water Desalination in The Emirate of Abu Dhabi,” *Sustainability*, vol.11, Article 1691, 2019.

[80] K. H. Chu, J. Lim, S. Kim, T. Jeong, M. Hwang, “Determination of optimal design factors and operating conditions in a large-scale seawater reverse osmosis desalination plant,” *Journal of Cleaner Production,* vol. 244, Article 118918, 2020.

[81] K. Elmaadawy, K. M. Kotb, M. R. Elkadeem, S. W. Sharshir, A. Dán, A. Moawad, B. Liu, “Optimal sizing and techno-enviro-economic feasibility assessment of large-scale reverse osmosis desalination powered with hybrid renewable energy sources,” *Energy Conversion and Management*, vol. 224, Article 113377, 2020.

[82] A. A. Alsarayreh, M. A. Al-Obaidi, A. M. Al-Hroub, R. Patel, I. M. Mujtaba, “Evaluation and minimisation of energy consumption in a medium-scale reverse osmosis brackish water desalination plant,” *Journal of Cleaner Production*, vol. 248, Article 119220, 2020.

[83] M. Kettani, P. Bandelier, “Techno-economic assessment of solar energy coupling with large-scale desalination plant: The case of Morocco,” *Desalination*, vol. 494, Article 114627, 2020.

[84] B. Ortega-Delgado, L. García-Rodríguez, D. Alarcón-Padilla, “Opportunities of improvement of the MED seawater desalination process by pretreatments allowing high-temperature operation,” *Desalination and Water Treatment*, vol. 97, pp. 94-108, 2017.

[85] M. Alsehli, M. Alzahrani, J. Choi, “A novel design for solar integrated multi-effect distillation driven by sensible heat and alternate storage tanks,” *Desalination*, vol. 468, Article 114061, 2019.

[86] C. Frantz, B. Seifert, “Thermal Analysis of a Multi Effect Distillation Plant Powered by a Solar Tower Plant,” *Energy Procedia*, vol. 69, pp. 1928-1937, 2015.

[87] H. R. Datsgerdi, H. T. Chua, “Thermo-economic analysis of low-grade heat driven multi-effect distillation based desalination processes,” *Desalination*, vol. 448, pp. 36-48, 2018.

[88] J. A. Carballo, J. Bonilla, L. Roca, A. De la Calle, P. Palenzuela, D. C. Alarcón-Padilla, “Optimal operating conditions analysis for a multi-effect distillation plant according to energetic and exergetic criteria,” *Desalination*, vol. 435, pp. 70-76, 2018.

[89] X. Wang, A. Christ, K. Regenauer-Lieb, K. Hooman, H. T. Chua, “Low grade heat driven multi-effect distillation technology,” *International Journal of Heat and Mass Transfer*, vol. 54, issue 25–26, pp. 5497-5503, 2011.

[90] M. Alhaj, A. Mabrouk, S. G. Al-Ghamdi, “Energy efficient multi-effect distillation powered by a solar linear Fresnel collector,” *Energy Conversion and Management*, vol. 171, pp. 576-586, 2018.

[91] P. Guo, T. Li, Y. Wang, J. Li, “Energy and exergy analysis of a spray-evaporation multi-effect distillation desalination system,” *Desalination*, vol. 500, Article 114890, 2021.

[92] M. Al-Hamahmy, H. E. S. Fath, K. Khanafer, “Techno-economical simulation and study of a novel MSF desalination process,” *Desalination,* vol. 386, pp. 1-12, 2016.

[93] A. M. K. El-Ghonemy, “Performance test of a sea water multi-stage flash distillation plant: Case study,” *Alexandria Engineering Journal*, vol. 57, issue 4, pp. 2401-2413, 2018.

[94] K. S. Reddy, K. R. Kumar, T. S. O'Donovan, T. K. Mallick, “Performance analysis of an evacuated multi-stage solar water desalination system,” *Desalination*, vol. 288, pp. 80-92, 2012.

[95] E. A. M. Hawaidi, I. M. Mujtaba, “Simulation and optimization of MSF desalination process for fixed freshwater demand: Impact of brine heater fouling,” *Chemical Engineering Journal*, vol. 165, issue 2, pp. 545-553, 2010.

[96] A. E. Al-Rawajfeh, S. Ihm, H. Varshney, A. N. Mabrouk, “Scale formation model for high top brine temperature multi-stage flash (MSF) desalination plants,” *Desalination*, vol. 350, pp. 53-60, 2014.

[97] A.Y. Kalendar, A. J. Griffiths, “Performance study of enhanced and smooth surface tubes in a system condenser of a multistage flash desalination unit,” *Desalination*, vol. 134, issue 1–3, pp. 269-283, 2001.

[98] I. Darawsheh, M. D. Islam, F. Banat, “Experimental characterization of a solar powered MSF desalination process performance,” *Thermal Science and Engineering Progress*, vol. 10, pp. 154-162, 2019.

[99] K. C Ng, K. Thu, Y. Kim, A. Chakraborty, G. Amy, “Adsorption desalination: an emerging low-cost thermal desalination method,” *Desalination,* vol. 308, pp. 161-179, 2013.

[100] K. C. Ng, K. Thu, G. Amy, M. Chunggaze, T. Al-Ghasham, “Regenerative adsorption distillation system,” Patent US20130341177A1, 2013.

[101] T. H. Rupam, M. A. Islam, A. Pal, A. Chakraborty, B. B. Saha, “Thermodynamic property surfaces for various adsorbent/adsorbate pairs for cooling applications,” *International Journal of Heat and Mass Transfer*, vol. 144, Article 118579, 2019.

[102] Y. Matsui, S. Nakao, A. Sakamoto, T. Taniguchi, L. Pan, T. Matsushita, N. Shirasaki, “Adsorption capacities of activated carbons for geosmin and 2-methylisoborneol vary with activated carbon particle size: Effects of adsorbent and adsorbate characteristics” *Water Research*, vol. 85, pp. 95-102, 2015.

[103] S. Woo, H. Lee, H. Ji, D. Moon, Y. Kim, “Silica gel-based adsorption cooling cum desalination system: Focus on brine salinity, operating pressure, and its effect on performance,” *Desalination,* vol. 467, pp. 136-146, 2019.

[104] A. Naeimi, S. M. Nowee, H. A. A. Amiri, “Numerical simulation and theoretical investigation of a multi-cycle dual-evaporator adsorption desalination and cooling system,” *Chemical Engineering Research and Design*, vol. 156, pp. 402-413, 2020.

[105] E.S. Ali, R. H. Mohammed, A. Askalany, “A daily freshwater production of 50m^3/ton of silica gel using an adsorption-ejector combination powered by low-grade heat,” *Journal of Cleaner Production*, vol. 282, Article 124494, 2021.

[106] R. Raj, V. Baiju, “Thermodynamic Analysis of a Solar Powered Adsorption Cooling and Desalination System,” *Energy Procedia*, vol. 158, pp. 885-891, 2019.

[107] S. Bai, T. C. Ho, J. Ha, A. K. An, C. Y. Tso, “Study of the salinity effects on the cooling and desalination performance of an adsorption cooling cum desalination system with a novel composite adsorbent,” *Applied Thermal Engineering*, vol. 181, Article 115879, 2020.

[108] M. Li, Y. Zhao, R. Long, Z. Liu, W. Liu, “Computational fluid dynamic study on adsorption-based desalination and cooling systems with stepwise porosity distribution,” *Desalination*, vol. 508, Article 115048, 2021.

[109] P.C. Thimmaiah, A. Sharafian, M. Rouhani, W. Huttema, M. Bahrami, “Evaluation of low-pressure flooded evaporator performance for adsorption chillers,” *Energy*, vol. 122, pp. 144-158, 2017.

[110] Q. Wang, M. Li, W. Xu, L. Yao, X. Liu, D. Su, P. Wang, “Review on liquid film flow and heat transfer characteristics outside horizontal tube falling film evaporator: Cfd numerical simulation,” *International Journal of Heat and Mass Transfer,* vol. 163, Article 120440, 2020.

[111] R. Kaushal, R. Kumar, G. Vats, “Experimental and numerical analysis for optimal design parameters of a falling film evaporator,” *Sadhana*, vol. 41, issue 6, pp. 643–652, 2016.

[112] Y. Shen, C. Shi, L. Zhang, S. Bu, W. Xu, Z. Zhang, B. Zhu, C. Xu, X. Liu, “Falling film evaporation in a vertical tube with a new type of liquid distributor designed using the brachistochrone principle,” *Vacuum*, vol. 187, Article 110023, 2021.

[113] F. Liu, D. Wang, Q. Wang, J. Ga, “The optimum design of falling-film evaporator and numerical simulation of distributor,” *Procedia Engineering*, vol. 205, pp. 3867-3872, 2017.

[114] A. Haasbroek, L. Auret, W. H. Steyn, “A comparison of control techniques for dairy falling film evaporators,” in *IFAC Proceedings,* vol. 46. issue 32, pp. 253-258, 2013.

[115] H. Chen, “Factors affecting heat transfer in a falling film evaporator,” Masters Thesis. Massey University, 1992.

[116] Z. Mdletshe , V. Msomi, O. Nemraoui, “The effect of modifying the external surface of copper tubes used in a falling film fluid of a horizontal tube bundle,” *Materials Today: Proceedings*, vol. 45, part 45, pp. 5689-5694, 2021.

[117] L. Yang, X. Song, Y. Xie, “Effect of the Dryout in Tube Bundles on the Heat Transfer Performance of Falling Film Evaporators,” *Procedia Engineering*, vol. 205, pp. 2176–2183, 2017.

[118] B. X. Wang, J. T. Zhang, X. F. Peng, “Experimental study on the dryout heat flux of falling liquid film,” *International Journal of Heat and Mass Transfer*, vol. 43, pp. 1897-1903, 2000.

[119] J. Chen, J. Zhang, Z. Hu, Z. Ma, “Falling Film Transitions on Horizontal Enhanced Tubes: Effect of Tube Spacing,” *Procedia Engineering*, vol. 205, pp. 1542-1549, 2017.

[120] P. Jin, Z. Zhang, I. Mostafa, C. Zhao, W. Ji, W. Tao, “Experimental study of falling film evaporation in tube bundles of doubly-enhanced, horizontal tubes,” *Applied Thermal Engineering,* vol. 170, Article 11500, 2020.

[121] S. Shen, G. Liang, Y. Guo, H. Mu, R. Liu, Y. Yang, “Heat transfer coefficient in falling film evaporators with different tube arrangements,” in *Proceedings of the ASME 2012 Summer Heat Transfer Conference*, 2012, pp.873-879.

[122] D. Gstöhl, “Heat transfer and flow visualization of falling film condensation on tube arrays with plain and enhanced surfaces,” Doctoral Thesis. ÉCOLE POLYTECHNIQUE FÉDÉRALE DE LAUSANNE, 2004.

[121] L. Yang, L. Zhang, A. Li, J. Wu, “Modelling thermal and geometrical effects on non-condensable gas desorption in horizontal-tube bundles of falling film evaporation,” *Desalination,* vol. 478, Article 114302, 2020.

[123] M. Gourdon, E. Karlsson, F. Innings, A. Jongsma, L. Vamling, “Heat transfer for falling film evaporation of industrially relevant fluids up to very high Prandtl numbers,” *Heat Mass Transfer*, vol. 52, pp. 379–391, 2016.

[124] M. W. Shahzad, M. Burhan, K. C. Ng, “Development of Falling Film Heat Transfer Coefficient for Industrial Chemical Processes Evaporator Design,” in *Statistical Approaches With Emphasis on Design of Experiments Applied to Chemical Process*, IntechOpen, 2017.

[125] R. H. Mohammed, A. A. Askalany, “Productivity Improvements of Adsorption Desalination Systems,” in *Solar Desalination Technology*, pp. 325-357, 2019.

[126] X. Wang, K. C. Ng, “Experimental investigation of an adsorption desalination plant using low-temperature waste heat,” *Applied Thermal Engineering*, vol. 25, issue 17–18, pp. 2780-2789, 2005.

[127] K. Thu, A. Chakraborty, Y. Kim, A. Myat, B. B. Saha, K. C. Ng, “Numerical simulation and performance investigation of an advanced adsorption desalination cycle,” *Desalination,* vol. 308, pp. 209-218, 2013.

[128] A. S. Kim, H. Lee, D. Moon, H. Kim, “Performance control on adsorption desalination using initial time lag (ITL) of individual beds,” *Desalination*, vol. 396. pp. 1-16, 2016.

[129] E. S. Ali, K. Harby, A. A. Askalany, M. R. Diab, A. S. Alsaman, “Weather effect on a solar powered hybrid adsorption desalination-cooling system: A case study of Egypt’s climate,” *Applied Thermal Engineering*, vol. 124, pp. 663-672, 2017.

[130] C. Olkis, S. Brandani, G. Santori, “A small-scale adsorption desalinator,” in *Energy Procedia 2019*, vol. 158, pp. 1425-1430. 2019.

[131] B. Du, J. Gao, L. Zeng, X. Su, X. Zhang, S. Yu, Hongting Ma, “Area optimization of solar collectors for adsorption desalination,” *Solar Energy*, vol. 157, pp. 298-308, 2017.

[132] K. Thu, H. Yanagi, B. B. Saha, K. C. Ng, “Performance investigation on a 4-bed adsorption desalination cycle with internal heat recovery scheme,” *Desalination*, vol. 402, pp. 88-96, 2017.

[133] B. B. Saha , I. I. El-Sharkawy, M. W. Shahzad, K. Thu, L. Ang, K. C. Ng, “Fundamental and application aspects of adsorption cooling and desalination,” *Applied Thermal Engineering,* vol. 97, pp. 68-76, 2016.

[134] H. Zhang, H. Ma, S. Liu, H. Wang, Y. Sun, D. Qi, “Investigation on the operating characteristics of a pilot-scale adsorption desalination system,” *Desalination*, vol. 473, Article 114196, 2020.

[135] A. A. Askalany, E. S. Ali, "A new approach integration of ejector within desalination cycle reaching COP higher than one," *Sustainable Energy Technologies and Assessments*, vol. 40, Article 100766, 2020.

[136] H. Ma, J. Zhang, C. Liu, X. Lin, Y. Sun, "Experimental investigation on an adsorption desalination system with heat and mass recovery between adsorber and desorber beds," *Desalination*, vol. 446, pp. 42-50, 2018.

[137] S. M. Ali, A. Chakraborty. "Adsorption assisted double stage cooling and desalination employing silica gel+water and AQSOA-Z02+water systems," *Energy Conversion and Management,* vol. 117, pp. 193-205, 2016.

[138] E. Elsayed, R. AL-Dadah, S. Mahmoud, P. Anderson, A. Elsayed, "Experimental testing of aluminium fumarate MOF for adsorption desalination," *Desalination*, vol. 475, Article 114170, 2020.

[139] P. G. Youssef, R. K. AL-Dadah, S. M. Mahmoud, H. J. Dakkama, A. Elsayed, "Effect of Evaporator and Condenser Temperatures on the Performance of Adsorption Desalination Cooling Cycle," *Energy Procedia*, vol. 75, pp. 1464-1469, 2015.

[140] P. G. Youssef, S. M. Mahmoud, R. K. Al-Dadah, "Effect of Evaporator Temperature on the Performance of Water Desalination/Refrigeration Adsorption System Using AQSOA-ZO2," *Engineering and Technology International Journal of Environmental and Ecological Engineering*, vol. 9, issue 6, pp. 701-705, 2015.

[141] A. Amirfakhraei, T. Zarei, J. Khorshidi, "Performance improvement of adsorption desalination system by applying mass and heat recovery processes," *Thermal Science and Engineering Progress,* vol. 18, Article 100516, 2020.

[142] C. Olkis, S. Brandani, G. Santori, "Cycle and performance analysis of a small-scale adsorption heat transformer for desalination and cooling applications," *Chemical Engineering Journal*, vol. 37, Article 122104, 2019.

[143] H. Rezk, A. S. Alsaman, M. Al-Dhaifallah, A. A. Askalany, M. A. Abdelkareem, A. M. Nassef, “Identifying optimal operating conditions of solar-driven silica gel based adsorption desalination cooling system via modern optimization,” *Solar Energy*, vol. 181, pp. 475-489, 2019.

[144] V. Baiju, P. Abhishek, K. L. Priya, P. A. Mohammed Shahid, “Performance investigation of silica gel based consolidated composite adsorbents effective for adsorption desalination systems,” *Materials Today Communications*, Article 104015, 2022.

[145] Z. Mdletshe, V. Msomi, O. Nemraoui, “Experimental investigation of the adsorbents using pressure and thermal swing for adsorption and desorption,” *Results in Engineering*, vol.15, Article 100513, 2022.

APPENDICIES

APPENDIX: A

Materials Safety Data Sheet (MSDS)

TABLE A: MSDS – SILICA GEL

Equipment/model	Silica gel, white non-indicating
Manufacturer	-
Function	Adsorption & Desorption
Supplier	Silica gel SA
Range	3-5mm

TABLE B: MSDS - ZEOLITE

Equipment/model	Zeolite, Molecular sieve 3A
Manufacturer	-
Function	Adsorption & Desorption
Supplier	Silica gel SA
Range	3-5mm sphere

TABLE C: MSDS - ETC UNIT

Equipment/model	20 tube manifold
Manufacturer	KWIKOT, KWIKSOL
Function	Harvest solar energy for solar water heating
Supplier	Plumblink

TABLE D: MSDS - VACUUM PUMP

Equipment/model	Speedivac, Value D10, Vacuum Pump
Manufacturer	Value

Function	Create & control vacuum conditions
Supplier	Vacuum SA
Range	<1.0 mbar, 10m^3/h, 6.0 CFM
Material	Cast iron, threaded female inlet ¼ ’’

TABLE E: MSDS - ELECTRIC GEYSER TO EVAPORATOR PUMP

Equipment/model	Clean water pump, CM2150
Manufacturer	Vansan
Function	Circulate clean water
Supplier	Afripumps (pty) ltd
Range	8.4 m^3/hr, Q_{max}
Material	Cast iron, threaded female inlet 1 ½’’, female outlet1 1/4”

TABLE F: MSDS - EVAPORATOR DISTRIBUTION PUMP

Equipment/model	Magnetic water pump, PT446951
Manufacturer	Flojet
Function	Circulate saline water under vacuum conditions
Supplier	RS Components
Range	52 l/min, Q_{max}
Material	Cast iron/plastic, threaded female inlet ½’’, female outlet ½’’

TABLE G: MSDS - ADSORPTION CIRCULATION PUMP

Equipment/model	Clean water pump, CM2150
Manufacturer	Vansan
Function	Circulate clean water
Supplier	Afripumps (pty) ltd

Range	8.4 m^3/hr, Q_{max}
Material	Cast iron, threaded female inlet 1 ½'', female outlet1 1/4"

TABLE H: MSDS - ETC MANIFOLD TO SOLAR GEYSER CIRCULATION PUMP

Equipment/model	Water pump, P 2000 G
Manufacturer	Metabo
Function	Circulate clean water to ETC Unit
Supplier	Brights
Range	2 m^3/hr, Q_{max}
Material	Cast iron, threaded female inlet & outlet 1''

TABLE I: MSDS - FLOWRATE TRANSMITTER

Equipment/model	YF-S201, liquid flow meter
Manufacturer	-
Function	Measure flow rate, digital signal
Supplier	Micro Robotics
Range	1-25 l/min
Material	Plastic, threaded male ends ½''

TABLE J: MSDS – PT100 THERMOCOUPLE

Equipment/model	PT100, RTD, 3 wire Sensor
Manufacturer	-
Function	Measure temperature, digital signal
Supplier	RS Components
Range	-50°C to 200°C
Material	Stainless steel sleeve

TABLE K: MSDS -PRESSURE GAUGE

Equipment/model	Pressure gauge
Manufacturer	SA Gauge
Function	Measure pressure, analogue signal
Supplier	N & Z Instruments Cape (pty) ltd
Range	-100 kPa to 500 kPa
Material	Stainless steel, glycerine full

TABLE L: MSDS -TERMINAL ADAPTER

Equipment/model	PP660 screw Terminal Adapter
Manufacturer	Pico technology
Function	Connect sensor to data logger's terminal
Supplier	Mantech & RS Components

TABLE M: MSDS - DATA LOGGER

Equipment/model	PT-104, PRT data logger
Manufacturer	Pico technology
Function	Digitally log temperature, ^{o}C
Channels	4 input channels
Supplier	Mantech & RS Components

TABLE N: MSDS – SPECIAL SCALE

Equipment/model	HKD electronic loadcell, 1kg
Manufacturer	-

Function	Digitally measure mass difference
Supplier	Communica

TABLE O: MSDS -AMPLIFIER

Equipment/model	HX711, weight sensor amplifier
Manufacturer	-
Function	Amplifies digital signal to Arduino Uno
Supplier	Communica

TABLE P: MSDS -ARDUINO UNO

Equipment/model	Arduino Uno R3 board
Manufacturer	Arduino
Function	Digitally processes data collected
Supplier	Micro Robotics

TABLE Q: MSDS -WEATHER STATION

Equipment/model	Weather station
Manufacturer	-
Function	Digitally logs weather conditions data
Supplier	In house

APPENDIX: B

Processes and equipment used

Below is a representation of the processes and equipment used to construct and testing the adsorption desalination model.

- Welding machines
    - MIG welding
    - Arc welding
- CNC drilling machine
- Lathe machine – for machining viewport flange
- Milling machine- for machining and drilling buffer plates
- Drill press machine – for ETC frame
- Hand grinding machine – for ETC frame, adsorbent chamber and evaporator
- Data logger – experimental data acquisition
- Arduino Uno- experimental data acquisition
- Variable transformer – for variable potential difference
- Pneumatic air-line- for leak testing shell and tube conduits
- PPE – for protection

APPENDIX: C

Error analysis

The test rig was unstable experiencing vibrations from nearby moving parts within the rig. Quantifying the error was important, especially for the areas around the loadcell at the adsorbent bed contributed to the systems deviation which contributed to the overall experimental error.

The system's deviation was gauged by switching on the vacuum pump to create a controlled testing environment in the adsorbent chamber, but the evaporator was isolated, such that there is no adsorption or desorption taking place. This was to assess if there are any systems errors giving false mass readings when the evaporator was isolated from the adsorbent bed. The dry test condition was run over a period of 2000 seconds and it was observed that the system's deviation occurred over the first 1000 seconds which account to a maximum of 7 grams, this mass then stabilised for the balance of the period. Therefore, the system deviation was based on this observation of 7 grams. This systems deviation was used in determining all errors of tests conducted.

$$q = \frac{m_t - m_{sg}}{m_{sg} + \Delta m_{sys}} \; x \; 100$$

eq.1

$$\mathrm{q} = \text{ the uptake percentage } (\%) \qquad \text{eq. 2}$$

$$m_t = \text{ total mass of adsorbent and adsorbate (g)} \qquad \text{eq. 3}$$

$$m_{sg} = \text{dry mass of adsorbent (g)} \quad \text{eq. 4}$$

$$m_{sys} = \text{system deviation (g)} \quad \text{eq. 5}$$

TABLE A: EXPERIMENTAL ERROR FOR SILICA GEL

Test	P (kPa)	m_t (g)	m_{sg} (g)	m_t-m_{sg} (g)	Dm_{sys} (g)	m_{sg}+m_{sys} (g)	3s	q (%error)
3	-50	238,35	200	38,35	7	207	3,5	18,5
5	-55	264,59	200	64,59	7	207	2,1	31,2

Note: the pressure indicated above is gauge pressure.

TABLE B: EXPERIMENTAL ERROR FOR ZEOLITE

Test	P (kPa)	m_t (g)	m_{sg} (g)	m_t-m_{sg} (g)	Dm_{sys} (g)	m_{sg}+m_{sys} (g)	3s	q (%error)
4	-50	230,26	200	30,26	7	207	1,3	14,6
6	-55	234,11	200	34,11	7	207	2,7	16,5

Note: the pressure indicated above is gauge pressure.

It should be noted that all adsorption phase was conducted at temperature between 25°C and 30°C, it was only the pressure that was varied to trigger desorption. The standard deviation was calculated using the last 400 seconds mass data of Test 3; Test 4, Test 5 and Test 6 for the steady conditions of the adsorption phase. It was observed that the errors of the tests were below 19% except for Test 5. It can be also concluded that the lower the vacuum testing conditions were this exposed the test rig to having higher system error.